DISSERTATION

submitted to the

Combined Faculty of Mathematics, Engineering and Natural Sciences

of

Heidelberg University, Germany

for the degree of

Doctor of Natural Sciences

Put forward by

Nele Volmer

born in Coesfeld

Oral examination: 30th of October 2024

Probing Astrophysical Neutrinos and Lepton Number Violation in Rare Events

Referees: Prof. Dr. Dr. h.c. Manfred Lindner
Prof. Dr. Joerg Jaeckel

Abstract

In the past decades, many experiments have been built to detect neutrinos and learn about their properties. An example is IceCube, which, with its extraordinary volume, measured a first Glashow resonance (GR) candidate event. In the first part of this thesis, we utilize the GR to infer astrophysical neutrino sources since it is an excellent probe to distinguish between neutrinos and antineutrinos. Assuming that the production is dominated by the Δ-resonance, we can exclude the μ-damped pγ source at about 2σ confidence level. Moreover, we perform a projection for IceCube-Gen2. While the GR is a process that can happen within the Standard Model, it can be sensitive to new physics as well. One such new physics model is discussed in the context of neutrinoless double beta decay ($0\nu\beta\beta$). We propose a complex scalar that carries two units of lepton number and argue that its capture can induce a signal that is indistinguishable from standard $0\nu\beta\beta$. For this, we do not require a Majorana neutrino mass or lepton number violation in the zero-density vacuum Lagrangian and thus we can circumvent the famous Schechter-Valle theorem. We also discuss the influence that such a scalar would have on measurements of the GR.

Zusammenfassung

In den letzten Jahrzehnten wurden viele Experimente gebaut, um mehr über Neutrinos und ihre Eigenschaften zu lernen. Ein Beispiel ist IceCube, das zum ersten Mal ein Event mit einer Energie detektiert hat, die der Glashow-Resonanz (GR) entspricht. Die GR ist sehr gut geeignet, um Neutrinos von Antineutrinos zu unterscheiden. Im ersten Teil dieser Arbeit nutzen wir die GR deshalb, um astrophysikalische Neutrinoquellen zu untersuchen. Wenn der Produktionsmechanismus über die Δ-Resonanz dominiert, können wir die μ-gedämpfte pγ-Quelle mit ungefähr 2σ ausschließen. Außerdem führen wir eine Projektion für IceCube-Gen2 durch. Die GR ist im Standardmodell erlaubt, kann aber auch durch neue Physik beeinflusst werden. Ein mögliches Modell neuer Physik wird zunächst im Zusammenhang mit neutrinolosem doppeltem Betazerfall ($0\nu\beta\beta$) diskutiert. Wir führen einen komplexen Skalar ein, dessen Leptonzahl den Betrag zwei hat. Der Einfang eines solchen Skalars kann ein Signal ergeben, welches von normalem $0\nu\beta\beta$ nicht unterschieden werden kann. Wir brauchen hierfür keine Majorana-Neutrinomasse und auch keine Leptonzahlverletzung im Lagrangian im Vakuum. Somit können wir das bekannte Schechter-Valle-Theorem umgehen. Wir diskutieren außerdem den Einfluss des Skalars auf die GR.

Disclaimer

This thesis is heavily based on work that has been completed in collaboration with others during the PhD studies of the author. Equations and tables are taken from these papers without additional reference. Wherever figures are taken from one of the following papers, this is indicated in the caption. Cited references in this thesis are similar to those cited in the papers given below. If a reference is used multiple times within one paragraph, it is cited once after the last period of that paragraph. The work presented in Ch. 3 was first published in

> G.-y. Huang, M. Lindner and N. Volmer, *Inferring astrophysical neutrino sources from the Glashow resonance*, JHEP **11** (2023) 164, arXiv:2303.13706.

In this thesis, we will refer to this paper as Ref. [1]. See also Ref. [2] for a contribution to the conference proceedings of the MAYORANA 2023 Workshop. Another project that is presented in Ch. 5 is mostly based on

> L. Gráf, S. Jana, O. Scholer and N. Volmer, *Neutrinoless double beta decay without vacuum Majorana neutrino mass*, arXiv:2312.15016,

which is currently under review. Within this thesis, we will refer to this work as Ref. [3]. Moreover, parts of Ch. 5 (mostly Sec. 5.2.4 but also small parts elsewhere) are based on the following work that is not public yet:

> L. Gráf, O. Scholer, M. Sen and N. Volmer, *to be published,* 2024.

This work is referenced as Ref. [4] in this thesis.

Conventions

Within this thesis, we use natural units for which

$$c = \hbar = k_B = 1\,. \tag{1}$$

For spinors, we use the commonly used notation for the Dirac adjoint

$$\bar{\Psi} = \Psi^\dagger \gamma_0\,, \tag{2}$$

where $\Psi^\dagger$ is the hermitian adjoint and γ_0 is one of the well-known Dirac matrices. Moreover, we will use

$$\Psi^C = C\bar{\Psi}^T \quad \text{with} \quad C = i\gamma_2\gamma_0 \tag{3}$$

for charge conjugation. At the end of some equations, we will add

$$+\ \text{h.c.}\,, \tag{4}$$

which means that we add the hermitian conjugate of the expression given in the equation. We also use bold print to denote three-vectors

$$\mathbf{p} = \begin{pmatrix} p_1 \\ p_2 \\ p_3 \end{pmatrix}\,. \tag{5}$$

For repeated indices, we use the Einstein sum convention

$$a_\mu b^\mu = \sum_{\mu\nu} g_{\mu\nu} a^\mu b^\nu \tag{6}$$

with the metric

$$g = \text{diag}(1, -1, -1, -1)\,. \tag{7}$$

Sometimes, we use the superscript E to indicate that we mean a quantity on Earth or a superscript S for a quantity at the source.

Contents

1

Introduction

I have done something very bad today by proposing a particle that cannot be detected; it is something no theorist should ever do.

Wolfgang Pauli

In 1914, James Chadwick made an odd observation: When he measured the electron spectrum in radioactive beta decay, he found that it is a continuous spectrum rather than a discrete one [5]. At that time, this was a puzzling discovery. Before the measurement, it was thought that beta decay happens when a neutron bound in a nucleus decays to a proton while emitting an electron. Because, in this picture, the electron is the only particle that leaves the nucleus and can thus carry away energy, it was expected that the energy spectrum of the outgoing electron would be discrete. This discrepancy even lead to some physicists questioning the concept of energy conservation. For example, Niels Bohr proposed that, instead of being valid for each process, energy conservation might only hold in a statistical sense [6]. However, this turned out to be wrong. Wolfgang Pauli came up with a different explanation in 1930. In his famous letter [7] to the participants of the Tübingen conference on radioactivity, he proposed that the continuous spectrum might be due to the fact that a second particle is emitted, which had not been seen until then. Such a particle should, according to Pauli, be electrically neutral and have spin 1/2. Even though Pauli said in his letter that he did not dare to publish this idea at that point, it turned out that he was right later on. The particle (which he called "neutron" at first) was detected in the famous Cowan-Reines experiment in 1956 [8]. While Pauli proposed the existence of these particles that are nowadays called "neutrinos", Enrico Fermi was the one who formulated a first theory for beta decay in 1934 [9]. [10–12]

It is conveyed that, after his proposal, Pauli said the words given in the beginning [10, 12]. Luckily, he was wrong and the neutrino could be detected but not without difficulty. Due to the fact that it carries neither electrical nor color charge, it only participates in the weak and most likely in the gravitational interaction. Both of these interactions are weak compared to the electromagnetic and the strong force. Moreover, since the mass of the neutrino is rather small (and it is not yet excluded that the lightest mass eigenstate might be massless [13]), its gravitational interaction is even smaller. While this makes the work of experimentalists harder when they want to detect neutrinos, it also has a positive side. Neutrinos can travel huge distances and pass through entire planets and other objects without being annihilated or scattered. Therefore, they are a valuable probe for processes and objects that are far away from Earth (see, e.g., Ref. [14]).

In this thesis, there will be a special focus on different astrophysical neutrino sources. Excitingly, in the last decades, so-called neutrino telescopes [15] have been built with which astrophysical neutrinos can be detected. With their large volume either in water or in ice, such neutrino telescopes are able to detect a reasonable amount of neutrinos. The first project that the author worked on [1], which will be discussed in this thesis, evolves around the recent detection of a Glashow resonance (GR) candidate event in IceCube [16], a large neutrino telescope that is located at the South Pole [17]. The Glashow resonance was predicted in 1960 by Sheldon L. Glashow [18] and, due to its unique features, it can help to distinguish between neutrinos and antineutrinos. We will make use of this quality to examine astrophysical neutrino sources and, to be more specific, to distinguish different types of neutrino sources that might be the ones that emit the (anti-)neutrinos that arrive on Earth. However, so far IceCube has only detected one such event [16]. This is again related to the fact that neutrinos interact so rarely. Even though the cross section is significantly enhanced at the energy that the GR is expected to happen at, the detection of a GR candidate event is still extremely rare. In the future, larger, more advanced neutrino telescopes [19–21] may be able to detect more such candidate events, leaving us with better statistics for our analysis.

The GR is a process that can happen within the Standard Model (SM) of particle physics [22]. Nonetheless, the GR and neutrino physics in general can also be a valuable probe for physics beyond the Standard Model (BSM). In fact, the first new physics not covered by the SM that is widely accepted within the community are neutrino oscillations [23, 24]. When the SM was first formulated, neutrinos were thought to be massless. However, it was found that neutrinos are not massless and that they can actually change their flavor while propagating through space due to this mass. This effect will be described in more detail later on.

Here, we want to focus on another type of possible new physics that is strongly related to neutrinos. Due to the fact that neutrinos can change their flavor, the lepton family number is not conserved [25]. Within the original SM, both lepton family number and lepton number are conserved (except for anomalies that break both the baryon number B and the lepton number L; the quantity $B - L$ is not broken by these). However, the corresponding symmetries in the SM are accidental, i.e., the SM was not designed such that lepton number and lepton family number are conserved, they just happen to be conserved [26]. Since we already know that

lepton family number is not conserved in nature, it is reasonable to ask whether lepton number really is conserved.

The second project that the author worked on in recent years and that will be presented in this thesis is strongly related to this question. So far, it is not clear if neutrinos have a Majorana mass or not. If they have a Majorana mass, they can be their own antiparticle, which would lead to the violation of lepton number. The standard probe for this is the lepton number violating (LNV) neutrinoless double beta decay ($0\nu\beta\beta$) [27]. Under certain conditions, an isotope cannot undergo standard beta decay but double beta decay is allowed. Here, the standard process would be two-neutrino double beta decay ($2\nu\beta\beta$): Two neutrons in the nucleus decay to two protons and emit an electron and an electron antineutrino each. If neutrinos are their own antiparticle, the two neutrinos can annihilate. This is then the famous $0\nu\beta\beta$. Moreover, the Schechter-Valle or black box theorem [28] states that the other direction is also true. Not only does the existence of a Majorana neutrino mass imply the existence of $0\nu\beta\beta$; if $0\nu\beta\beta$ is ever found, this immediately implies that neutrinos have a Majorana mass. In this thesis, we will examine a specific model that can circumvent the Schechter-Valle theorem. We introduce a scalar that carries two units of lepton number and we will see that, if such a scalar is captured, it can lead to a signal that looks like a standard $0\nu\beta\beta$ signal. The proof-of-concept was first published in Ref. [3]. Moreover, we will also discuss parts that will be published in Ref. [4].

Both the GR and $0\nu\beta\beta$ are rare events. It is also possible that $0\nu\beta\beta$, as we usually think of it, is forbidden. However, there is a similar process that is allowed within the SM such that, technically, if experiments searching for $0\nu\beta\beta$ are running for an extremely long time, we would expect to see a signal at some point even without any new physics. This process is the double capture of two relic neutrinos and it has been investigated in Refs. [29, 30], where they find that the number of expected events is very small. Thus, this is a rather theoretical consideration. Within the scope of this thesis, we will see that such rare events can be very valuable probes for interesting physics and that a non-observation can also teach us about the characteristics of particles and their interactions. In this thesis, we will not only discuss the two topics the author worked on during her PhD studies. We will also see how they are connected by looking at the influence that the existence of a complex scalar as proposed in Refs. [3, 4] would have on measurements of the GR.

This thesis is structured as follows: In Ch. 2, we will discuss the theoretical foundations that are needed for the two different topics later on. There, we start with a general introduction to neutrino physics in and beyond the SM in Sec. 2.1, covering the different flavors of neutrinos in the SM, neutrino oscillations as confirmed BSM physics and what we can learn about neutrino masses from them, the Pontecorvo-Maki-Nakagawa-Sakata (PMNS) matrix, neutrino mass ordering, the difference between Majorana and Dirac neutrino masses and, finally, the smallness of neutrino masses. Next, we give a short introduction to neutrino sources with a focus on astrophysical neutrino sources in Sec. 2.2 and, after that, we discuss neutrino telescopes in Sec. 2.3. Both of these are relevant for the project that aims to infer information about astrophysical neutrino sources with the help of the GR. To finish the basics, there will be a detailed introduction of $0\nu\beta\beta$ in Sec. 2.4, which

will be relevant for the second project. We start with the first project in Ch. 3. In Sec. 3.1, the GR and its cross section is introduced. Moreover, we show how to calculate two relevant higher-order corrections to the cross section. Before we can start with the main calculation, we introduce the two different flux models we make use of in said calculation in Sec. 3.2. The main calculation is presented in Sec. 3.3 and we discuss its results in Sec. 3.4. To finish that chapter, we briefly look into projections for the future to do justice to the promising neutrino telescopes that will be available in coming years. Thereafter, in Ch. 4, we move on to BSM physics by discussing proposals how physicists could make use of the GR to detect new physics in Sec. 4.1. After that, we introduce the lepton number carrying complex scalar in Sec. 4.2. The influence of this scalar on $0\nu\beta\beta$ is the topic of Ch. 5. There, we first look at the role of the scalar in $0\nu\beta\beta$ in Sec. 5.1. Subsequently, we discuss the influence of the density of the scalar in Sec. 5.2. Depending on the density of the scalar background, it might form a Bose-Einstein (BE) condensate. This issue and also the details of $0\nu\beta\beta$ in both the free and the condensate phase are addressed in this section. While we expect the signal of $0\nu\beta\beta$ to look just like the signal of the capture mode of the scalar we introduce under certain circumstances, there is still a way to distinguish the two modes if a signal is ever seen as long as the scalar is in the free phase. This possibility is based on measurements in different isotopes and it is also described in Sec. 5.2. Next, we discuss phenomenological implications that the existence of our scalar would have beyond double beta decay measurements (except for implications on the GR) in Sec. 5.3 and we briefly look into the capture of dark vector bosons and fermions in Sec. 5.4. There, we also describe the capture of two relic neutrinos that was already mentioned in this introduction. We finish the chapter with a conclusion in Sec. 5.5. Since we have excluded the GR when we discussed the phenomenological implications of the scalar in Sec. 5.3, we will give a few examples in how the existence of such a scalar would affect measurements of the GR in Ch. 6. Lastly, we end this thesis with a summary and an overall conclusion in Ch. 7.

2

Theoretical foundations

In this chapter, we will discuss the basics that will be needed in the scope of this thesis. We will start with a general introduction to neutrinos in and beyond the SM. After that, we will focus on more specific prerequisites for the work that is presented later on in this thesis. As discussed in Ch. 1, there are two main projects that will be reviewed in this thesis. For the first project [1] that aims to distinguish astrophysical neutrino sources using the GR candidate event that was measured in IceCube [16], we will first discuss neutrino sources with a focus on astrophysical neutrino sources in Sec. 2.2. These are the ones that we aim to distinguish in the work presented later on. Moreover, we discuss how neutrino telescopes function, which ones have been built so far and which ones are planned for the future (Sec. 2.3). For the second project [3], we will discuss the basics of $0\nu\beta\beta$ in Sec. 2.4.

2.1 Neutrinos in and beyond the Standard Model

The SM of particle physics is a very successful model when it comes to describing the interactions of elementary particles. It describes the electromagnetic, the strong and the weak force, all within the framework of quantum field theory (QFT). The SM is a gauge theory, which is based on the direct product of three gauge groups:

$$\mathrm{SU}(3)_C \times \mathrm{SU}(2)_L \times \mathrm{U}(1)_Y \,. \tag{2.1}$$

Here, C stands for the color in quantum chromodynamics, L for the left-handed chirality and Y is the weak hypercharge. The eight generators of $\mathrm{SU}(3)_C$ correspond to eight massless gluons, which mediate the strong force while the three generators of $\mathrm{SU}(2)_L$ and the one generator of $\mathrm{U}(1)_Y$ correspond to three massive gauge bosons (W^+, W^- and Z boson) and the photon, a massless gauge boson. Moreover, there is the Higgs boson, which plays a unique role within the SM by giving mass to all the massive particles via the famous Higgs mechanism [31–33]. Besides the bosons

that mediate the forces, there is another group of particles: the so-called fermions. These are divided into quarks and leptons. Both quarks and leptons come in three generations. For the leptons, there are the charged leptons e^-, μ^- and τ^- and the corresponding neutrinos ν_e, ν_μ and ν_τ. These different types of neutrinos are also referred to as flavor. For each of these particles, there is a corresponding antiparticle, which has opposite quantum numbers. We denote the antineutrinos with a bar: $\bar{\nu}_e$, $\bar{\nu}_\mu$ and $\bar{\nu}_\tau$. [10, 25, 34]

So far, everything that was discussed here is covered by the SM. However, in the SM neutrinos were originally thought to be massless. Nowadays we know that this is not true. A first experimental hint was found by the Homestake solar neutrino detector when measurements showed that the flux of solar neutrinos on Earth is much smaller than it was expected from solar-model calculations [35]. After a construction phase and a few initial tests, the Homestake Detector took data from 1970 to 1994 [36]. The mechanism that is responsible for the missing neutrinos are the so-called neutrino oscillations. The initial idea for neutrino oscillations came from the physicist Bruno Pontecorvo already in 1957, even before the first measurements of the Homestake experiment were performed. Back when Pontecorvo published his first paper on neutrino oscillations, it was not known that there are different neutrino flavors. Because of that, he proposed that the neutrino has different "components" [23]. He was inspired by the possibility of kaon oscillations, which were proposed before [37]. It is now accepted that Pontecorvo was right. The reason why the Homestake experiment measured less neutrinos on Earth than we would expect from the solar-model calculations is that neutrinos change their flavor on the way from the Sun to the Earth. Inside the Sun the only neutrinos that are produced are ν_e. Due to the change of flavor that happens on the way to Earth, less ν_e arrive on Earth and less electron neutrinos can, in turn, be detected in the Homestake experiment. The detection mechanism in the Homestake detector was based on the inverse beta decay [36]

$$\nu_e + {}^{37}\mathrm{Cl} \rightarrow {}^{37}\mathrm{Ar} + e^- \,, \tag{2.2}$$

which is only sensitive to ν_e and thus it cannot detect those neutrinos that changed their flavor on the way to Earth. Conceptually, neutrino oscillations rely on the fact that neutrinos have a mass. Besides the well-known flavor eigenstates ν_e, ν_μ and ν_τ, there are also the mass eigenstates ν_1, ν_2 and ν_3 with masses m_1, m_2 and m_3. For the underlying calculation, it is crucial that neutrinos propagate in their mass eigenstates, which changes the probability for a neutrino to be detected as a certain flavor along the way. For reasons of brevity, we will not give a full derivation here and instead refer the interested reader to the standard literature, e.g., Refs. [10, 34]. The transition probability for a neutrino that started propagating as a neutrino of flavor α to be detected as a neutrino of flavor β can be approximated as [10]

$$P_{\nu_\alpha \rightarrow \nu_\beta}(t, E) = \sum_{k,j} U^*_{\alpha,k} U_{\beta k} U_{\alpha j} U^*_{\beta j} \exp\left(-i \frac{\Delta m^2_{kj} t}{2E}\right) . \tag{2.3}$$

Here, t is the time the neutrino propagates, E is its energy and we defined the squared-mass difference

$$\Delta m^2_{kj} = m^2_k - m^2_j \tag{2.4}$$

of two different masses of the mass eigenstates. Here, we can already see that oscillation experiments are only sensitive to the squared masses. Another quantity that was introduced in Eq. 2.3 is the PMNS matrix. This matrix connects the flavor eigenstates and the mass eigenstates via [25]

$$|\nu_\alpha\rangle = U_{\text{PMNS}}|\nu_i\rangle \quad \text{with} \quad \alpha = e, \mu, \tau;\ i = 1, 2, 3\,. \tag{2.5}$$

In components, it can be written as

$$U_{\text{PMNS}} = \begin{pmatrix} U_{e1} & U_{e2} & U_{e3} \\ U_{\mu 1} & U_{\mu 2} & U_{\mu 3} \\ U_{\tau 1} & U_{\tau 2} & U_{\tau 3} \end{pmatrix}\,. \tag{2.6}$$

Later on, in Sec. 5.2.4, we will use the following parametrization for this unitary 3×3 matrix [25]:

$$U_{\text{PMNS}} = \begin{pmatrix} c_{12}c_{13} & s_{12}c_{13} & s_{13}e^{-i\delta_{cp}} \\ -s_{12}c_{23} - c_{12}s_{23}s_{13}e^{i\delta_{cp}} & c_{12}c_{23} - s_{12}s_{23}s_{13}e^{i\delta_{cp}} & s_{23}c_{13} \\ s_{12}s_{23} - c_{12}c_{23}s_{13}e^{i\delta_{cp}} & -c_{12}s_{23} - s_{12}c_{23}s_{13}e^{i\delta_{cp}} & c_{13}c_{23} \end{pmatrix} \cdot V_M\,. \tag{2.7}$$

In this equation, we used the short notation

$$s_{ij} = \sin\theta_{ij},\ c_{ij} = \cos\theta_{ij};\ i, j = 1, 2, 3\,, \tag{2.8}$$

where the θ_{ij} are the three mixing angles and δ_{cp} is the Dirac charge conjugation parity (CP) phase. The matrix V_M summarizes the Majorana CP phases α_1 and α_2 as [25]

$$V_M = \text{diag}\left(1, e^{i\alpha_1}, e^{i\alpha_2}\right)\,. \tag{2.9}$$

These Majorana CP phases and thus the matrix V_M are only relevant in the Majorana case. We will discuss the difference between Dirac and Majorana neutrinos later on. [10, 24, 25, 36]

We already introduced the masses m_1, m_2 and m_3 of the neutrino mass eigenstates. Please note that they were defined by their mixing with the flavor eigenstates. While it is accepted in the community that the mass eigenstates and their corresponding masses exist, we know surprisingly little about the magnitude of the masses m_1, m_2 and m_3. In fact, so far even the ordering is not known for sure. This is strongly related to neutrino oscillation experiments: They revealed that [38]

$$|\Delta m^2_{21}| \ll |\Delta m^2_{31}| \tag{2.10}$$

holds. The sign of Δm^2_{21} is known to be positive, but the sign of Δm^2_{31} is yet unknown. The current best-fit values for differences of the squared masses according to the Particle Data Group [39] are

$$\Delta m^2_{21} = (7.53 \pm 0.18) \times 10^{-5}\,\text{eV}^2 \tag{2.11}$$

and

$$\Delta m^2_{23} = \begin{cases} (-2.529 \pm 0.029) \times 10^{-3}\,\text{eV}^2 & \text{for inverted ordering} \\ (2.455 \pm 0.028) \times 10^{-3}\,\text{eV}^2 & \text{for normal ordering} \end{cases}\,. \tag{2.12}$$

Here, we already used the terms inverted ordering (IO) and normal ordering (NO). What does that mean? Due to the fact that masses are always bigger than or equal to zero, it is possible to deduce two different mass orderings that are allowed with the current experimental data. The first is the so-called NO for which

$$m_1 < m_2 \ll m_3 \tag{2.13}$$

holds. The second one that is allowed is the IO

$$m_3 \ll m_1 < m_2\,, \tag{2.14}$$

where m_3 is the lightest mass. The two orderings are sometimes also called normal or inverted hierarchy. A plot that depicts the two different orderings is shown in Fig. 2.1. There we can see that, for NO, two of the masses are much smaller than the third one while for IO two of the masses are much larger than the third one. Even though there is no clear result yet, experimental results favor NO at the moment. Recently, the collaboration working on the NuMi Off-Axis ν_e Appearance (NOνA) experiment presented new results at the Neutrino 2024 conference in Milan. They claim that their data favors NO with a preference of almost $7:1$ [40]. If this preference turns out to be correct, the sign of Δm^2_{31} would be positive. [38]

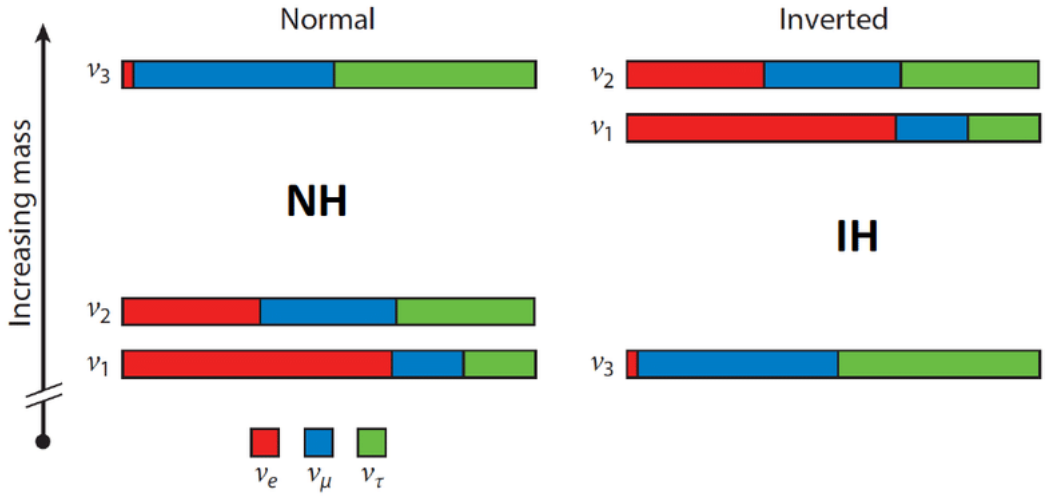

Figure 2.1: The two possible hierarchies for the neutrino mass ordering. On the left, the normal ordering is shown and the inverted ordering is shown on the right. Figure taken from Ref. [41] (licensed under CC BY).

The neutrino mass is strongly intertwined with the question whether neutrinos are Dirac or Majorana particles. As discussed before, neutrino masses are not zero as it is assumed in the SM. However, there are more subtleties when it comes to neutrino masses. When the SM Lagrangian is extended such that neutrino masses are included, there are two different options for the mass term. The first and most widely used option is a so-called Dirac mass term

$$-m_D\bar{\nu}\nu = -m_D(\bar{\nu}_L\nu_R + \text{h.c.})\,, \tag{2.15}$$

where m_D is the Dirac neutrino mass and ν_L and ν_R are left- and right-handed chiral Dirac spinors. In this scenario, lepton number is conserved. However, from neutrino oscillations we already know that the lepton family number is not conserved. As discussed in the introduction (Ch. 1) it is therefore possible that lepton number is not conserved either. If neutrinos are their own antiparticles (which would clearly violate lepton number), we say that they are of Majorana nature. Then we can also introduce a Majorana mass term

$$-\frac{1}{2}m_L\left(\bar{\nu}_L\nu_L^C + \text{h.c.}\right) . \tag{2.16}$$

In this framework first introduced in 1937 by Ettore Majorana [42], a left-handed neutrino is identical to a right-handed antineutrino (except for a phase). In other words: If the neutrino has a Majorana mass, it can be its own antiparticle. It is also possible to introduce a Majorana mass term for both the left- and the right-handed neutrinos. If both the Dirac and the Majorana mass term are present, we can write the mass term in the Lagrangian as

$$\mathcal{L}_{\text{mass}} = -m_D\bar{\nu}_L\nu_R - \frac{1}{2}\left(m_L\bar{\nu}_L\nu_L^C + m_R\bar{\nu}_R\nu_R^C\right) + \text{h.c.} \tag{2.17}$$

This mass term can also be written as

$$2\mathcal{L}_{\text{mass}} = \begin{pmatrix}\bar{\nu}_L & \bar{\nu}_L^C\end{pmatrix}\begin{pmatrix}m_L & m_D\\ m_D & m_R\end{pmatrix}\begin{pmatrix}\nu_R^C\\ \nu_R\end{pmatrix} + \text{h.c.} \tag{2.18}$$

in matrix notation. [25, 38]

One last issue we want to address here is the smallness of neutrino masses. Cosmology sets an upper limit on the sum of neutrino masses. While there are many different limits set by different experiments [39], we will utilize the commonly used limit set by the Planck satellite in 2018 throughout this thesis [43]:

$$\sum_{i=1}^{3} m_i < 260\,\text{meV} . \tag{2.19}$$

When we look at the masses of other particles in the SM, they are orders of magnitude larger. This by itself raises the question why neutrino masses are so much smaller than the masses of other particles. While this is not fully understood yet, there are a few approaches to explain the smallness of neutrino masses. Here, we will introduce a mechanism that will also appear later on in Sec. 5.2.4: the seesaw mechanism.

While there are different types of seesaw mechanisms, we will focus on the type 1 seesaw mechanism here since this is the one that will appear later on. For each of the three light active neutrinos, the type 1 seesaw mechanism introduces a very heavy sterile neutrino. For each generation, the mass matrix reads

$$\begin{pmatrix}0 & m_D\\ m_D & m_R\end{pmatrix} \tag{2.20}$$

and its eigenvalues are

$$m^{\pm} = \frac{m_R}{2} \pm \sqrt{\frac{m_R^2}{4} + m_D^2} . \tag{2.21}$$

For $m_D \ll m_R$, these are approximately

$$m^+ \approx m_R \quad \text{and} \quad m^- = \frac{m_R}{2}\left(1 - \sqrt{1 + \frac{4m_D^2}{m_R^2}}\right) \approx \frac{m_R}{2}\left(1 - 1 - \frac{2m_D^2}{m_R^2}\right) = -\frac{m_D^2}{m_R}\,. \tag{2.22}$$

It is easy to see that for a large Majorana mass of the right-handed sterile neutrinos the smaller eigenvalue m^- is very small. Therefore, the type 1 seesaw mechanism is one approach to explain the smallness of the masses of the active neutrinos. For our purposes here, the type 1 seesaw mechanism is sufficient. For a more detailed discussion of the different seesaw mechanisms see, e.g., Refs. [44, 45].

2.2 Neutrino sources

Next, let us take a look at neutrino sources and especially those that are relevant for the work described in Ch. 3, where we use the GR candidate event to distinguish different astrophysical neutrino sources. In general, neutrino sources can be divided into two categories: They are either artificial or natural. Some examples for artificial neutrino sources are accelerators and nuclear reactors. To produce a neutrino beam using an accelerator, protons are typically shot onto a target. This leads to the production of kaons and pions, which then decay to neutrinos and antineutrinos. An example of a well-known accelerator neutrino experiment is T2K [46]. Nowadays, neutrino beam experiments are used to determine unknown neutrino parameters. For reactor neutrinos, the situation is similar. In nuclear reactors antineutrinos are produced via beta decay:

$$^A_Z X \rightarrow {}^A_{Z+1} X' + e^- + \bar{\nu}_e\,. \tag{2.23}$$

Hence, nuclear reactors produce electron antineutrinos (on average six per fission). Typically, reactor neutrino experiments look for the disappearance of electron antineutrinos, $\bar{\nu}_e \rightarrow \bar{\nu}_X$. The energy is too low to produce (anti-)neutrinos of the other two flavors and thus appearance of these in a beam stemming from a nuclear reactor is a strong probe for neutrino oscillations. [10, 25, 47]

Within this thesis, the natural neutrino sources are more relevant than the artificial ones. Natural neutrino sources can also be distributed into different categories. One natural neutrino source that produced neutrinos that nowadays have very low energies ($\approx 10^{-4}\,\text{eV}$) is the Big Bang. The so-called cosmic neutrino background [49, 50], also known as relic neutrinos, is similar to the cosmic microwave background (CMB). Another natural neutrino source, which produces neutrinos with an energy that is a bit higher than the energy of relic neutrinos, is the Sun. These so-called solar neutrinos are produced in thermonuclear fusion processes in the core of the Sun. This fusion

$$4p + 2e^- \rightarrow {}^4\,\text{He} + 2\nu_e + 26.73\,\text{MeV} \tag{2.24}$$

produces energy and is the energy source of the Sun (and other stars). We can see that the neutrinos produced in the Sun are electron neutrinos. The dominant fusion

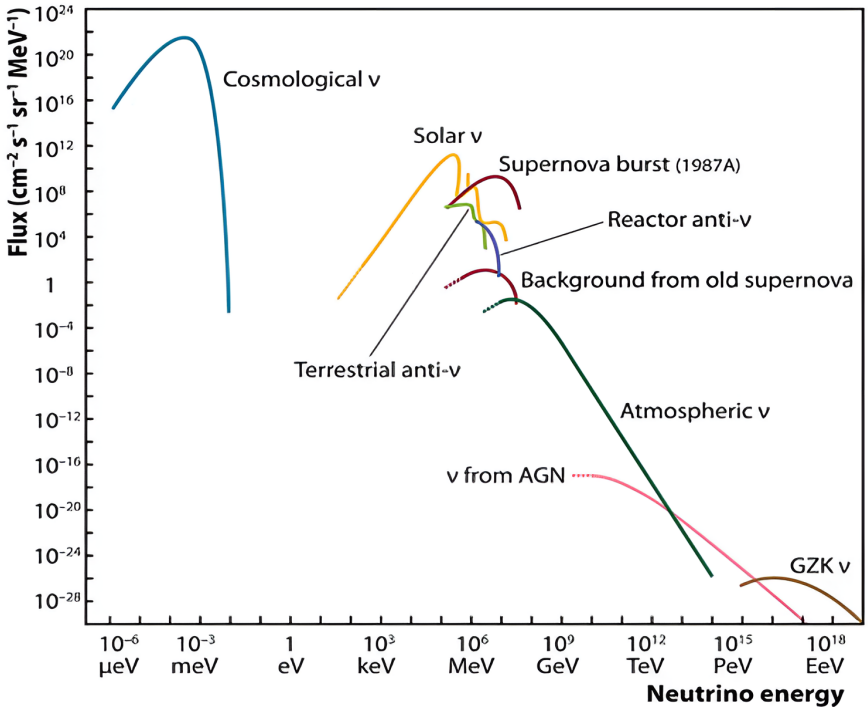

Figure 2.2: Neutrino fluxes and corresponding energies for natural and reactor neutrinos. Figure taken from Ref. [48] (licensed under CC BY).

process is the pp-chain and a small part of the energy of the sun is produced in the carbon-nitrogen-oxygen (CNO) cycle, where the fusion is catalyzed by heavier elements. However, in stars that are at least 1.3 times heavier than the Sun, the CNO cycle is expected to be the dominant fusion mechanism. [10, 25, 47]

Nuclear fusion processes are not the only way neutrinos are produced in the Sun. There are also thermal solar neutrinos, which are produced by, e.g., bremsstrahlung or plasmon decay. Another powerful neutrino source are core collapse supernovae [51]. About 10^{58} neutrinos are emitted during a supernova burst. Neutrinos are an important carrier of both energy and lepton number and they also play a significant role in the explosion mechanism. The emission of neutrinos happens in two major steps: First, within a few milliseconds, the deleptonization burst happens. This burst emits electron neutrinos. Afterwards, during a cooling phase all flavors and both neutrinos and antineutrinos are emitted. [10, 25, 47, 52]

While the natural neutrino sources we mentioned so far are far away from Earth, there are two that are much closer to us. Neutrinos can also be produced in the atmosphere and even in the crust of the Earth. When primary cosmic rays (which mostly consist of protons) interact with nuclei in the atmosphere, many secondary pions are produced. These then decay to neutrinos, which are then the atmospheric neutrinos. Mainly muon (anti-)neutrinos are produced. At high energies, kaons are also produced, which then decay to muons and neutrinos as well. Some of the muons will also decay before hitting the Earth, producing electrons, positrons and muon and electron (anti-)neutrinos. An overview over neutrino fluxes and corresponding energies on Earth for different neutrino sources is shown in Fig. 2.2. [10, 25, 47]

Here, we are mostly interested in ultrahigh-energy (UHE) astrophysical neutrinos detected in IceCube. In Fig. 2.2, the energy range and flux for these are also shown. So far, it is unknown where exactly these neutrinos come from. In this thesis, we want to shed a bit of light on them by using the GR candidate event measured in IceCube to perform a statistical analysis and thus infer information on the astrophysical sources of these neutrinos. One of the most popular mechanisms are accelerated cosmic rays, which collide with targets around the source [53–58]. Depending on the target particle, these are usually classified into pp and pγ type sources. For a pp source, the target particle is a proton while it is a photon for a pγ source. There is a variety of source models describing the production of the UHE neutrinos [59–62]. Now we will focus on pp and pγ sources and their phenomenology, which we will later on use for our analysis.

Since we want to distinguish different types of sources, it is important to think about measurable quantities we could use for this distinction. First of all, neutrino flavor is not necessarily the best probe for this since the neutrinos are produced far away from Earth. On their way to Earth they therefore have to cover a huge distance and during the flight they undergo neutrino oscillations. After traveling long distances, we expect an almost democratic flavor composition on Earth [63]

$$\phi^E_{\nu_e} + \phi^E_{\bar{\nu}_e} : \phi^E_{\nu_\mu} + \phi^E_{\bar{\nu}_\mu} : \phi^E_{\nu_\tau} + \phi^E_{\bar{\nu}_\tau} \approx 1 : 1 : 1\,. \tag{2.25}$$

Here, ϕ^E is the corresponding (anti-)neutrino flux on Earth. Since this ratio is approximately the same for all source types we want to distinguish, flavor is not a good observable for our purposes. However, for the pγ source, there is a small subtlety. This subtlety is discussed in Sec. 2.2.2. In general, we will use the neutrino to antineutrino ratio, which is defined in the next section, to distinguish between the different source types.

2.2.1 Cosmic rays colliding with a target: the pp source

When hadronic cosmic rays interact with a dense target at high energies (e.g., when cosmic ray protons interact with gas in the acceleration region or the medium surrounding it like, e.g., in a galaxy cluster [64]), this leads to the production of pions. The neutrinos we are interested in are decay products of these pions. For pp sources, we expect the following mixture of pions due to isospin invariance [65]:

$$p + p \to \begin{cases} \pi^0 + \text{anything} & 1/3 \text{ of cases} \\ \pi^+ + \text{anything} & 1/3 \text{ of cases} \\ \pi^- + \text{anything} & 1/3 \text{ of cases} \end{cases}. \tag{2.26}$$

Then, the charged pions decay to muons [65, 66]

$$\pi^+ \to \mu^+ \nu_\mu,\ \pi^- \to \mu^- \bar{\nu}_\mu \tag{2.27}$$

and the muons subsequently decay via [65, 66]

$$\mu^+ \to e^+ \nu_e \bar{\nu}_\mu,\ \mu^- \to e^- \bar{\nu}_e \nu_\mu\,. \tag{2.28}$$

For the pp source, the production of the pion is purely hadronic. Since the dominant decay mode of the π^0 is the decay to two photons, this one does not change the ratio and the final ratio we expect is

$$\phi_\nu^{\mathrm{S}} : \phi_{\bar{\nu}}^{\mathrm{S}} = 1 : 1\,, \tag{2.29}$$

i.e., the amount of neutrinos is equal to the amount of antineutrinos. Here, ϕ^{S} is the flux at the source. Since this is not affected by neutrino oscillations while the neutrinos travel from the source to the detector on Earth, this ratio is the same on Earth - at least as long as we do not consider any new physics. In this thesis, the parameter we will discuss is the $\bar{\nu}_e$ fraction:

$$f_{\bar{\nu}_e} = \phi_{\bar{\nu}_e}/(\phi_{\bar{\nu}_e} + \phi_{\nu_e})\,. \tag{2.30}$$

For an ideal pp source, we expect $f_{\bar{\nu}_e}^E \approx 0.5$ on Earth. [39, 65, 66]

2.2.2 Cosmic rays colliding with photons: the pγ source

Cosmic rays can also produce pions when they collide with photons if the center-of-mass (COM) energy exceeds about 0.2 GeV. Some examples for the origin of such photons are active galactic nuclei or synchrotron radiation from electrons that are accelerated in the cosmic rays alongside the protons [64]. At low energies, resonances dominate the cross section with the most prominent one being the Δ-resonance [65]:

$$p + \gamma \to \Delta^+ \to \begin{cases} p + \pi^0 & 2/3 \text{ of cases} \\ n + \pi^+ & 1/3 \text{ of cases} \end{cases}. \tag{2.31}$$

Overall, the charged pions that are produced are mostly π^+. As for the pp source, this one then decays to $\mu^+\nu_\mu$ and the muon decays further to $e^+\nu_e\bar{\nu}_\mu$. Therefore, the expected neutrino to antineutrino ratio for pγ sources is

$$\phi_\nu^{\mathrm{S}} : \phi_{\bar{\nu}}^{\mathrm{S}} = 2 : 1\,, \tag{2.32}$$

which is different from the pp case. [65, 66]

However, on Earth we expect $f_{\bar{\nu}_e}^E \approx 0.23$, which differs from the one at the source ($f_{\bar{\nu}_e}^S \approx 0.33$). To understand this, we have to go beyond the basic assumption of a democratic flavor composition on Earth as given in Eq. 2.25 and look at neutrinos and antineutrinos separately. Let us do a simple analysis to understand how the flavor of the antineutrinos changes on their way to Earth. Due to neutrino oscillations, the final amount of $\bar{\nu}_e$ measured on Earth also consists of antineutrinos that were $\bar{\nu}_\mu$ at the source. However, this leads to an important question: Why does this affect the pγ source but not the pp source? For a detailed discussion of the oscillation effects see Ref. [65]. There, they calculate the neutrino and antineutrino flavors on Earth using the so-called tri-bimaximal mixing model. In Eq. 11, they find

$$\xi_{\bar{\nu}_e}^E \approx \frac{5}{9}\xi_{\bar{\nu}_e}^S + \frac{2}{9}\xi_{\bar{\nu}_\mu}^S\,, \tag{2.33}$$

where $\xi_{\bar{\nu}}^E$ is the ratio of the corresponding antineutrino compared to the total flux of neutrinos and antineutrinos on Earth and $\xi_{\bar{\nu}}^S$ is the one at the source. For the pp

source, $\xi^S_{\bar{\nu}_\mu} \approx 2\xi^S_{\bar{\nu}_e}$ and hence $\xi^E_{\bar{\nu}_e} \approx \xi^S_{\bar{\nu}_e}$. However, for the p$\gamma$ source, we only have $\bar{\nu}_\mu$ at the source and no $\bar{\nu}_e$. When a careful calculation is performed, we can see that $f^E_{\bar{\nu}_e}$ is smaller than the share of antineutrinos at the source. Please note that the definition of $f^E_{\bar{\nu}_e}$ differs from $\xi^E_{\bar{\nu}_E}$, which explains that the value we expect for $f^E_{\bar{\nu}_e}$ is significantly larger than what Eq. 2.33 would give for $\xi^E_{\bar{\nu}_e}$.

2.2.3 Muon damping

In this work, we do not only take pp and pγ sources into account but also the muon-damped pγ source. Muon-damping typically takes place in an environment with strong magnetic fields ($B \gtrapprox 10^3\,\mathrm{G}$). Then the muons in the decay chain lose energy by synchrotron radiation or via adiabatic losses before they can decay. For pp sources, this mode is $pp \to \pi^\pm$ pairs $\to \nu_\mu, \bar{\nu}_\mu$ and for pγ sources $p\gamma \to \pi^+ \to \nu_\mu$ [65]. Therefore, we expect $f^E_{\bar{\nu}_e} \approx 0$ for the ideal muon-damped pγ source. For the muon-damped pp source, the ratio $f^E_{\bar{\nu}_e}$ does not change compared to the undamped pp source and therefore we do not treat this as a separate case.

2.2.4 Comment on multi-pion production

All we have discussed so far holds in the case of ideal pp and (μ-damped) pγ sources. For the pγ source, the idealized picture includes only the production via the Δ-resonance given in Eq. 2.31. However, the reality is not as simple. At higher energies, on top of higher resonances, multi-pion processes become relevant. Unlike for the Δ-resonance, these processes do not only produce π^+ (and π^0) but also π^- [67, 68]. Therefore, multi-pion production will shift $f^E_{\bar{\nu}_e}$ towards 0.5. This clearly makes the distinction harder. If we assume that the multi-pion mode dominates over the other pγ production mechanisms, we would need additional multimessenger information to distinguish the different production mechanisms. In this thesis, we will discuss mostly ideal pp, pγ and muon-damped pγ sources. For ideal pγ sources, we assume production via the Δ-resonance. However, since multi-pion production is relevant at higher energies as well, we will also consider a pγ source with both multi-pion production and production via the Δ-resonance. In general, it is important to understand that we constrain the fraction $f^E_{\bar{\nu}_e}$ as given in Eq. 2.30. The result is subsequently interpreted in terms of the values we would expect for $f^E_{\bar{\nu}_e}$ for the different types of neutrino sources.

2.3 Neutrino telescopes

Neutrino astronomy is a branch of astronomy that aims to use neutrinos to detect and examine astronomical objects. For this, neutrinos are well suited due to the same reason that makes them hard to detect: They are unlikely to scatter with matter on their way to Earth since they rarely interact. Thus, we can extract information from neutrinos that we could not get with other experiments like optical telescopes.

2.3.1 How neutrino telescopes work

To detect neutrinos, sophisticated settings are necessary. One class of experiments that is widely used for neutrino astronomy are so-called neutrino telescopes. The detection mechanism of neutrino telescopes heavily relies on Cherenkov radiation, which was first discovered by the Soviet physicist Pavel Cherenkov while he was working on his PhD. While performing his studies, he discovered the radiation that is now named after him by surprise: He noticed faint blue light stemming from γ-radiation in pure sulphuric acid. [69, 70]

When a charged particle moves through an electrically isolating medium, it induces short-time polarization of the atoms it passes. This dipole moment varying over time then emits electromagnetic waves. The waves emitted by different atoms interfere with each other. If the particle has a velocity v that is bigger than c/n, where c is the speed of light and n is the refractive index of the material, then there is an angle θ_C at which the interference is constructive:

$$\sin(\theta_C) = \frac{c}{vn} = \frac{1}{\beta n}\,. \tag{2.34}$$

In this direction the so-called Cherenkov radiation is emitted. From Eq. 2.34 it is easy to deduce that only particles that are faster than c/n can induce Cherenkov radiation since $|\sin(\theta_C)| \leq 1$. [71]

Since Cherenkov radiation can only be emitted by charged particles, neutrinos themselves do not emit any Cherenkov radiation. So how are they detected in neutrino telescopes? When a neutrino travels through the medium, it can interact with the medium, which can lead to charged product particles that then emit Cherenkov radiation. However, even neutrinos of very high energies often travel through a detector without interacting with the medium because the interaction cross section is very small. Since this is the case, it is important to increase the number of targets (in our case, these are the electrons in ice or water) within our detector. This can be achieved by building experiments with a huge volume. The Cherenkov radiation can then be detected using a photomultiplier tube (PMT). PMTs rely on the photoelectric effect to detect the Cherenkov light. The signals are then digitized and sent to a computer. Usually, the signal is sent to a facility at the surface via a cable going through a string on which the PMTs are placed. [72]

The events that are measured in neutrino telescopes can be classified into different categories. Two typical topologies are track and shower events. If a charged particle like, e.g., a muon, travels through the detector for a long distance, this is classified as a track event. An example measured in IceCube is shown in Fig. 2.3a. Another option is that the energy of the incoming particle is released into several electromagnetic and/or hadronic showers. Such an event is shown in Fig. 2.3b. [75]

2.3.2 Historical development

Here, we will briefly discuss the historical development of neutrino telescopes, which lead up to the construction of IceCube. The Deep Underwater Muon And Neutrino Detector (DUMAND) was the first project aiming to build a neutrino telescope [76]. While DUMAND was terminated before it even started to take any data, many ideas

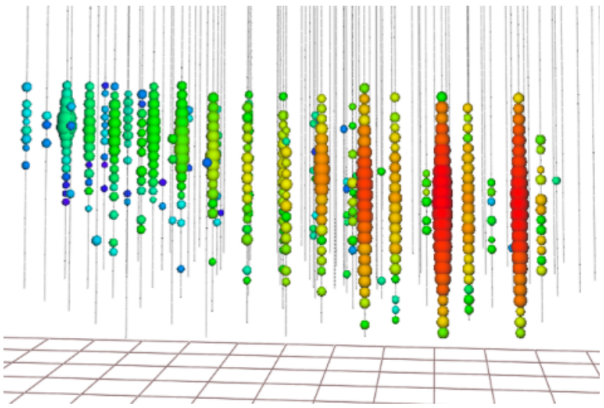

(a) A high-energy track event. Figure taken from Ref. [73] (licensed under CC BY).

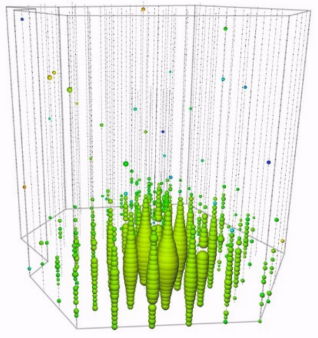

(b) A shower event. Figure taken from Ref. [74] (licensed under CC BY-NC-ND).

Figure 2.3: Two events that have been measured in IceCube.

and technologies used in neutrino telescopes later on were developed by scientists working on DUMAND. It was supposed to be located in the Pacific Ocean near Hawaii since the water there is deep enough relatively close to the shore. The location was found during a first DUMAND workshop, which was held in 1975 at Washington state university. One year later, the next workshop took place in Honolulu. There, three different alternatives for a neutrino telescope in the sea were discussed. Eventually, two of these were combined leading to DUMAND. [77]

Exploiting the rich information carried by neutrinos, DUMAND was supposed to be a multipurpose experiment - just as modern neutrino telescopes. First of all, the experiment was aiming to find astrophysical point sources of high-energy neutrinos. Furthermore, it was supposed to examine two phenomena in particle physics, namely UHE hadronic interactions and neutrino oscillations. For the UHE hadronic interactions, indirect detection of events both in extraterrestrial sources and in the detector were considered. Also, back when DUMAND was first planned, neutrino oscillations had not been observed so far and were not as well understood as nowadays. Thus, DUMAND was also an excellent candidate to shed light on these. Another potential use of DUMAND was to study cosmic rays. In addition to detecting neutrinos, high-energy downgoing muons that were produced in the atmosphere could have also been detected. [78]

Originally, the first conception for DUMAND aimed for a cubic kilometer neutrino telescope using more than 20.000 large-size PMTs protected by glass spheres. This vision was very demanding when it comes to financial and also technical resources. Since it was not feasible, the first idea and also a few subsequent ones were discarded. Eventually, the collaboration ended up with a project called DUMAND-II, requiring only 216 PMTs arranged in an octagonal shape with a string in each corner of an octagon and one in the middle. The diameter would have been 100 m and the height 230 m. This setup could have detected about 3500 atmospheric neutrinos per year and three downgoing muons per minute. In 1993, the first three strings of PMTs were attached to the ground of the sea. Unfortunately, this endeavor was not successful: The communication with facilities on the shore was stopped by leaks and

a short circuit. In the end, DUMAND was canceled in 1995, due to the technical difficulties and consequential difficulties to get funding; the main funding agency, the Department of Energy in the United States, terminated the project. [77, 79]

There were many Russian scientists participating in DUMAND until 1980. Then, due to the Soviet invasion in Afghanistan, the administration under Reagan, the president of the United States, ended the cooperation. At that time, A. Chudakov proposed to build a "Russian DUMAND" in lake Baikal in Siberia [77]. After a few initial tests, a first stationary string with up to twelve PMTs was installed and operated using a cable connecting it to the shore. In a first experiment, strings with up to 36 PMTs were operated. During this period, technologies were developed, especially for deploying and retrieving the instruments in the water. On the physics side, the experiment set stringent limits on the flux of magnetic monopoles that catalyze baryon decays [80]. Afterwards, consecutive experiments with 72 and later 96 and 144 optical modules were operated. Next, an experiment making use of about 200 PMTs was planned. This one was called Neutrino Telescope 200 (NT-200). NT-200 started operating in 1998 and eventually it consisted of 192 PMTs on eight strings that were carried by a frame [81]. Each optical module has a pressure glass housing with a phototube inside. These optical modules are arranged in pairs along the strings of the telescope. A basic building block of NT-200 consisted of two of these pairs and an electronics module, which is responsible for power supply and front-end electronics, in between. It also contained control units. These basic building blocks were called "svjaska", which is Russian for bundle [82]. NT-200 was completed in 1998 and afterwards it took data for about ten years. While it was struggling with a large number of failures of individual channels, it was still able to compete with the Antarctic Muon And Neutrino Detector Array (AMANDA), which was a much larger experiment. This was possible since it was also able to search for high-energy cascades below the experimental setup, increasing the volume NT-200 itself covered by a factor of ten [77]. The detector in lake Baikal gets upgraded to Baikal Gigaton Volume Detector (Baikal-GVD) nowadays, see Sec. 2.3.4. [77, 81]

Now we will focus on AMANDA, the predecessor of IceCube. While Russian scientists focused on their experiment in lake Baikal, two scientists working in the United States proposed to build a neutrino telescope in deep polar ice. In their proposal, they also discussed the possibility of detecting the Cherenkov light coming from high-energy muons going through optically clear deep polar ice and showed that this yields a cost-effective opportunity to build neutrino telescopes [83]. A few transparency measurements of natural ice were performed and in parallel, a group of scientists proposed to construct AMANDA. In 1991 and 1992, the AMANDA collaboration started to deploy PMTs into the ice at the South Pole using a hot water drilling technique. After Swedish collaborators joined AMANDA, a first detector with four strings and 80 optical modules in total was designed. In 1993 and 1994, a first array was deployed 800 to 1000 meters deep into the ice. This exploratory phase found that, at this depth, residual air bubbles still caused strong scattering of light. Therefore, in 1995 and 1996, an array was deployed at depths between 1540 and 2040 m. At these depths, the concentration of air bubbles is smaller. This array consisted of 86 optical modules on four strings. Later on, six more strings with 216 additional optical modules were added. One year later, in 1997 and 1998, this

setup was upgraded by adding three additional strings at depths between 1150 and 1350 m in preparation for next generation experiments and to test new technologies used for data transmission [84]. Until January 2000, the AMANDA detector was upgraded stepwise. Eventually, it consisted of 677 optical modules, distributed over 19 strings. This setup was called the AMANDA-II detector. AMANDA-II took data until April 2009 for a total of nine years. All in all, the neutrino sky map it measured consisted of 6959 events. There was no excess that was statistically significant, hence only upper limits on point source fluxes could be derived. In the end, AMANDA was a predecessor for IceCube (see Sec. 2.3.3). The final goal of having a kilometer-scale neutrino telescope was declared by one of the lead scientists already in 1994. [77, 85, 86]

After DUMAND was stopped, the European groups that had participated in the project were looking for other possibilities to realize a neutrino telescope in water, leading to three other noteworthy projects aiming to detect neutrinos in the Mediterranean Sea, the Astronomy with a Neutrino Telescope and Abyss environmental RESearch project (ANTARES) [87], the NEutrino Mediterranean Observatory (NEMO) [88] and the Neutrino Extended Submarine Telescope with Oceanographic Research Project (NESTOR) [89]. Note that there is the Neutrino Ettore Majorana Observatory [90], which is also abbreviated as NEMO. We do not refer to that one this thesis.

The first one of these three projects was NESTOR. A first hexagonal structure carrying only ten PMTs was deployed in 1991 near Pylos in Greece. Originally, the collaboration working on NESTOR was international but centered in Greece. Some French and Italian institutes also joined in the beginning, but later on they left to work on their own neutrino telescopes ANTARES and NEMO. The NESTOR collaboration put a lot of effort into identifying suitable sites where the experiment could have been located. After spending a long time on technical development, a cable was installed connecting a site with a depth of 4 km to the shore. Later on, in 2004, a prototype floor with twelve optical modules was installed. However, this one could only be operated for one month before the cable to the shore failed. While this was the end of NESTOR, the collaboration was able to measure the atmospheric muon flux with the prototype and found that the measurement agreed with expectations. Moreover, they developed a triangular working platform facilitating deployment of floors into the sea. [77, 79]

A second project on which Italian groups started working in 1998 is NEMO. The purpose of NEMO was to investigate whether a cubic-kilometer deep sea neutrino telescope is feasible and to find a suitable site for such an experiment. NEMO lead to new technical solutions, an important one being “flexible towers”, allowing the towers containing the optical modules to be folded together, which made deploying the experiment easier, taking away tension from the electro-optical cable and giving a 3D structure to the positions of the optical modules in a single tower. Moreover, a site near Sicily was found to be suitable. Over the years, several versions of these towers have already been deployed. Now the site that has been identified will be one of the locations for the Cubic Kilometre Neutrino Telescope (KM3NeT) (see Sec. 2.3.4). [77, 79]

The most prominent of these three projects is ANTARES, located at the French

coast near Toulon. While NESTOR and NEMO contributed to the technical development needed to successfully run such experiments in the deep sea, ANTARES succeeded in installing and operating the first working neutrino telescope in the deep sea. It is located 40 km off the shore at a depth of 2475 m and it was completed in 2008. The detector consists of twelve strings carrying 885 optical modules in total and a 13th so-called instrumentation line monitoring the environment. The strings are arranged in an octagonal shape. ANTARES took data until 2022. The Southern sky was explored with a special focus on central regions of our galaxy looking for point-like objects. Due to the good angular resolution for cascades, they could be included into searches for point-like objects. [77, 79, 91]

2.3.3 The IceCube observatory

For the study we perform in this thesis, we use an event detected in IceCube. It comes as no surprise that the first event of this kind was detected in IceCube since it is the first gigaton neutrino telescope that has ever been built. Thus it is an excellent observatory for astrophysical neutrinos. In the future, its successor and other large-scale experiments (see Sec. 2.3.4) will most likely be able to provide increased statistics, which would give us the opportunity to refine our analysis.

As discussed before, AMANDA was a precursor for IceCube and scientists back then already had the goal to build a kilometer-scale neutrino telescope. With IceCube, this was finally realized at the South pole near the Amundsen-Scott South Pole Station. IceCube was first proposed in 1999 essentially by members of the AMANDA collaboration. A new collaboration was formed that coexisted with the AMANDA collaboration until they merged in 2005. Not only did the AMANDA collaboration become a part of the IceCube collaboration, AMANDA also became a part of the IceCube detector. To be more precise, AMANDA is part of the portion of IceCube that is located deep inside the ice. This in-ice array consists of 5160 digital optical modules located in depths from 1450 to 2450 m, each containing a PMT and associated electronics. 60 of these optical modules are arranged on each string. In total, there are 86 strings frozen into the ice on a hexagonal grid with 125 m spacing in between them. Vertically, the distance between two modules is 17 m. In the center of the array, eight strings are arranged in a denser way with only 70 m in between two strings and a vertical spacing of seven meters allowing for a lower neutrino energy threshold of about 10 GeV. Because of this, IceCube is also suitable for studying neutrino oscillations. This denser part deep in the ice is called DeepCore and it replaced the AMANDA detector that was part of the in-ice array until 2009. The surface part of the detector, IceTop, consists of 81 stations, each one located on top of a string carrying optical modules of the in-ice part of the detector. All of these stations contain two tanks, which are equipped with two downward facing digital optical modules. In between the two tanks there is a surface junction box connected to the optical modules aligned on the string. These boxes are then connected to a central counting house, where all data is collected and then sent to the University of Wisconsin-Madison. IceTop fulfills multiple purposes: It is a veto and calibration detector for IceCube and it can also detect air showers stemming from cosmic rays with an energy between 300 TeV and 1 EeV. For such

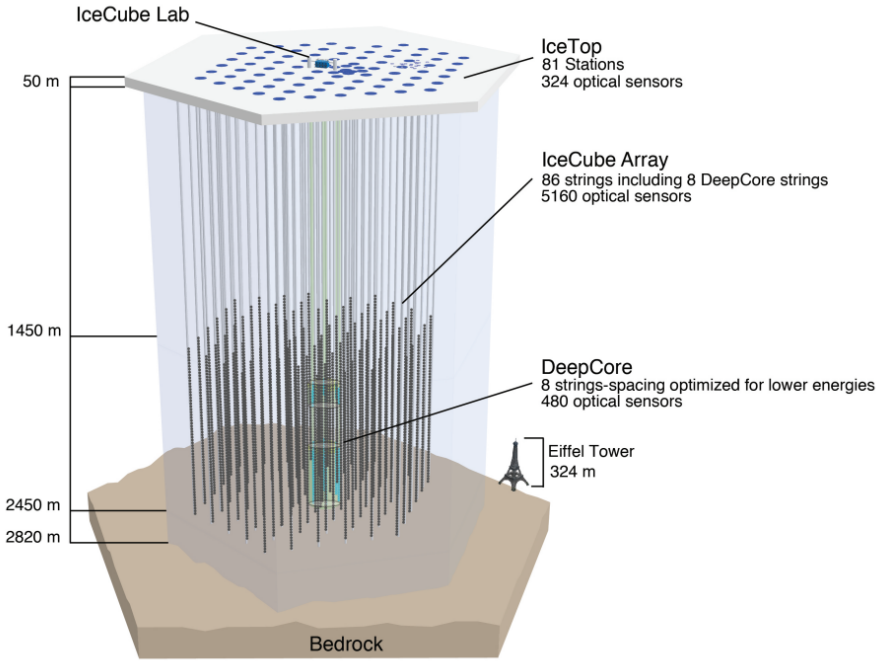

Figure 2.4: The IceCube detector. Besides the in-ice array, the part at the surface called IceTop and the more densely instrumented region DeepCore are also displayed. Figure taken from Ref. [95] (licensed under CC0).

cosmic rays, it also measures the flux and composition and the arrival direction in the Southern sky. The whole setup including not only the in-ice array but also IceTop and DeepCore is displayed in Fig. 2.4. [77, 92–94]

The construction of IceCube started with the deployment of the first string in January 2005. After that, construction went on during the following austral summers until the last string was deployed in December 2010. The detector was thus finished a decade after the proposal was submitted by the collaboration. To deploy the strings, holes with a diameter of 60 cm were drilled. The sensors were then lowered into these holes filled with water which then refroze, leaving the instruments frozen into the ice. While IceCube already started taking data in 2005, it became fully operational in May 2011 after construction was complete. [77, 92, 96]

With its unprecedented volume, IceCube was able to perform some remarkable measurements. Here, we will give an overview over part of the results from IceCube, focusing on those that will be relevant for the analysis performed in this thesis. Quite early, in 2013, the IceCube collaboration reported on the detection of two neutrinos with PeV energies. The first one with the nickname "Bert" was detected on the 8th of August 2011 with an energy of 1.04 ± 0.16 PeV and the second one ("Ernie") was seen on the 3rd of January 2012, carrying an energy of 1.14 ± 0.17 PeV. The observation of these two events was a first indication of an astrophysical origin of the neutrino flux. At that time, the probability to observe two or more such candidate events was 2.9×10^{-3} under the hypothesis that there is only atmospheric background. While this was a strong lead, it was not possible to come to a definite conclusion just with this measurement [97]. However, later on in the same year, the collabo-

ration announced the detection of 26 additional events in the range between 30 TeV and 1.2 PeV, leading to 28 detected UHE events in total. This is substantially more than expected for a purely atmospheric neutrino background. Moreover, flavors and directions did not match the expectation for atmospheric neutrinos either. With these measurements, the hypothesis of a purely atmospheric neutrino background could be rejected at 4σ-level. It can be concluded that there is an extraterrestrial component to the neutrino background [75]. In September 2014, yet another paper was published, reporting on the observation of the highest energy neutrino interaction ever measured at that time with an energy of 2 PeV. This event was nicknamed "Big Bird" [98]. Later on in our analysis, "Bert", "Ernie" and "Big Bird" will be used to fix the normalization and shape of the neutrino flux (cf. Sec. 3.1.1 and Sec. 3.3). In 2015, the observation of an astrophysical neutrino flux was confirmed again by studying muon neutrinos from the Northern sky. Unlike for the Southern sky, neutrinos from the Northern sky have to pass through Earth on their way to IceCube. While most particles are not able to pass through Earth, neutrinos can do this since they rarely interact. By looking at the Northern sky, Earth naturally blocks muons originating in cosmic ray air showers as long as they pass through enough material. When a muon is seen from such a direction, part of the distance must have been covered by a neutrino. These are the events that were taken into account in the analysis. Most neutrinos in the sample are stemming from cosmic ray interactions in the atmosphere of the Earth. However, the collaboration found that the events with the highest energies were not consistent with this hypothesis. Instead, they can be explained by an astrophysical origin, which is consistent with what IceCube found earlier in studies dominated by neutrinos from the Northern sky. [99]

In 2018, IceCube was the first detector that was able to use a neutrino to locate a source of high-energy astrophysical neutrinos. On the 22nd of September, IceCube detected a high-energy neutrino with an energy of 290 TeV [100]. This neutrino came from a direction that was known to be consistent with the location of a gamma-ray blazar. Also, the time of its detection was consistent with other measurements indicating a flaring episode of the blazar [101]. After this, IceCube also played a role in finding other neutrino source candidates like tidal disruption events [102, 103] and an active galactic nucleus [104]. In 2016, IceCube measured a neutrino with an even higher energy compared to the events measured before. With an energy of 6.05 ± 0.72 PeV, it is consistent with the GR [16], see also Ch. 3.1.

While we are mainly interested in measurements of UHE neutrinos, these are not the only results from IceCube so far. For example, it also contributed to the understanding of neutrino oscillations by measuring the atmospheric muon neutrino disappearance using DeepCore to detect atmospheric muon neutrinos with an energy between 10 GeV and 100 GeV. In this energy region, a strong disappearance signal was expected. Neutrino oscillation parameters were determined [105] and updated in 2017 [106] and 2023 [107]. Atmospheric tau neutrino appearance was measured as well [108].

2.3.4 The future of neutrino telescopes

While the detection of one GR candidate event is a great achievement and enables us to perform a first analysis aiming to distinguish astrophysical neutrino sources, we need better statistics to perform a more detailed analysis. Fortunately, there are already plans for new experiments and future generations of existing neutrino telescopes. First of all, IceCube will be upgraded to IceCube-Gen2. A first step in this is the so-called IceCube upgrade, where seven additional strings are lowered into the ice in the center of the existing IceCube detector. These strings will be densely instrumented at the bottom-center of the detector. They will improve the detection of unscattered photons from interactions with an energy above 1 GeV. This will yield a high sensitivity to neutrino properties that can be inferred from measurements of neutrino oscillations. For example, measurements of tau neutrino appearance from atmospheric oscillations are a probe for the unitarity of the neutrino mixing matrix (cf. Eqs. 2.5 and 2.6). Moreover, the angular resolution will be improved. Work on this upgrade is already in progress. However, for our purpose, the second step is more relevant to increase statistics of GR candidate events. For IceCube-Gen2, the volume of the detector will be increased by about a factor of eight to a volume of 7.9 km^3. The annual rate of observed cosmic neutrinos will be increased by a factor of ten and it will be able to detect much weaker sources than the first IceCube detector. By adding an additional radio array, the energy range that can be detected will be significantly increased, yielding sensitivity to events above 10 PeV. Construction of IceCube-Gen2 is supposed to be finished by 2032 [109]. [21, 110, 111]

Besides IceCube-Gen2, there are other promising future experiments. The Russian experiment in lake Baikal is being upgraded to Baikal-GVD, a kilometer-scale neutrino telescope looking at the Northern sky. Construction was started in 2015. The upgraded telescope is designed to detect astrophysical neutrinos with an energy between a few TeV and 100 PeV. While construction is still ongoing, the detector is taking data at the same time. In Europe, the dominating setup - or rather setups - will be KM3NeT, the successor of ANTARES, NEMO and NESTOR. As already mentioned in Sec. 2.3.2, KM3NeT will be installed in several sites in the Mediterranean sea, namely off-shore Toulon in France, near Capo Passero in Italy and near Pylos in Greece. These sites were chosen due to the distance to the shore, local infrastructure and optical properties of the water. Currently, two detectors are under construction, a cubic kilometer detector called Astroparticle Research with Cosmics in the Abyss (ARCA) near Sicily in Italy and one called Oscillation Research with Cosmics in the Abyss (ORCA). While ARCA is build to cover a huge volume and thus to be sensitive to low neutrino fluxes, ORCA is instrumented more densely and aims to measure neutrino oscillations of atmospheric neutrinos. Other promising projects are the Pacific Ocean Neutrino Experiment (P-ONE) [112], the Tau Air Shower Mountain-Based Observatory (TAMBO) [113] and The tRopIcal DEep-sea Neutrino Telescope (TRIDENT) [114]. [19, 20, 115, 116]

2.4 Neutrinoless double beta decay

The second project that will be discussed in this thesis proposes a new physics scenario in the context of $0\nu\beta\beta$. Therefore, we want to introduce this process, the related Schechter-Valle or black box theorem, some details that are relevant for the calculation of the half-life and the current experimental status in this section.

Due to the fact that neutrino oscillations have been found in experiment [117], we know that neutrinos are not massless as it is assumed in the SM. However, this does not tell us whether the neutrino mass is of Dirac or Majorana nature (c.f. Sec. 2.1). If neutrinos are of Majorana nature, this also means that lepton number is not conserved and thus the search for Majorana neutrinos is also a search for lepton number violation. In the SM of particle physics, lepton number is a conserved quantity. However, it is already known that lepton family number is not conserved in nature due to neutrino oscillations. Because of this, it is fair to ask whether lepton number is conserved in nature.

The most popular probe for this search is $0\nu\beta\beta$, a process that was hypothesized by W. Furry in 1931 [27]. $0\nu\beta\beta$ is based on standard beta decay, which is the well-known process given in Eq. 2.23, i.e., a neutron (usually inside a nucleus) decays to a proton, an electron and an electron antineutrino. This process is lepton number conserving since the electron carries a lepton number of 1 and the electron antineutrino has lepton number -1 while both the proton and the neutron do not carry any lepton number.

For some isotopes, single beta decay does not happen due to energetic restrictions. The decay can only happen if the atomic mass of the final nucleus is smaller than the mass of the initial nucleus. Nuclei for which both the number of neutrons N and the atomic number Z are even (even-even nuclei) are bound in a stronger way than the ones with both these numbers being odd (odd-odd nuclei) due to the nuclear pairing force. This leads to cases where single beta decay is energetically forbidden for a certain isotope while double beta decay is allowed. An example for this is shown in Fig. 2.5. The even-even nuclei are marked in green and the odd-odd ones in red. For example, ^{136}Xe is even-even and the isotope that it would decay to via standard beta decay (^{136}Ce) has a higher atomic mass than ^{136}Xe. Therefore, the standard beta decay is forbidden for this isotope. Decay to ^{136}Ba via double beta decay, on the other hand, is not forbidden. This double beta decay is marked with a blue arrow in the Fig. 2.5. In nature, 35 nuclides are known where double beta decay is energetically favored. These are potential probes for double beta decay for both the $2\nu\beta\beta$ mode that is allowed in the SM and also for the $0\nu\beta\beta$ mode. [118]

A Feynman diagram for $0\nu\beta\beta$ mediated by the so-called light-neutrino exchange mechanism (LνEM) is shown in Fig. 2.6. This one is the most commonly shown mechanism for $0\nu\beta\beta$ and it is mediated by a Majorana mass insertion for the neutrino. However, as we will discuss later in Sec. 2.4.1, even if the $0\nu\beta\beta$ potentially found in experiment is mediated by different new physics, it would directly imply that neutrinos have a Majorana neutrino mass. In $0\nu\beta\beta$ as shown in Fig. 2.7, two neutrons decay to two protons and two electrons:

$$2n \rightarrow 2p + 2e^- \,. \tag{2.35}$$

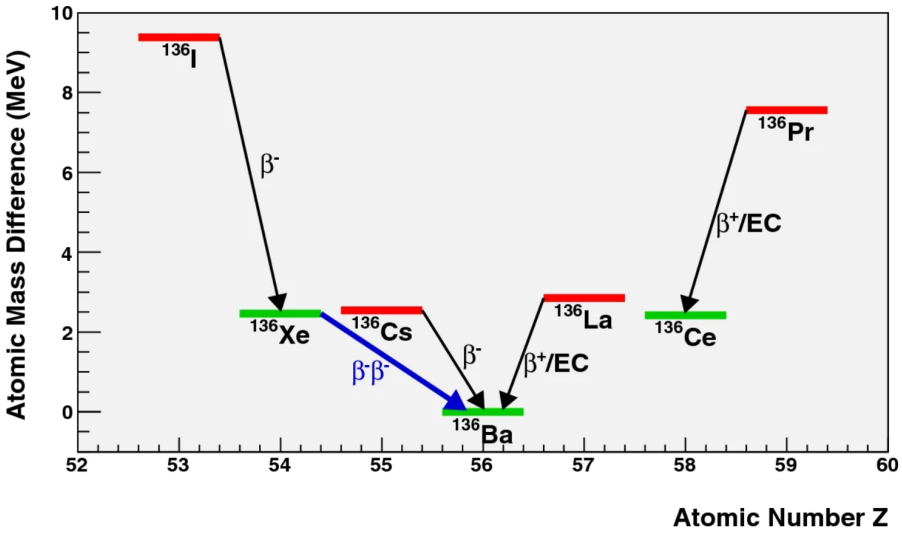

Figure 2.5: Atomic masses for different isotopes with the atomic mass number $A = 136$. All atomic masses are given as differences from the mass of the most bound isotope (^{136}Ba). The isotopes marked in green are even-even and the ones in red are odd-odd nuclei and the arrows mark the different types of decay that are possible, namely beta$^-$ decay (β^-), beta$^+$ decay (β^+), double beta decay ($\beta^-\beta^-$) and electron capture transitions (EC). Figure taken from Ref. [118] (licensed under CC BY).

This is twice the standard beta decay denoted in Eq. 2.23 without the final state antineutrinos and therefore lepton number is not conserved (the lepton number of the initial state is zero while the lepton number of the final state is two). The two neutrinos that come out of the two beta decays annihilate via the Majorana neutrino mass. In Fig. 2.6, the mass insertion is indicated with a cross. Moreover, the figure shows the standard Fermi interaction mediated by the W^- boson. In general, this interaction could also be mediated by new physics.

The standard scenario - if $0\nu\beta\beta$ is ever found - would be that the decay is mediated by Majorana neutrinos. However, this does not have to be the case. There might be other LNV new physics that mediates $0\nu\beta\beta$. While it is possible that this other LNV new physics is negligible, it is also possible that it represents the main contribution that mediates $0\nu\beta\beta$. Even if the latter one is the case, the detection of $0\nu\beta\beta$ still leads to the conclusion that a Majorana neutrino mass exists. This is explained by the so-called Schechter-Valle theorem. [119]

2.4.1 The Schechter-Valle theorem

In 1982, J. Schechter and J. W. F. Valle argued that the observation of $0\nu\beta\beta$ would automatically imply that a Majorana mass term exists for neutrinos [28]. This is the so-called Schechter-Valle or black box theorem. The relevant process (shown in Fig. 2 of the original paper by Schechter and Valle [28] in a similar way) is depicted in Fig. 2.7. The diagram contains a black box that represents the new physics that mediates $0\nu\beta\beta$. For example, the standard $0\nu\beta\beta$ process mediated by the LνEM in Fig. 2.6 can be inserted into the black box and thus mediate the process. As

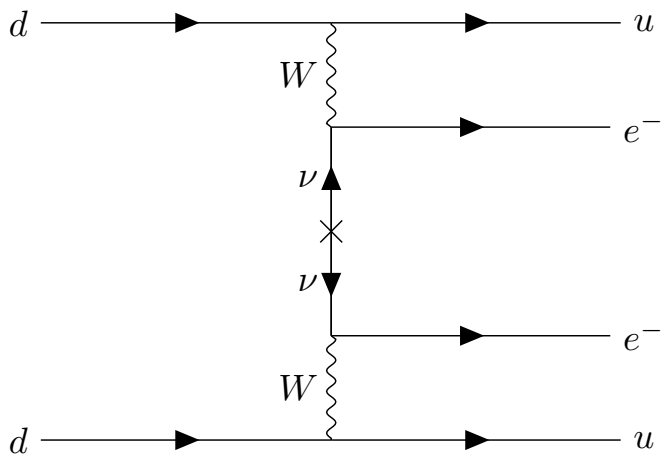

Figure 2.6: The Feynman diagram for neutrinoless double beta decay mediated by the light-neutrino exchange mechanism. Here, we show the standard Fermi interaction via the W^- boson. Additionally, the Majorana mass insertion for the neutrino is indicated with a cross.

already discussed, there could be other LNV new physics contributions mediating $0\nu\beta\beta$. This new physics can also be the mediator that goes into the black box as long as both the incoming and the outgoing particles are the same as in Fig. 2.6. Overall, the process can change an antineutrino into a neutrino and vice versa. Since no other external particles contribute to the process, this violates lepton number by two units and it generates a Majorana mass for the neutrino. The Schechter-Valle theorem leads to a bidirectional logic: If $0\nu\beta\beta$ exists, it implies that the neutrinos have a Majorana mass at least via the diagram given in Fig. 2.7; on the other hand, if neutrinos have a Majorana mass, it automatically means that $0\nu\beta\beta$ exists - at least mediated by the LνEM shown in Fig. 2.6 [120]. A bit after Schechter and Valle published their version, E. Takasugi published another paper that comes to the conclusion that - if $0\nu\beta\beta$ is found - the electron neutrino has a Majorana mass [121]. He was writing in response to another paper [122] that claimed that $0\nu\beta\beta$ can also occur for neutrinos that only have a Dirac mass. Takasugi showed that this is wrong in a more mathematical way.

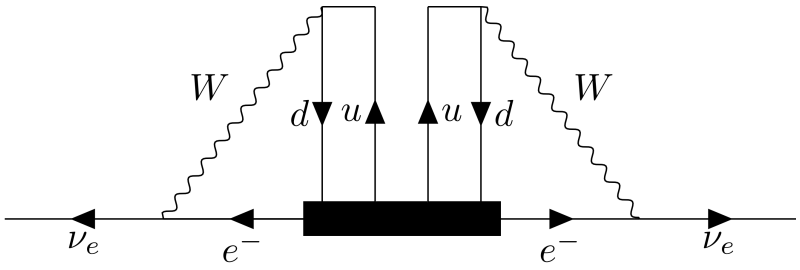

Figure 2.7: The process that generates a Majorana neutrino mass in case neutrinoless double beta decay is a process that takes place in nature. Here, the black box represents the new physics that generates neutrinoless double beta decay. Diagram similar to Fig. 9 in Ref. [120].

Qualitatively, it is well established that the Schechter-Valle theorem is true. However, the theorem only states that a Majorana neutrino mass exists (given that a $0\nu\beta\beta$ signal is found). It does not determine the absolute scale of said Majorana mass. A quantitative analysis was performed in Ref. [123]. The authors estimated the masses generated by the four-loop diagram shown in Fig. 2.7 and they find that these masses are smaller than the neutrino masses observed in experiment by many orders of magnitude. In their calculation of the correction, they consider effective point-like operators that could mediate $0\nu\beta\beta$, which are then plugged into the black rectangle in Fig. 2.7. In Ref. [123], they perform this calculation for two such operators. For one of the operators, they find a contribution to the Majorana neutrino mass of 5×10^{-28} eV and for the other one they even find that it does not contribute to the neutrino Majorana mass at all at the leading, i.e., four-loop, order in perturbation theory. Thus, the actual contribution to the neutrino Majorana mass is most likely even more suppressed. These contributions are too small to explain the neutrino masses that have been observed so far. The authors conclude that other leading contributions to the neutrino mass need to exist and that it would be misleading to translate an observed rate of $0\nu\beta\beta$ into neutrino masses.

2.4.2 Calculating the half-life

Later on, in Ch. 5, the half-life of different $0\nu\beta\beta$ processes will be an important quantity. Therefore, we will describe how the half-life is calculated and discuss the different constituents in detail. However, in order to not lengthen the discussion of the basics unnecessarily, we will not give a detailed derivation here. The interested reader is referred to Ch. 8 of Ref. [34] and to Part 2 of Ref. [124] for a more detailed calculation. We will focus on the standard mechanism, where the LNV physics mediating $0\nu\beta\beta$ is the exchange of the light Majorana neutrino as shown in Fig. 2.6. Without going into too much detail, it can be seen that the amplitude will be proportional to the following quantity for the LνEM:

$$\mathcal{A}_{L\nu EM} \propto \sum_i U_{ei}^2 P_L \frac{\not{q} + m_i}{q^2 - m_i^2} P_L \,. \tag{2.36}$$

Here, U_{ei} is a component of the PMNS matrix (see Eqs. 2.5 and 2.6), $\not{q} = q^\mu \gamma_\mu$ and q is the momentum of the internal neutrino. Moreover, $P_L = (1 - \gamma_5)/2$. Since $P_L \not{q} P_L = 0$, this simplifies to

$$\mathcal{A}_{L\nu EM} \propto \sum_i U_{ei}^2 \frac{m_i}{q^2} P_L \,, \tag{2.37}$$

where we also assumed that the neutrino mass is small compared to the momentum ($m_i \ll q$). Here, we can already identify one important constituent of the half-life formula. It is the effective electron neutrino Majorana mass $\langle m_{ee} \rangle$. This one reads [125]

$$\langle m_{ee} \rangle = \sum_j U_{ej}^2 m_j \,, \tag{2.38}$$

where the sum runs over all light neutrino mass eigenstates j that couple to the SM W-boson and the electron and the m_j are the neutrino masses.

The full expression for the decay rate can be given as

$$\Gamma^{0\nu\beta\beta} = G^{0\nu\beta\beta}(Q, Z)|\mathcal{M}^{0\nu\beta\beta}|^2 \frac{\langle m_{ee}\rangle^2}{m_e^2} \,. \tag{2.39}$$

Besides $\langle m_{ee}\rangle$ and the electron mass m_e there are two other factors. $G^{0\nu\beta\beta}(Q, Z)$ is the phase space factor (PSF), which depends on the atomic number Z and on the Q-value of the decay (denoted by Q). The Q-value is the energy that is released or absorbed during the reaction

$$Q = M_i - M_f \,, \tag{2.40}$$

where M_i is the mass of the atom before the decay and M_f is its mass after the decay. For the decay to occur in nature, the Q-value needs to be positive. Moreover, $\mathcal{M}^{0\nu\beta\beta}$ is the nuclear matrix element (NME). Usually, such NMEs are of order one ($\mathcal{O}(1)$) and, just like the value of the PSF, they depend on the isotope the $0\nu\beta\beta$ is happening in. The electron mass m_e is there for dimensional reasons. Sometimes it is included into the PSF $G^{0\nu\beta\beta}(Q, Z)$. [119]

The half-life is the inverse of the decay rate:

$$T^{1/2}_{0\nu\beta\beta} = \frac{\log(2)}{\Gamma^{0\nu\beta\beta}} \,. \tag{2.41}$$

Now we will discuss how the two leftover factors contributing to Eq. 2.39 can be calculated. Let us start with the NME $\mathcal{M}^{0\nu\beta\beta}$ that describes the nuclear physics aspects of the process. Calculating the NME is complicated and requires the knowledge of many body nuclear physics. Here, we will find the NME for the exchange of a light neutrino; for the project outlined in Ch. 5 we will need different ones. These are given later on in Sec. 5.2.2 for the free phase and in Sec. 5.2.4 for the condensate phase (with additional information given in Appendix C). For the LνEM, the NME can be written as [126]

$$\mathcal{M}^{0\nu\beta\beta} = \mathcal{M}^{0\nu\beta\beta}_{GT} - \frac{g_V^2}{g_A^2}\mathcal{M}^{0\nu\beta\beta}_{F} + \mathcal{M}^{0\nu\beta\beta}_{T} \,, \tag{2.42}$$

where $g_V = 1$ and $g_A \approx 1.27$. $\mathcal{M}^{0\nu\beta\beta}_{GT}$ is the so-called Gamow-Teller NME, $\mathcal{M}^{0\nu\beta\beta}_{F}$ is the Fermi NME and $\mathcal{M}^{0\nu\beta\beta}_{T}$ is the tensor NME. These three expressions are very similar. Their main difference is an operator that appears in the expressions. One way of denoting the three NMEs is [127]

$$\mathcal{M}^{0\nu\beta\beta}_{GT} = \sum_k (0^+_f || \sum_{mn} h_{GT}(r_{mn}, E_k)(\boldsymbol{\sigma}_m \cdot \boldsymbol{\sigma}_n)||0^+_i) \,, \tag{2.43a}$$

$$\mathcal{M}^{0\nu\beta\beta}_{F} = \sum_k (0^+_f || \sum_{mn} h_{F}(r_{mn}, E_k)||0^+_i) \,, \tag{2.43b}$$

$$\mathcal{M}^{0\nu\beta\beta}_{T} = \sum_k (0^+_f || \sum_{mn} h_{T}(r_{mn}, E_k) S^T_{mn}||0^+_i) \,, \tag{2.43c}$$

where the tensor operator S^T_{mn} is given by

$$S^T_{mn} = 3[(\boldsymbol{\sigma}_m \cdot \hat{\mathbf{r}}_{mn})(\boldsymbol{\sigma}_n \cdot \hat{\mathbf{r}}_{mn})] - \boldsymbol{\sigma}_m \cdot \boldsymbol{\sigma}_n \,. \tag{2.44}$$

Moreover, 0_i^+ is the initial ground state, 0_f^+ is the final one and the $\boldsymbol{\sigma}_i$ are the Pauli spin matrices. The $h_X(r_{mn}, E_k)$ are the neutrino potentials (for concrete expressions, see Ref. [127]), r_{mn} is the distance between the two neutrons that decay and $\hat{\mathbf{r}}_{mn} = \mathbf{r}_m - \mathbf{r}_n$. The summation over k runs over all states of the intermediate odd-odd nucleus and m and n are the labels of the two decaying neutrons. As mentioned before, calculating these NMEs is a complicated and tedious task. There are many different methods, which are used to find these NMEs. Later on, we will use NMEs that are calculated within the Interacting Boson Model-2 (IBM2) framework. Overall, the outcome vastly differs for NMEs calculated with different methods. The NME therefore usually contributes the most to the uncertainty that we get for the resulting half-life. [119, 126, 127]

The last factor that we want to discuss is the PSF $G^{0\nu\beta\beta}(Q, Z)$. This one is of huge importance for the second project discussed in this thesis. Because of that, there will be a detailed discussion in Ch. 5. Here, we will only discuss the basics. For the LνEM, the PSF is proportional to [124]

$$\begin{aligned} G^{0\nu\beta\beta}(Q, Z) \propto \int & F_0(Z, E_1) F_0(Z, E_2) E_1 E_2 p_1 p_2 \\ & \times \delta(E_1 + E_2 + M_f - M_i) dE_1 dE_2 d(\hat{\mathbf{p}}_1 \cdot \hat{\mathbf{p}}_2) \,, \end{aligned} \tag{2.45}$$

where [124]

$$F_0(Z, E) \approx 4 \left(\frac{|\Gamma(\gamma + iy)|}{\Gamma(2\gamma + 1)} \right)^2 (2pR)^{2(\gamma - 1)} \exp(\pi y) \tag{2.46}$$

is the Fermi function. In Eq. 2.45, E_1 and E_2 are the energies of the two final state electrons. Similarly, p_1 and p_2 are their momenta, which can be written in terms of the energies via the well-known relation

$$p_i = \sqrt{E_i^2 - m_e^2} \,. \tag{2.47}$$

Moreover, M_f is the mass of the nucleus after $0\nu\beta\beta$ and M_i is its mass before the decay. The δ thus ensures energy conservation and the $\hat{\mathbf{p}}_i$ are the normalized momentum vectors. Therefore, we can also rewrite $d(\hat{\mathbf{p}}_1 \cdot \hat{\mathbf{p}}_2)$ as

$$d(\hat{\mathbf{p}}_1 \cdot \hat{\mathbf{p}}_2) = d \cos\theta \,, \tag{2.48}$$

with θ being the angle in between the momenta of the two final state electrons. In Eq. 2.46, p is again the momentum, R is the nuclear radius and γ and y are defined as

$$\gamma = \sqrt{1 - (\alpha Z)^2} \quad \text{and} \quad y = \frac{\alpha Z E}{p} \,. \tag{2.49}$$

Here, α is the fine structure constant. Even though it is quite obvious, let us point out something that will be relevant later on. The PSF as given in Eq. 2.45 only depends on the final state particles. The initial state only enters through the mass of the nucleus before $0\nu\beta\beta$. [124]

Before we move on to the experimental measurements, let us briefly comment on a few approximations that are often used when the calculating the half-life. The first one is the closure approximation. This one is based on the observation that

the transfer of momentum between the two nucleons must be of the order of the inverse of an average spacing between the nucleons. This is about 100 MeV and it has to be carried by the virtual intermediate neutrino. Then it is possible to neglect the quantity $E_k - E_i$ that depends on the intermediate state energy E_k (E_i is the energy of the initial state) since it typically shows up in a denominator in the neutrino potentials $h_X(r_{mn}, E_k)$ alongside the energy of the intermediate virtual neutrino, which is much larger than the excitation energy of the intermediate state. Incorporating this approximation into the calculation avoids the explicit calculation of exited states of the intermediate nucleus in Eq. (2.43). The second common approximation is the long-wave approximation. Here, it is assumed that the two electrons that are involved in $0\nu\beta\beta$ are in the s-state. Moreover, small neutrino masses are sometimes neglected in parts of the calculation (i.e., when they are added to or subtracted from much larger quantities). Naturally, they cannot be neglected in $\langle m_{ee} \rangle$. Another approximation that is used fairly often is the impulse approximation for hadronic currents. [34, 124, 126]

2.4.3 Experimental measurements of the half-life

There are several experiments that have been trying to observe $0\nu\beta\beta$. However, until now it has not been found. Therefore, the main result experiments gave so far are lower limits on the half-life of $0\nu\beta\beta$. As discussed before, $0\nu\beta\beta$ can only be observed experimentally if usual beta decay is forbidden. Experiments make use of certain even-even nuclei like ^{76}Ge or ^{136}Xe that fulfill this condition. The relevant experimental signal is the energy of the two final state electrons combined. Using this observable, two modes have to be distinguished - the $0\nu\beta\beta$ mode and $2\nu\beta\beta$, which is allowed in the SM. $2\nu\beta\beta$ is an irreducible background. Fortunately, the energy spectrum of the final state electron looks different for the two modes. For $0\nu\beta\beta$, all the energy from the decay is carried away by the two final state electrons. Due to this, we expect that the kinetic energy of the two final state electrons is

$$T = E_1 + E_2 - 2m_e = Q \tag{2.50}$$

besides experimental uncertainties. On the other hand, the spectrum for the variable T for $2\nu\beta\beta$ is continuous since the final state neutrinos carry away a variable amount of energy. Hence, the experimental signal we would expect if $0\nu\beta\beta$ is observed is a peak at $T = Q$ in addition to the continuous spectrum from the two neutrino background. [119]

So far, $0\nu\beta\beta$ has not been observed, but $2\nu\beta\beta$ has been found in several isotopes. This is not surprising since $2\nu\beta\beta$ is allowed in the SM. The very first experiment that was designed to observe $2\nu\beta\beta$ in ^{124}Sn was performed in 1948 using Geiger counters [128, 129]. This first experiment found a lower limit on the half life of $2\nu\beta\beta$ of 3×10^{15} yr [129].

After this, the first well-known experiment searching for $0\nu\beta\beta$ is the Heidelberg-Moscow experiment, which was performed by a collaboration of the Max-Planck-Institut für Kernphysik in Heidelberg (Germany) and the Kurchatov Institute in Moscow (Russia). For their experiment, the collaboration used the isotope ^{76}Ge and the detector was located in the Gran Sasso underground laboratory in Italy,

operating five detectors, which were trying to find $0\nu\beta\beta$ in 19.2 kg of enriched germanium. The Gran Sasso underground laboratory was chosen due to its excellent shielding to keep the background low. From 1990 to 2003, the experiment took data. In 2001, part of the collaboration famously claimed that they had observed $0\nu\beta\beta$ at $\sim 4\sigma$ [130]. In the same publication, they claim that the best-fit value for the half-life of $0\nu\beta\beta$ is 1.5×10^{25} yr. Another analysis was performed later by a part of the collaboration that has a huge overlap with the authors of Ref. [130]. This analysis included the data taken until May 2003 and found a best-fit value of $T^{1/2}_{0\nu\beta\beta,^{76}\mathrm{Ge}} = 1.19 \times 10^{25}$ yr for the half-life of $0\nu\beta\beta$ in ^{76}Ge [131]. However, this was very controversial within the community; nowadays, there is a consensus that the Heidelberg-Moscow experiment did not find $0\nu\beta\beta$. For example, the authors of Ref. [132] come to the conclusion that there is no basis for such a claim. [131,133,134]

To resolve the controversy around this finding, the claim had to be tested in an experiment that uses the same isotope. An experiment that emerged in the following years that uses ^{76}Ge is the GERmanium Detector Array (GERDA). The detector was also located in Gran Sasso and it made use of material that was isotopically enriched in ^{76}Ge. The first phase of GERDA took place from November 2011 to September 2013 and collected 23.5 kg yr of exposure. After an upgrade, the second phase took data from December 2015 to November 2019. In 2020, the final results of GERDA were reported. GERDA did not find $0\nu\beta\beta$ and it set a lower limit on the $0\nu\beta\beta$ half-life for ^{76}Ge. This lower limit is

$$T^{1/2}_{0\nu\beta\beta,^{76}\mathrm{Ge}} > 1.8 \times 10^{26}\,\mathrm{yr} \tag{2.51}$$

at 90% confidence level. These findings contradict the claim that was made by part of the collaboration of the Heidelberg-Moscow experiment in Refs. [130, 131]. [135]

Besides these two, another early experiment searching for $0\nu\beta\beta$ in ^{136}Xe was the Enriched Xenon Observatory (EXO). The EXO-200 detector was operated in two phases, the first one taking place from September 2011 to February 2014 and the second one from May 2016 to December 2018. This experiment did not find statistically significant evidence for $0\nu\beta\beta$ either. The lower limit on the half-life that was found at 90% confidence level is

$$T^{1/2}_{0\nu\beta\beta,^{136}\mathrm{Xe}} > 3.5 \times 10^{25}\,\mathrm{yr}\,. \tag{2.52}$$

Please note that this one is for a different isotope than the half-life given in Eq. 2.51. A successor called next EXO (nEXO) is already planned. It is proposed as a ton-scale detector, which uses about 5000 kg of xenon enriched to 90% in the relevant isotope ^{136}Xe. It is expected that nEXO will be sensitive to a half-life of $\sim 10^{28}$ yr. [136,137]

Now let us move on to two current experiments. One experiment that also makes use of the isotope ^{136}Xe is the Kamioka Liquid Scintillator Antineutrino Detector (KamLAND) or, for double beta decay searches, KamLAND ZEro-Neutrino double-beta decay (KamLAND-Zen). The KamLAND detector already existed and now KamLAND-Zen uses the existing detector to study double beta decay. The experiment is located in the Kamioka mine in Gifu (Japan) and it makes use of Xe-loaded liquid scintillators. KamLAND-Zen is still running. However, intermediate results were published in 2022 [138] finding no $0\nu\beta\beta$ signal. Moreover, there was

a very recent publication by the KamLAND-Zen collaboration. Still, no $0\nu\beta\beta$ was found and their current lower limit for the half-life is [139]

$$T^{1/2}_{0\nu\beta\beta,^{136}\mathrm{Xe}} > 3.8 \times 10^{26}\,\mathrm{yr}\,. \tag{2.53}$$

This result is at 90% confidence level. [138, 140]

The second ongoing experiment we want to briefly mention here is the Cryogenic Underground Observatory for Rare Events (CUORE). CUORE uses ^{130}Te, an isotope none of the experiments mentioned so far uses. Like the Heidelberg-Moscow experiment and GERDA, CUORE is also located in the Gran Sasso underground laboratory. It started to take data in 2017. In 2022, the CUORE collaboration published the latest intermediate result. They did not find any evidence for $0\nu\beta\beta$ yet and set a lower bound on the half-life of

$$T^{1/2}_{0\nu\beta\beta,^{130}\mathrm{Te}} > 2.2 \times 10^{25}\,\mathrm{yr} \tag{2.54}$$

at 90% confidence level. [141]

Even though $0\nu\beta\beta$ has not been found yet, the precision of existing measurements is still very impressive and it might be found in ongoing or future experiments. In Ch. 5, we will consider the case that a $0\nu\beta\beta$ signal is detected in the future. While the Majorana neutrino mass can be extremely small even if $0\nu\beta\beta$ is found in experiment [123], it is generally thought that the detection of a $0\nu\beta\beta$ signal implies a non-zero Majorana neutrino mass. We introduce a BSM model, which describes a framework in which the detection of a $0\nu\beta\beta$ signal in experiment does not necessarily imply that there is a Majorana neutrino mass in the vacuum Lagrangian. This does not mean that the Schechter-Valle theorem is wrong, it just does not apply in our case.

3

Inferring astrophysical neutrino sources from the Glashow resonance

Neutrinos are an excellent probe for astrophysics, mostly because they rarely interact. As such, they can cover huge distances and even travel through planets without interaction. Therefore, they can arrive at research facilities on Earth without decaying or annihilating first, leaving us with rich information about objects that are very far away. Unfortunately, the fact that neutrinos interact so rarely also impedes the work of research facilities, which are aiming to detect neutrinos. Because of that, huge detection volumes and long observation times are needed to increase the chance of actually detecting neutrinos. A good example for this is the IceCube experiment, which we have described in detail in Sec. 2.3.3. Excitingly, IceCube observed a first GR candidate event in recent years [16]. In the work described in this chapter, we use this GR candidate event to infer the astrophysical neutrino source, i.e., we perform a likelihood analysis with the one GR candidate event that IceCube measured so far. The possibility to use the GR to distinguish different astrophysical neutrino sources has been foreseen already in Refs. [65, 142–157]. Here, we focus on the $\overline{\nu}_e$ fraction $f^{\mathrm{E}}_{\overline{\nu}_e}$ as it is defined in Eq. 2.30 since we know what value this variable should have on Earth for the different astrophysical neutrino sources. For a different approach to distinguish high-energy neutrino sources, see, e.g., Ref. [158]. There, the authors go beyond the assumption of a democratic flavor composition and consider the energy dependence of the flavor composition of neutrinos that come from astrophysical neutrino sources.

This chapter is structured as follows: In Sec. 3.1, we discuss what the GR is in detail. Next, we take a look at PeV energy events that have been measured in IceCube so far in Sec. 3.1.1. After that, we include two higher-order corrections

into the GR cross section, namely the Doppler broadening effect (Sec. 3.1.2) and the initial state radiation (ISR), which is described in Sec. 3.1.3. Next, in Sec. 3.2, we will introduce different flux models that will be used in our calculation later on. After that, we present the calculation itself in Sec. 3.3 and discuss its results in Sec. 3.4. To finish this chapter, we will outline some projections for the future and give an outlook in Sec. 3.5. The work presented in this chapter is based on Ref. [1].

3.1 The Glashow resonance and higher-order corrections of the cross section

As discussed in Sec. 2.2, different astrophysical neutrino sources lead to different ν:$\bar{\nu}$ ratios on Earth. Hence it would be beneficial to identify a process that can be measured in experiment and that can distinguish between neutrinos and antineutrinos. One process that fulfills these criteria is the so-called GR. While electron antineutrinos can induce such a process, electron neutrinos cannot. This is due to the fact that natural targets like ice or water contain electrons while positrons immediately annihilate with an electron if they enter the target. Therefore, the GR is a valuable probe to distinguish different astrophysical neutrino sources.

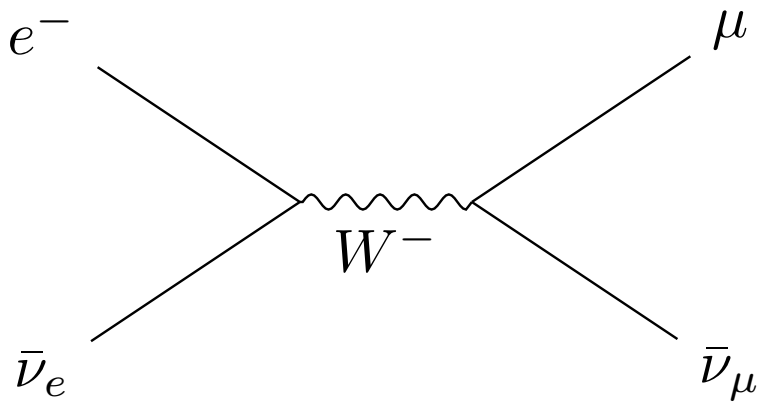

Figure 3.1: Glashow resonance process $\bar{\nu}_e + e^- \to W^- \to \bar{\nu}_\mu + \mu^-$ as predicted by Glashow in 1960 [18].

In 1960, Sheldon L. Glashow predicted resonant scattering of antineutrinos by electrons via an intermediary boson [18]:

$$\bar{\nu} + e^- \to W^- \to \bar{\nu} + \mu^- \,. \tag{3.1}$$

Back then, Glashow called the intermediary boson Z^-. Nowadays, the boson mediating this process is called the W^- boson. The process predicted by Glashow is shown in Fig. 3.1. In his original publication [18], Glashow also noted that the cross section for the process in Eq. 3.1 has the form of a typical resonance

$$\sigma_{\mathrm{GR}}^{\mathrm{orig}} = \sigma_0 \frac{E_0^2}{(E - E_0)^2 + \Gamma^2} \,, \tag{3.2}$$

where E_0 is the resonance energy, Γ is the width and σ_0 is an overall parameter. Since the cross section σ_{GR} is enhanced at the resonance energy, it is more likely to measure an event near the resonance energy in experiment.

In Eq. 3.1, Glashow only took one decay channel into account. In fact, for the W boson, the decay mode $W \to \bar{\nu}_\mu + \mu^-$ only accounts for 10.6 % of the decays. The dominating decay mode is the decay to hadrons with a branching ratio of 67.4 % [39]. In this thesis, we will use the following form for the GR cross section:

$$\sigma^{(0)}_{\mathrm{GR}}(s) = 24\pi\Gamma_W^2 \mathrm{Br}_{W^-\to\bar{\nu}_e e^-} \frac{s/M_W^2}{(s-M_W^2)^2 + \Gamma_W^2 M_W^2} \,. \tag{3.3}$$

Here, $\Gamma_W \approx 2.09\,\mathrm{GeV}$ is the total decay width of the W boson, $M_W \approx 80.433\,\mathrm{GeV}$ is its mass and $\mathrm{Br}_{W^-\to\bar{\nu}_e e^-} \approx 10.7\%$ is the branching ratio of the W^- decay channel $W^- \to \bar{\nu}_e e^-$ [39, 159]. The resonance energy reads [16]

$$E_R = \frac{M_W^2}{2m_e} \approx 6.32\,\mathrm{PeV} \,. \tag{3.4}$$

3.1.1 Measurement of events with PeV energy in IceCube

As discussed in Sec. 2.3.3, the measurement of UHE neutrinos has been successfully established in IceCube in recent years. For our analysis, we are particularly interested in events with an energy close to the the resonance energy given in Eq. 3.4. However, the other events at PeV energies - especially the events named "Bert", "Ernie" and "Big Bird" - are valuable for our analysis as well to fix both the shape and the normalization of the UHE neutrino flux.

In general, events measured in neutrino telescopes are divided into two different classes of events. An event can be a PeV energy partially contained event (PEPE). Here, the particle shower(s) are not fully contained in the fiducial volume of the detector. On the other hand, an event can also be a high energy starting event (HESE) for which the event - including the interaction vertex - is fully contained in the fiducial volume. Events that are contained in the HESE sample are excluded from the PEPE sample [160]. The three PeV events with an energy below 3 PeV have all been measured in the HESE sample [161].

On the 8th of December 2016, IceCube observed an event with an energy deposited in the detector of $E_{\mathrm{dep}} = 6.05 \pm 0.72\,\mathrm{PeV}$ in the PEPE sample [16]. An event with such a visible energy is consistent with a W boson at the resonance energy of the GR that decays to hadrons since it is expected that 5% of the energy is carried away by particles that do not emit Cherenkov radiation [16]. Therefore, we will refer to this event as the GR candidate event in the scope of this thesis. In the future, we expect that more such GR candidate events will be measured in IceCube-Gen2 and other neutrino telescopes, leaving us with better statistics for an analysis like the one presented in this chapter.

3.1.2 The Doppler broadening effect

With more events detected in current and future neutrino telescopes and hence better statistics, it becomes more and more important to have a detailed knowledge

of the cross section involved. For this, we will incorporate two subleading effects - the Doppler broadening (DB) effect and the ISR. Here, we will start with the DB. For this, we will follow the method given in [162]. The electrons in ice (or in water, for neutrino telescopes like, e.g., the Baikal Deep Underwater Neutrino Telescope that are installed in a lake or sea) are not exactly at rest, leading to a slightly different COM energy of the $\bar{\nu}_e$ - e^- system. In fact, a simple estimate shows that the electrons move with a velocity of the order $\mathcal{O}(\alpha c)$, α being the fine-structure constant and c being the speed of light. We can estimate that this will shift the square of the COM energy from $s = 2m_e E_{\bar{\nu}}$, with m_e being the mass of the electron and $E_{\bar{\nu}}$ the energy of the incoming $\bar{\nu}$, to

$$s \approx 2m_e E_{\bar{\nu}}(1 - \beta\cos(\theta))\,. \tag{3.5}$$

Here, β is the electron velocity and θ is the angle between the velocity of the electron and the velocity of the antineutrino. For a more detailed discussion, see Ref. [162]. Starting from the cross section given in Eq. 3.3, we can find the Doppler broadened cross section by replacing $E_{\bar{\nu}}$ by $E_{\bar{\nu}}(1 - \beta\cos(\theta))$:

$$\sigma_{\mathrm{DB}}(E_{\bar{\nu}}) = \frac{1}{4\pi}\int \mathrm{d}\phi \int \mathrm{d}\beta F(\beta) \int \mathrm{d}x' \sigma^{(0)}_{\mathrm{GR}}[E_{\bar{\nu}}(1 - \beta x')]\,. \tag{3.6}$$

$F(\beta)$ is the velocity distribution of the target electrons and ϕ is the azimuth angle. First, we perform the angular integration over x and ϕ. This yields

$$\sigma_{\mathrm{DB}}(E_{\bar{\nu}}) = \frac{6\pi\Gamma_W^2 \mathrm{Br}_{W^-\to\bar{\nu}_e e^-}}{M_W m_e E_{\bar{\nu}}} \int d\beta \frac{F(\beta)}{\beta} \left\{ \frac{1}{2M_W}\left[\ln(y_h^2+1) - \ln(y_l^2+1)\right] + \frac{1}{\Gamma_W}\left[\arctan(y_h) - \arctan(y_l)\right]\right\}, \tag{3.7}$$

where

$$y_h = \frac{2m_e E_{\bar{\nu}}(1+\beta) + m_e^2 - M_W^2}{\Gamma_W M_W} \quad \text{and} \quad y_l = \frac{2m_e E_{\bar{\nu}}(1-\beta) + m_e^2 - M_W^2}{\Gamma_W M_W}\,. \tag{3.8}$$

Next, we need to find the averaged electron velocity distribution for - in our case - ice. Details on how to find the electron velocity distribution for electrons in a given atom are given in Appendix A. For ice, we consider the standard water molecule (H_2O). We weigh the distribution functions by the amount of electrons each atom in the water molecule carries:

$$F_{\mathrm{ice}}(\beta) = \frac{2F_{\mathrm{H}}(\beta) + 8F_{\mathrm{O}}(\beta)}{10}\,. \tag{3.9}$$

Using this velocity distribution function, we can integrate over β in Eq. 3.7 and find the Doppler broadened cross section. The result is shown in Fig. 3.2. There, the black line depicts the cross section without taking any subleading effects into account (as given in Eq. 3.3) and the orange dashed line shows the one where DB has been included. It can be seen that the DB leads to a reduction of the maximum peak by about 12% while the width of the cross section is increased. When integrating the cross section over the initial antineutrino energy, the result is almost the same. However, if we consider an antineutrino spectrum that is not uniform, the DB will significantly alter results. Hence it is crucial to account for DB once experiments yield more statistics. [162]

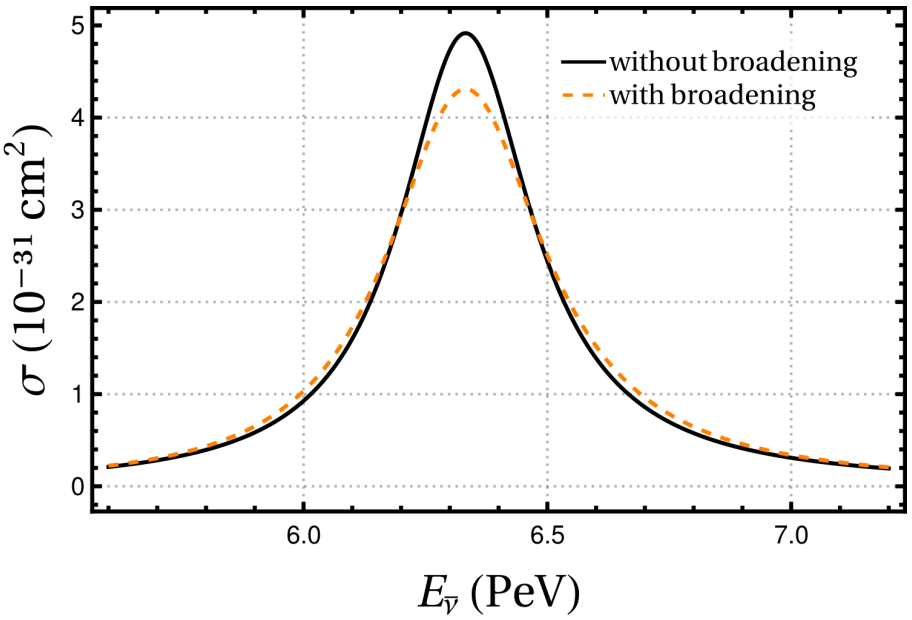

Figure 3.2: Glashow resonance cross section with (orange, dashed) and without (black) Doppler broadening. Figure also published in Ref. [1] (licensed under CC BY).

3.1.3 Photon radiation off the initial state electron

Another subleading effect that alters the cross section more substantially than the DB is the ISR, which is the emission of one or more photons from a charged particle in the initial state. For the process we consider here, the charged lepton is the electron in the initial state. The effect becomes more relevant with an increasing COM energy. Once the COM energy exceeds the mass of the initial charged lepton - in our case the electron - collinear emission of photon(s) from this lepton will alter the cross section in a significant way. For example, the ISR has been found to be relevant in the Large Electron-Positron Collider (LEP) for examining the Z boson peak. In 2005, collaborations of relevant experiments like LEP found that, for the Z boson peak, the effects the ISR has are more than two orders of magnitude larger than the experimental precision [163].

For the process considered in this thesis, radiation of one or more photons off the target electron (cf. Fig. 3.3) considerably changes the cross section. We use the structure function approach to include the ISR into our calculation. Then, the modified cross section reads [164]

$$\sigma(E_\nu) = \int \mathrm{d}x\, \Gamma_{e/e}(x, Q^2)\sigma^{(0)}_{\mathrm{GR}}(x, Q^2, E_\nu)\,. \tag{3.10}$$

Here, x is the longitudinal momentum fraction of the electron after the radiation of the photon, Q is the energy scale and, as before, the cross section $\sigma^{(0)}_{\mathrm{GR}}$ without subleading effects is given in Eq. 3.3. Moreover, $\Gamma_{e/e}$ is the structure function of the electron. In this work, we use the structure function given in Eq. 3.2 of Ref. [165]. It includes soft photons resummed to all orders and hard photons up to $\mathcal{O}(\alpha^3)$. The result is shown - among others - in Fig. 3.4, where the blue dashed line depicts the

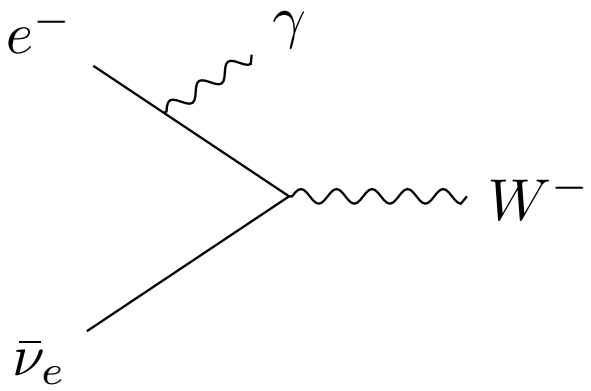

Figure 3.3: Initial state radiation from the process $\bar{\nu}_e + e^- \to W^-$. Here, a photon is emitted from the target electron.

cross section with ISR. There are two main features to this curve. First of all, the peak at the resonance energy is reduced by almost 20%. The second feature is the so-called radiative return. For energies above the resonance energy ($\approx 6.3\,\mathrm{PeV}$), the cross section is enhanced by more than a factor of two. This is due to the fact that energy is carried away by the emitted photon(s) and thus the W^- production can also be on-shell for $\sqrt{s} > M_W$.

In Fig. 3.4, we show the cross section without any subleading effects (black), the cross section with DB (orange, dashed), the one with ISR (blue, dashed) and also the one with both subleading effects combined (red), which is obtained using a convolution, alongside the charged current (CC) background (black, long dash) and the neutral current (NC) background (black, short dash). For better visibility, the cross sections are shown on a logarithmic scale. The cross section with both subleading effects combined exhibits a reduction of the peak at the resonance energy by about 30%. Moreover, the radiative return is clearly visible. Note that these effects may eventually be smeared out by the finite energy resolution of the detector in IceCube. The data points for the curve including both effects is published in the supplementary material of Ref. [1].

3.2 Flux models

Before we start with the actual calculation, let us briefly introduce the two models we will use to describe the neutrino flux. As mentioned in Sec. 2.2, we assume a democratic flavor composition of the neutrino flux on Earth (see Eq. 2.25). However, for our analysis we need the energy dependence of the overall neutrino flux. Here, we will use two rather simple flux models. The first one is the single power law flux model, which describes the neutrino flux as [166]

$$\frac{\mathrm{d}\Phi_{6\nu}}{\mathrm{d}E_\nu} = \Phi_0 \left(\frac{E_\nu}{100\ \mathrm{TeV}}\right)^{-\gamma} \times 10^{-18}\ \mathrm{GeV}^{-1}\mathrm{cm}^{-2}\mathrm{s}^{-1}\mathrm{sr}^{-1}\,, \tag{3.11}$$

where γ is the spectral index and $\Phi_{6\nu}$ is the neutrino flux including all three flavors and neutrinos and antineutrinos at an energy of 100 TeV.

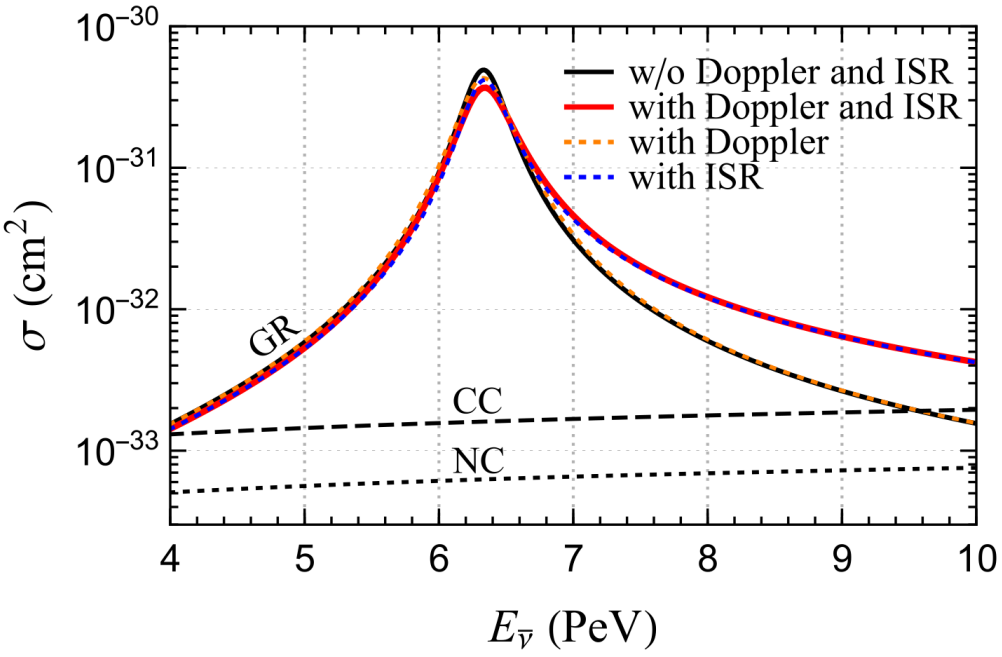

Figure 3.4: Glashow resonance cross section without any subleading effects (black), with Doppler broadening (orange, dashed), with initial state radiation (blue, dashed) and with both Doppler broadening and initial state radiation (red). Moreover, the charged (black, long dash) and neutral current (black, short dash) backgrounds are shown. For the Glashow resonance cross sections for which Doppler broadening was taken into account, we averaged over the electrons in H_2O for the target. Figure also published in Ref. [1] (licensed under CC BY).

For the second flux model considered in this thesis, we also incorporate the Hillas criterion [167]. This criterion states that there is a maximum energy an accelerated charged particle can reach and thus it imposes an energy cutoff onto our flux model. While neutrinos are not charged and thus they cannot undergo such an acceleration within an electromagnetic field, they are decay products of charged particles. Therefore, the maximum energy these charged particles can be accelerated to within an electromagnetic field around a typical source also affects the maximum energy of the neutrinos. For a charged particle in a magnetic field, the Larmor radius [168]

$$r_L = \left| \frac{m v_\perp}{qB} \right| \tag{3.12}$$

gives the radius of the circle a charged particle moves on in a magnetic field. Here, m is the mass and q the charge of the particle, $v_\perp$ is the velocity of the particle perpendicular to the magnetic field and B is the strength of the magnetic field. The Hillas criterion now exploits the fact that the region containing the field, where the particle is accelerated, has a finite size. For the particle to stay inside this region, the size of the region has to be bigger that $2r_L$. Since the Larmor radius increases with $v_\perp$ and thus also with the particle energy, the maximum energy of the accelerated particle is

$$E_{\max} \sim L q v_\perp B \,, \tag{3.13}$$

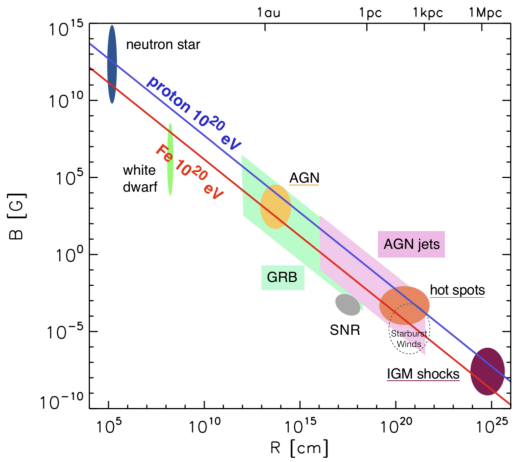

Figure 3.5: An example for a Hillas plot. Here, the energy of the charged particle is $10^{20}\,\mathrm{eV}$. The magnetic field B is then obtained by requiring the characteristic source size to be bigger than the Larmor radius. Shown are the limits for iron nuclei (red) and protons (blue) alongside astrophysical objects that could meet the requirements. Figure taken from Ref. [169] (licensed under CC BY).

where L is the size of the region. The two parameters that describe the source are the region size and the magnetic field. A common way to display this is a so-called Hillas plot. For a certain particle energy, the limits on region size and magnetic field are depicted. An example is shown in Fig. 3.5. [167, 170]

The easiest way to incorporate the energy cutoff is by adding an exponential damping factor to Eq. 3.11, yielding [166]

$$\frac{\mathrm{d}\Phi_{6\nu}}{\mathrm{d}E_\nu} = \Phi_0 \left(\frac{E_\nu}{100\ \mathrm{TeV}}\right)^{-\gamma} e^{-E_\nu/E_{\mathrm{cutoff}}} \times 10^{-18}\ \mathrm{GeV}^{-1}\mathrm{cm}^{-2}\mathrm{s}^{-1}\mathrm{sr}^{-1}\,, \tag{3.14}$$

where E_{cutoff} is another parameter of the flux model.

We want to emphasize that these two rather simplistic flux models were chosen due to the low statistics of GR candidate events available so far. In the future, when more such candidate events have been measured, one could also consider flux models that are more sophisticated than the single power law flux models we use here.

3.3 Outline of the calculation

To not deviate from the calculation too much, the basics on maximum likelihood theory including the Bayesian and the frequentist approach are given in Appendix B. The two flux models introduced in the previous section depend on two (for the single power law flux model) or three (with cutoff at high energies) parameters. Our next step will be to confine their values. As discussed in Sec. 3.1.1, the GR candidate event is the only UHE event measured in the PEPE sample and three such events have been measured in the HESE sample. Here, we use the HESE sample to fix the parameters. The data we use is taken from Ref. [171], where the IceCube collaboration has analyzed HESEs that were measured within a period of 7.5 years.

We apply energy cuts that we will integrate over for the PEPE sample for which the deposited energy E_{dep} is between 4 PeV and 10 PeV. The GR candidate event is so far the only event that was found in the PEPE sample within the energy cuts even though the effective volume for the PEPE sample is nearly twice as large as the one for the HESE sample. For this analysis, we assume again a democratic flavor composition. It would be reasonable to assume a completely free flavor ratio for a more thorough analysis. Nevertheless, the assumption we make here is an

approximation that is widely used in literature.

For the parameters γ and Φ_0, we construct the likelihood (based on Gaussian distributions) as follows:

$$-2\ln\mathcal{L}_{6\nu} = \frac{(\Phi_0 - \Phi_0^{\mathrm{bf}})^2}{\sigma(\Phi_0)^2} + \frac{(\gamma - \gamma^{\mathrm{bf}})^2}{\sigma(\gamma)^2}\,. \tag{3.15}$$

Both the best-fit values $\Phi_0^{\mathrm{bf}} = 6.37$ and $\gamma^{\mathrm{bf}} = 2.87$ and the values for the 1σ errors $\sigma(\Phi_0) = 1.54$ and $\sigma(\gamma) = 0.2$ are taken from Ref. [171]. For the 1σ errors, we averaged over the errors in the positive and negative direction from the best-fit values. This treatment is adequate since the errors in both directions are very similar for both parameters; also, they differ less than 10 % from the averaged value. For the cutoff model, we also need to derive the likelihood for E_{cutoff}. As before, this is also derived from the HESE sample utilizing Fig. VI.9 of Ref. [171]. For the parameters, we have ignored any correlations between γ, Φ_0 and E_{cutoff} since these are not given in Ref. [171].

Now that we know the priors for all the parameters, the next step is to fit $f^E_{\overline{\nu}_e}$ to PEPE, i.e., we need to find the likelihood $\mathcal{L}_{\overline{\nu}_e}(f^E_{\overline{\nu}_e})$ with the GR candidate event measured so far. Once this is known, the total likelihood can be determined as

$$\mathcal{L}_{\mathrm{tot}} = \mathcal{L}_{6\nu} \times \mathcal{L}_{\overline{\nu}_e}\,. \tag{3.16}$$

The likelihood $\mathcal{L}_{\overline{\nu}_e}$ is calculated as

$$\mathcal{L}_{\overline{\nu}_e} = \prod_{i=1}^{n} \left[\mu_{\mathrm{DIS}} P_{\mathrm{DIS}}(\#i|\Theta) + \mu_{\mathrm{GR}} P_{\mathrm{GR}}(\#i|\Theta)\right] \times \frac{1}{n!} \mathrm{e}^{-(\mu_{\mathrm{DIS}}+\mu_{\mathrm{GR}})}\,, \tag{3.17}$$

with μ_{GR} and μ_{DIS} being the expected event numbers for the GR and for the deep inelastic scattering (DIS) within the energy interval $E_{\mathrm{dep}} \in [4, 10]$ PeV. Here, E_{dep} is the energy deposited in the detector when an event is detected and $\#i$ runs over all GR candidate events. Since so far only one of these was measured, $n = 1$ in this thesis. μ_{GR} and μ_{DIS} are the expected event numbers for GR candidate and DIS events. Lastly, for a given model parameter set Θ, $P_{\mathrm{DIS/GR}}(\#i|\Theta)$ are the normalized probabilities for measuring an event at the energy at which event $\#i$ was measured.

Our next task is to find the expected event numbers μ_{GR} and μ_{DIS} by integrating cross sections and flux with the detector configuration. Following Ref. [172], we can find the differential event distribution as a function of the deposited energy

$$\frac{\mathrm{d}N^r_{\overline{\nu}_\alpha}}{\mathrm{d}E_{\mathrm{dep}}} = T_{\mathrm{IC}} \cdot N_{\mathrm{A}} \int_{E_{\mathrm{min}}}^{\infty} \mathrm{d}E_\nu \frac{\mathrm{d}\Phi^{\mathrm{IC}}_{\overline{\nu}_\alpha}}{\mathrm{d}E_\nu} \int_0^1 \mathrm{d}y \frac{\mathrm{d}\sigma^r_{\overline{\nu}_\alpha}(E_\nu)}{\mathrm{d}y} \frac{\mathrm{d}P(E_{\mathrm{sh}})}{\mathrm{d}E_{\mathrm{dep}}} M_{\mathrm{eff}}(E_{\mathrm{sh}}) \tag{3.18}$$

for the different reaction types r (GR, DIS-CC, DIS-NC). Here, T_{IC} is the collection time of IceCube, N_{A} is the Avogadro constant and $\mathrm{d}\Phi^{\mathrm{IC}}_{\overline{\nu}_\alpha}/\mathrm{d}E_\nu$ is the $\overline{\nu}_\alpha$ flux integrated over the direction of the incoming (anti-)neutrinos. We average the cross section over the number of nucleons. E_{sh} is the energy of the charged final state particles that initiate the shower and M_{eff} is the effective target mass of IceCube for HESE or PEPE. y denotes the energy fraction that is carried by one of the two final state fermions. It is an integration variable that is integrated from 0 to 1, i.e., from all

the energy being carried by one of the fermions to all of it being carried by the other one. The second integration variable is the neutrino energy E_ν, which is integrated from E_{min} to infinity. Here, we set the lower bound E_{min} to 1 PeV.

Before we can find the expected event numbers by performing the integrals in Eq. 3.18, we need to find its constituents.

- Let us start with T_{IC}, the collection time of IceCube. In their analysis given in Ref. [16], the IceCube collaboration analyzed data that was taken from May 2012 to May 2017 with a total live-time of

$$T_{\text{IC}} = 4.6\,\text{yr}. \tag{3.19}$$

- The well-known Avogadro constant is

$$N_{\text{A}} \approx 6.022 \cdot 10^{23}\,. \tag{3.20}$$

- For the flux $\mathrm{d}\Phi^{\text{IC}}_{\overline{\nu}_\alpha}/\mathrm{d}E_\nu$, we take either the single power law flux model given in Eq. 3.11 or the one including a cutoff (Eq. 3.14), assuming a democratic flavor composition and integrating over the directions where the (anti-)neutrinos come from. The neutrino flux that arrives at IceCube is calculated numerically. Here, we made use of the Preliminary Reference Earth Model [173] to model the density profile of Earth. We did not take uncertainties into account.

- Next, we need to find the contribution from the cross section $\mathrm{d}\sigma^r_{\overline{\nu}_\alpha}(E_\nu)/\mathrm{d}y$. Naturally, this looks rather different for the three reaction types. Let us start with the GR cross section. This one we already found in Ch. 3.1, where we introduced the cross section without any higher-order corrections in Eq. 3.3. Afterwards, we took corrections from ISR and the Doppler broadening effect into account. Note that for this one we do not need to integrate over y since we found the cross section and not its derivative. For the CC and NC interactions, we calculate the cross sections with the help of parton distribution functions (cf. Refs. [174,175]). For this, we used the CT18 parton distribution files [176] and read them with ManeParse [177].

- $\mathrm{d}P(E_{\text{sh}})/\mathrm{d}E_{\text{dep}}$ is the derivative of the probability for the energy of the charged final state particles that initiate the shower to be E_{sh} with respect to the deposited energy E_{dep}. Why do we even need this? When the shower develops, neutral particles carry away a bit of energy. These particles are not detected by the detector. Therefore, the deposited energy E_{dep} is generally smaller than E_{sh}. In this work, we follow Appendix A of Ref. [178] and model the probability as a Gaussian distribution:

$$\frac{\mathrm{d}P(E_{\text{sh}})}{\mathrm{d}E_{\text{dep}}} = N \exp\left[-\frac{(E_{\text{dep}} - rE_{\text{sh}})^2}{2(E_{\text{sh}}\Delta)^2}\right] \Theta(E_{\text{sh}} - E_{\text{dep}})\,. \tag{3.21}$$

  Here, N is the normalization factor and we use $r = 0.95$ and $\Delta = 0.06$. $\Theta(x)$ is the Heaviside step function.

- The last constituent that we need to find is the effective target mass $M_{\text{eff}}(E_{\text{sh}})$. For the HESE sample, it is available in Fig. 7 of Ref. [75]. For the PEPE sample, we extract the ratio between the HESE and PEPE sample from the Monte-Carlo results for the effective area in Fig. 7a of Ref. [160], which is reproduced in Fig. 3.6.

After finding all these, we can now calculate $\mathrm{d}N^{r}_{\overline{\nu}_\alpha}/\mathrm{d}E_{\text{dep}}$ for all three interaction types. However, there is one exception: For ν_τ CC interactions, Eq. 3.18 does not hold. The reason is that it produces an outgoing tau, which decays hadronically or leptonically. For this, we need to consider the distribution of the energy over the visible decay products. For example, an event induced by a ν_τ at the GR energy can lead to a double-cascade signature [179, 180]. This is then clearly distinguishable from the cascade we would expect from a ν_e event.

The next step is to calculate the expected event numbers μ_{GR} and μ_{DIS}. With the differential distributions in Eq. 3.18, we can calculate μ_{GR} as

$$\mu_{\text{GR}} = \int_{\text{cut}} \mathrm{d}E_{\text{dep}} \cdot \left(\frac{\mathrm{d}N^{\text{GR},jj}_{\overline{\nu}_e}}{\mathrm{d}E_{\text{dep}}} + \frac{\mathrm{d}N^{\text{GR},e\nu}_{\overline{\nu}_e}}{\mathrm{d}E_{\text{dep}}} \right) \tag{3.22}$$

and μ_{DIS} as

$$\mu_{\text{DIS}} = \int_{\text{cut}} \mathrm{d}E_{\text{dep}} \cdot \left(\frac{\mathrm{d}N^{\text{CC}}_{\nu_e+\overline{\nu}_e}}{\mathrm{d}E_{\text{dep}}} + \sum_\alpha \frac{\mathrm{d}N^{\text{NC}}_{\nu_\alpha+\overline{\nu}_\alpha}}{\mathrm{d}E_{\text{dep}}} \right) . \tag{3.23}$$

As mentioned before, the energy regime we integrate over is $E_{\text{dep}} \in [4, 10]$ PeV. For μ_{DIS}, we take both the CC and the NC interactions into account. Please note that for the NC interactions we take incoming neutrinos of all flavors into account while for the CC one electron (anti-)neutrinos are the relevant ones. On the other hand, for the GR interactions only incoming electron antineutrinos are relevant.

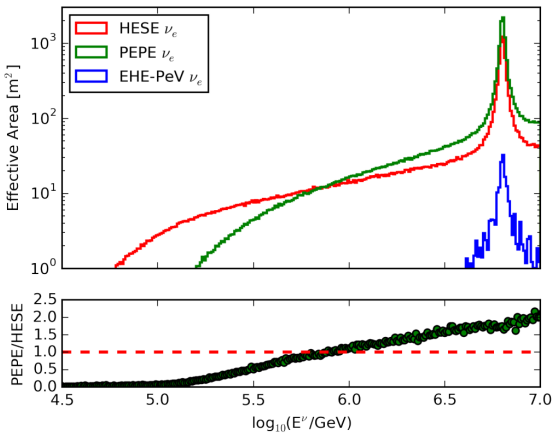

Figure 3.6: Effective area for electron (anti-)neutrinos for the different samples of events. Figure taken from Ref. [160] (licensed under CC BY-NC-ND).

Now we know how to find the expected event numbers for both the GR and for DIS. However, we are not done yet. Looking at Eq. 3.17, we still need to find $P_{\text{DIS}}(\#i|\Theta)$. It can be found from two known quantities with a convolution over E_{dep}:

$$P_{\text{DIS/GR}}(\#i|\Theta) = \int \mathrm{d}E_{\text{dep}} P(\#i|E_{\text{dep}}) f_{\text{DIS/GR}}(E_{\text{dep}}|\Theta) \, . \tag{3.24}$$

For an event $\#i$, the deposited energy is distributed over a range with the probability function $P(\#i|E_{\text{dep}})$ since the energy resolution of the detector is limited. For now,

since only one GR candidate event has been detected so far, we only need this probability for this specific event. Fortunately, for this event a posterior probability density of the deposited energy is available in Fig. 3a of Ref. [16]. We use this in our calculation. $f_{\mathrm{DIS/GR}}$ is the probability density function (PDF), which is normalized within the energy cuts. This one can be inferred from Eq. 3.18 when the expression is normalized.

With the prerequisites sorted out, we can now do the likelihood analysis using both the Bayesian and the frequentist approach. For both, the starting point is the likelihood function $\mathcal{L}_{\mathrm{tot}}$ (see Eq. 3.16), which we compute using the framework given above. This likelihood is then a function of the parameters Φ_0, γ and $f^{\mathrm{E}}_{\overline{\nu}_e}$ for the single power law flux model. In the case of the flux model with an energy cutoff, E_{cutoff} is another parameter. For the frequentist interpretation, the maximum of the likelihood $\mathcal{L}^{\mathrm{max}}_{\mathrm{tot}}(f^{\mathrm{E}}_{\overline{\nu}_e})$ is obtained by marginalizing over the other two or three parameters. On the other hand, for the Bayesian interpretation, we need to choose priors for the parameters. In this work, we choose flat priors for Φ_0, γ, $f^{\mathrm{E}}_{\overline{\nu}_e}$ and $\ln E_{\mathrm{cutoff}}$. With these, we can also derive the posterior distribution for E_{cutoff}.

3.4 Results

The main results of the calculation outlined in the previous section are shown in Fig. 3.7. The frequentist interpretation gives the likelihood function, which is shown in blue, and the Bayesian interpretation yields the posterior distribution, which is shown in brown. Both of these use the IceCube 4.6 year data sample. To constrain $f^{\mathrm{E}}_{\overline{\nu}_e}$, we included uncertainties of the neutrino flux parameters and marginalized over these. Fig. 3.7 is divided into two panels. The upper one shows the results we get for the single power law flux model without a cutoff at high energies and for the lower one we did incorporate an energy cutoff [171]. We also marked a few relevant values of $f^{\mathrm{E}}_{\overline{\nu}_e}$ with vertical dashed lines. Three of these vertical lines mark expected values of $f^{\mathrm{E}}_{\overline{\nu}_e}$ for ideal sources: $f^{\mathrm{E}}_{\overline{\nu}_e} \approx 0$ for the ideal μ-damped pγ source, $f^{\mathrm{E}}_{\overline{\nu}_e} \approx 0.23$ for the ideal pγ source and $f^{\mathrm{E}}_{\overline{\nu}_e} \approx 0.5$ for the ideal pp source. Moreover, as discussed in Sec. 2.2.4, it is not enough to just consider ideal sources since multi-pion processes become relevant at higher energies. Therefore, we also consider a pγ source where an equal mixture of single- and multi-pion production contributes at the source. The expected $\overline{\nu}_e$ fraction for this case is $f^{\mathrm{E}}_{\overline{\nu}_e} \approx 0.36$ and we also marked it with a vertical dashed line.

For the blue likelihood curves from the frequentist analysis, we show horizontal lines at $\exp(-1/2)$ and $\exp(-4/2)$ as blue dotted lines. The points where these intersect with the likelihood curves, $-2\ln\mathcal{L} = 1$ or, respectively, $-2\ln\mathcal{L} = 4$, roughly mark the 1σ and 2σ confidence levels. In the case of the Bayesian analysis, the 1σ and 2σ credible intervals have been marked from dark to light shades of brown. So what can we learn from this? The strongest claim we can make is that, for all cases, the ideal μ-damped pγ source ($f^{\mathrm{E}}_{\overline{\nu}_e} \approx 0$) can be excluded at around 2σ. Out of the other ideal sources (i.e., the ideal pp and pγ source), the ideal pp source is favored. However, this is a very weak preference and the ideal pγ source cannot

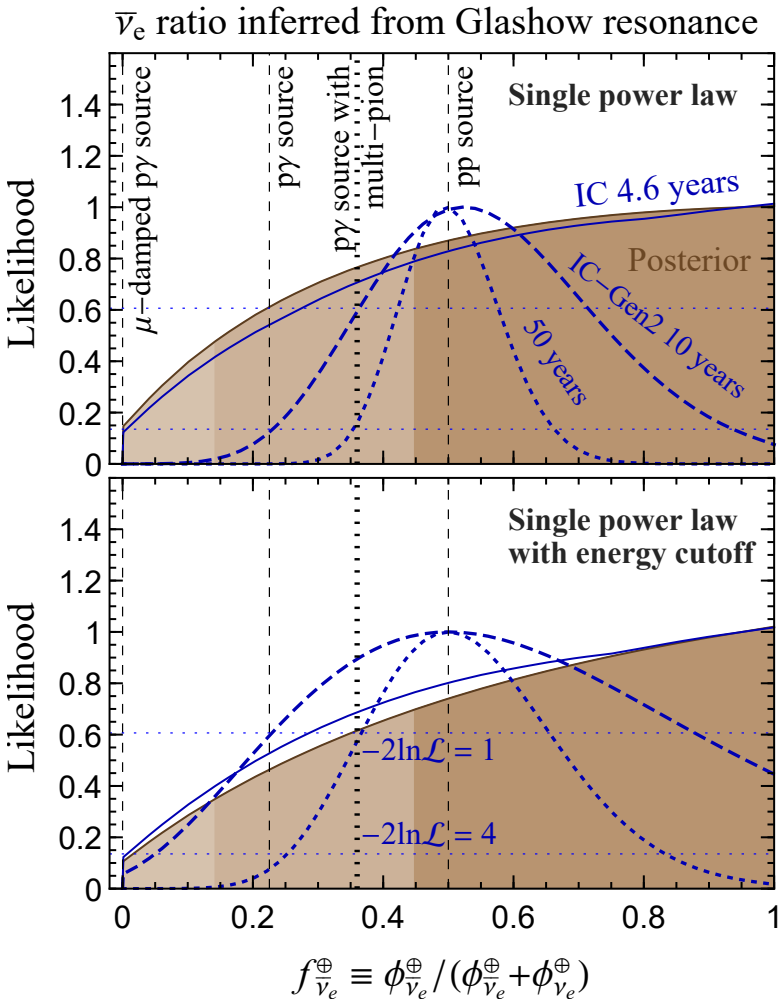

Figure 3.7: Results for both the Bayesian and the frequentist interpretation. In blue, the likelihood from the frequentist interpretation is shown while the posterior obtained with the Bayesian interpretation is shown in brown. Both infer the $\overline{\nu}_e$ fraction $f^{\mathrm{E}}_{\overline{\nu}_e}$ from the Glashow resonance candidate event detected by IceCube in 4.6 yr of taking data. For the upper plot, we assumed a single power law flux model with central values and uncertainties as given in Ref. [171] for the neutrino flux. The lower plot is using the same flux just with an additional energy cutoff at high neutrino energies. The expected $f^{\mathrm{E}}_{\overline{\nu}_e}$ are shown as vertical dashed lines for three neutrino source models, namely the ideal μ-damped pγ ($f^{\mathrm{E}}_{\overline{\nu}_e} \approx 0$), the ideal p$\gamma$ ($f^{\mathrm{E}}_{\overline{\nu}_e} \approx 0.23$) and the ideal pp ($f^{\mathrm{E}}_{\overline{\nu}_e} \approx 0.5$) source. To account for the fact that, in nature, neutrino sources are not ideal, we also show an example that deviates from these ideal models. For the pγ source, we find an expected value of $f^{\mathrm{E}}_{\overline{\nu}_e} \approx 0.36$ when assuming an equal mixture of single- and multi-pion production at the source. This is also shown in the plot. Besides the results for the measurements obtained so far, projections for future sensitivities of IceCube-Gen2 with effective exposures of ten and fifty years are shown as the two blue dashed lines. For these projections, we assumed that the pp source is dominant and for the flux parameters we took $\Phi_0 = 6.37$, $\gamma = 2.7$ and $E_{\mathrm{cutoff}} = 5$ PeV. Also published in Ref. [1] (licensed under CC BY).

be excluded (only at around 1σ). For the pγ source with single- and multi-pion production included, we can say less since the $\overline{\nu}_e$ fraction for this one is closer to the ideal pp source. Also, keep in mind that the 1:1 mixture of single- and multi-pion production is just an assumption. For high energies, the multi-pion production might be more dominant and thus the value of $f^{\mathrm{E}}_{\overline{\nu}_e}$ for the pγ source with the single- and multi-pion production mechanisms mixed could be even closer to the one of the ideal pp source for these sources. In the case of multi-pion production, more information would thus be required, e.g., from multi-wavelength observations of the source in question such that we can distinguish between the different sources. Please note that, while multi-pion production shifts the $\overline{\nu}_e$ fraction $f^{\mathrm{E}}_{\overline{\nu}_e}$ to higher values for the pγ source, the same is not true for the pp source.

While we cannot make strong claims with the one GR candidate event measured so far, there are promising experiments that will measure more such events in the future. A thorough analysis and discussion is given in Sec. 3.5.

Before we move on to projections for the future, let us have a quick look at what we can learn about another parameter. When assuming the single power law neutrino flux with energy cutoff, the GR candidate event can be used to constrain the cutoff energy E_{cutoff}. An analysis without the GR candidate event gave a value of about 5 GeV for E_{cutoff} [171]. In the same reference, the lower boundary was found to be at about 0.5 PeV at 2σ. With the GR candidate event, the lower boundary at 2σ is significantly higher (at 2.2 PeV). A plot of the two log-likelihood functions is shown in Fig. 3.8.

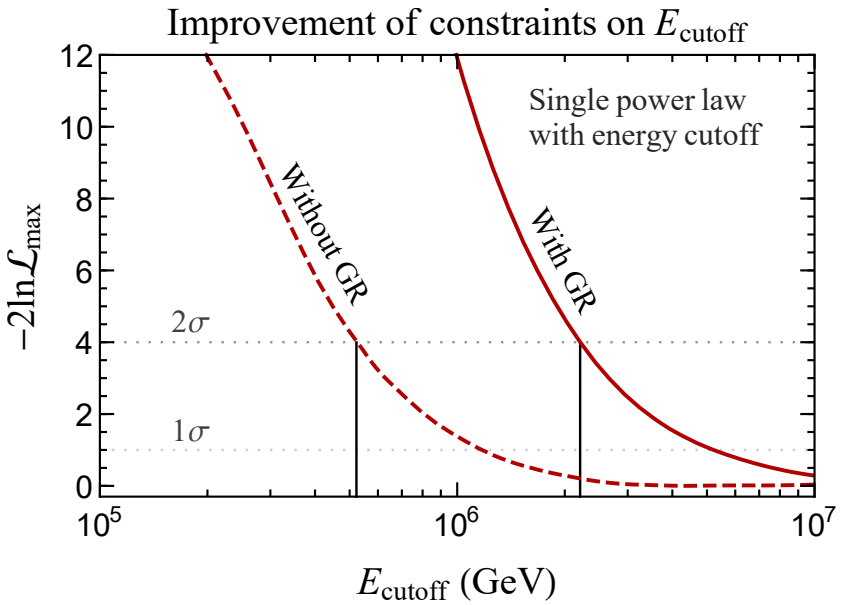

Figure 3.8: Log-likelihood function for the cutoff energy E_{cutoff}. The curve that does not take the Glashow resonance candidate event into account (dashed red) is taken from Fig. VI.9 of Ref. [171]. The second curve (solid red) is the log-likelihood function derived from the Glashow resonance candidate event. Here, we marginalized over the other model parameters. Also published in Ref. [1] (licensed under CC BY).

3.5 Projections for the future and outlook

Besides the posterior and the likelihood we get from the one GR candidate event measured until today, we also show projections for future sensitivities of IceCube-Gen2 in Fig. 3.7. So far, the strongest claim we can make is that the ideal μ-damped pγ source is excluded at 2σ confidence level. With more data, the discriminatory power of such an analysis will increase.

To demonstrate how the sensitivity will increase with future experiments, we take IceCube-Gen2 as an example (see Sec. 2.3.4 for more details). We rescale the current target mass of IceCube by a factor of ten. Then we perform a count analysis within the energy window we considered before, $E_{\mathrm{dep}} \in [4, 10]\,\mathrm{PeV}$. Afterwards, the projection is done for a runtime of ten and fifty years. For both, we assume that the source really is of pp type, i.e., $f^{\mathrm{E}}_{\overline{\nu}_e} \approx 0.5$. In the future, the flux parameters Φ_0, γ and E_{cutoff} can be determined in a very precise way [21]. Therefore, we choose a rather optimistic spectrum for our forecast. The parameters we use are $\Phi_0 = 6.37$, $\gamma = 2.7$ and $E_{\mathrm{cutoff}} = 5\,\mathrm{PeV}$. In Fig. 3.7, we show the ten year projection as the blue dashed line with the longer dash and the fifty year projection as the blue dashed line with the shorter dash. Both these projections are for the frequentist interpretation, which means that the likelihood functions are shown.

With the assumption of the true source being of pp type, the expected number of GR candidate events in ten years of runtime of IceCube-Gen2 is eleven events within the framework of the single power law model for the neutrino flux. If we extend the flux model by an exponential cutoff with the parameters as given beforehand, this number is reduced to three expected events. For the best-fit single power law flux model, ten years of runtime of IceCube-Gen2 would already be enough to distinguish the ideal pp and pγ source at 2σ confidence level. Since we would expect less events when the flux model is extended by the exponential cutoff, we need a longer runtime for a 2σ distinction between the ideal pp and pγ source for such a flux model. For the fifty year projection, we get that the ideal pp and pγ sources can be distinguished at 2σ confidence level also for the single power law model with an exponential cutoff. Please note that it is reasonable that we see such a difference between the single power law with and without an energy cutoff. The model with the cutoff has an additional parameter, which will dilute the information on the $\overline{\nu}_e$ fraction $f^{\mathrm{E}}_{\overline{\nu}_e}$. This effect can already be seen in the analysis that only takes the GR candidate event measured so far into account and it becomes even more apparent in the curves of the ten and fifty year projections given in Fig 3.7 (the curves are in general less wide for the flux model without the energy cutoff).

In Sec. 2.3.4, we gave an overview over neutrino telescopes that will be taking data in the future. Besides IceCube-Gen2 for which we already did the projection, the other neutrino telescopes will also contribute to the search for more GR candidate events (and in general to more statistics). The results that we got for IceCube-Gen2 can also be applied to other neutrino telescopes if the effective exposure is adjusted correctly. Here, the effective volume and the runtime are the most important variables. Overall, the combination of multiple neutrino telescopes will increase the future sensitivity to distinguish different astrophysical neutrino sources.

If the neutrino spectrum is measured more precisely in the future, it will be

reasonable to go beyond the single power law model for the neutrino flux and take a more general energy dependence into account. With increased statistics that we expect to be found in the future, GR candidate events could also be used to produce a map of the sky. For this, associated PeVatrons might also be identified [181–183]. All in all, with measurements of future neutrino telescopes we will learn more about (astrophysical) neutrino sources. With this improved knowledge, new physics studies will also be possible. A few of those will be discussed in more detail in Ch. 4.

4

The Glashow resonance as a probe for physics beyond the Standard Model

The GR is a process that takes place within the SM, i.e., no new physics is needed to describe this process. For the analysis presented in Ch. 3, we did not use any BSM physics either. Once future neutrino telescopes yield enough statistics, the GR can also be a sensible probe for BSM physics. Here, we will outline a few ideas presented in the literature first. Afterwards, we will present one model that will also be investigated in the context of $0\nu\beta\beta$ in chapter 5. We will come back to its effects on measurements of the GR later on in Ch. 6.

4.1 Relevant new physics

Since we are especially interested in lepton number violation in this thesis, we will focus on neutrinos that are of Majorana nature first. For these, the magnetic moment allows for a conversion of neutrinos into antineutrinos and vice versa. As pointed out in Ref. [184], this is especially relevant for the μ-damped pγ source. Since we would expect a $\overline{\nu}_e$ fraction of $f^{\mathrm{E}}_{\overline{\nu}_e} \approx 0$ for this source, the conversion between neutrinos and antineutrinos would change what is measured on Earth by a lot; it might even lead to the measurement of GR candidate events, which are naively not expected from such sources. As they also point out, this conversion would be facilitated by a magnetic field. An interesting case study that looks at Majorana neutrinos that are produced within a strong magnetic field of some astrophysical object is given in Ref. [185]. In the following, we will summarize their findings. When neutrinos propagate through a strong magnetic field, the neutrinos undergo spin-flavor precession induced by their magnetic moments. This affects both the

helicity and flavor composition that is measured on Earth. The study focuses on neutrinos that are produced at high energies in sources with a strong magnetic field. A possible candidate for such sources are magnetars. High-energy neutrinos could be produced in their surroundings. Since the magnetic field of magnetars is relatively well understood, the authors of Ref. [185] chose them for a benchmark study. Their study is based on the effective interaction term

$$\mathcal{L} \supset \mu_{\alpha\beta}\nu_{L,\alpha}\sigma_{ab}\bar{\nu}^{C}_{L,\beta}F^{ab} + \text{h.c.}\,, \tag{4.1}$$

where $\mu_{\alpha\beta}$ is an element of the neutrino magnetic moment matrix, ν_L is the left-handed neutrino field, σ is a Pauli matrix and F^{ab} is the electromagnetic field strength tensor. Besides this contribution, the authors also consider neutrino oscillations in vacuum and the Mikheyev-Smirnov-Wolfenstein effect [186] (however, they find that the latter is not relevant). A nonzero neutrino magnetic moment $\mu_{\alpha\beta}$ will cause additional helicity and flavor mixing when the neutrino passes through a magnetic field. The results they get are shown in Fig. 9 of Ref. [185]. We can see that the neutrino magnetic moment can change the $\overline{\nu}_e$ fraction $f^{\mathrm{E}}_{\overline{\nu}_e}$ drastically. The results also reflect what was predicted in Ref. [184] for the μ-damped pγ source. For certain choices of parameters, $f^{\mathrm{E}}_{\overline{\nu}_e}$ can even exceed a value of 0.4 for neutrinos that come from such a source. Normally, finding a GR event would immediately exclude the μ-damped pγ source. However, for Majorana neutrinos coming from an environment with a strong magnetic field, it is fair to conclude that this is not true. On the other hand, the authors also conclude that, if there are no GR candidate events found from μ-damped pγ sources like magnetars, this would lead to constraints on the neutrino magnetic moment due to the fact that at high enough neutrino magnetic moment all considered sources will yield a non-negligible $\overline{\nu}_e$ fraction $f^{\mathrm{E}}_{\overline{\nu}_e}$. However, to find such constraints, better statistics from future neutrino telescopes are crucial. [185]

A recent study given in Ref. [187] investigates the connection between the GR and dark matter (DM), which we will also briefly investigate later on in Ch. 6. However, the authors of Ref. [187] follow a different approach. While we consider capture or emission of a lepton number carrying scalar (that accounts for the ratio α of the observed total DM density), they consider the decay of both symmetric and asymmetric DM. The idea of asymmetric DM is strongly based on the hypothesis that the current DM abundance comes from the same origin as visible matter. It is a well-known fact that there is an observable imbalance between baryons and their antiparticles (the so-called baryon asymmetry of the universe); there are more baryons than antibaryons. Asymmetric DM is routinely assumed to be charged under $B-L$ and models typically have certain operators that enable transferring an asymmetry between the SM and the dark sector. This link can lead to an asymmetry between SM decay products of DM decay, i.e., while symmetric DM might decay to, e.g., $\nu\bar{\nu}$, the asymmetric DM might lead to a different ratio between particles and antiparticles. Therefore, it might also affect the ratio of neutrinos and antineutrinos, which would, in turn, alter GR measurements. In Ref. [187], this issue is addressed. The authors find limits on DM decay to neutrino pairs and also the first constraints on heavy asymmetric DM which decays to neutrinos. With the one GR event that has currently been measured in IceCube, they find a lower limit for the lifetime of

asymmetric DM of $10^{27} - 10^{29}$ s when the mass of the asymmetric DM is bigger than 10 PeV. The constraints they set are competitive with those from gamma ray searches (and in some ranges they are even stronger). [187, 188]

The GR is also a valuable probe for neutrino decay. If neutrino decay is observed, it would be a strong hint towards BSM physics. The UHE astrophysical neutrinos we consider when looking at the GR are a good probe for neutrino decay. This is due to the fact that they have cosmological-scale baselines. The idea that was proposed in Ref. [189] goes as follows: Assuming inverted mass ordering for neutrinos (where ν_3 is the lightest mass eigenstate), we can consider the case where ν_1 and ν_2 decay to ν_3 while traveling to Earth. Since ν_3 only has a very small electron flavor content, such decays would lead to a significantly reduced amount of detected GR candidate events in neutrino telescopes. Within a few years of runtime of current neutrino telescopes, even a single GR candidate event hints towards the presence of ν_1 and ν_2. This then allows to find lower limits for the lifetime of the two heaviest mass eigenstates. Such an analysis [190] found the following lower limits for the lifetimes:

$$\frac{\tau_1}{m_1} > 2.91 \times 10^{-3}\,\mathrm{s\ eV^{-1}} \quad \text{and} \quad \frac{\tau_2}{m_2} > 1.26 \times 10^{-3}\,\mathrm{s\ eV^{-1}}\,. \tag{4.2}$$

Here, $\tau_{1/2}$ is the lifetime of the corresponding mass eigenstate. For the analysis, the authors assumed that the neutrinos are of Majorana nature and thus that there is no helicity suppression for the daughter particles. Due to the assumed Majorana nature of neutrinos, this is a LNV scenario again. It can be seen that the limit they get is more strict for ν_1 than for ν_2. This is because ν_1 has a larger electron flavor content and thus the GR is more sensitive to it. [189, 190]

Another idea where the GR could be useful to test new physics is Lorentz violation. This is presented in Ref. [191]. Here, the Lorentz violation would affect neutrino oscillations and therefore also the $\overline{\nu}_e$ flux that reaches Earth and can possibly cause GR events in IceCube and other neutrino telescopes. With the Hamiltonian considered in Ref. [191], they find a noticeable damping of the GR event rate in the case where the UHE neutrinos are mostly from a source in which the production of muon (anti-)neutrinos dominates. [191]

A related field of study are Glashow-like resonances that could appear in the UHE neutrino spectrum. Let us quickly introduce two slightly different approaches here that have been studied in the literature. The first one [192,193] depends on light charged scalars in the context of radiative neutrino mass models. Here, the authors focus mainly on the Zee model [194], which comes with a second Higgs doublet and and a charged $SU(2)_L$ scalar singlet. These additions lead to a neutrino mass at one-loop level via an effective lepton number violating operator. Within the Zee model and variants of it there exist new scalar mediators. These will also lead to new resonances when UHE neutrinos interact with matter. However, in such models, the resonances are not restricted to electron antineutrinos as it is the case for the GR. Depending on the mediator, other (anti-)neutrinos can also induce resonances. The authors of Ref. [193] claim that resonances from scalars within the Zee model can be probed in IceCube and the extension IceCube-Gen2. Moreover, such models can also induce observable non-standard neutrino interactions. The second study [195] that we want to mention here is very similar. However, they consider a scenario that is a bit more simplistic as it only includes the extension

of the SM by a single charged Higgs. As before, this charged Higgs does not only induce Glashow-like resonances but also neutrino non-standard interactions. So far, the authors of Ref. [195] found that other neutrino experiments set more stringent limits than IceCube data. However, they expect that IceCube will be able to set more stringent bounds when it reaches four times the exposure existing to date.

As we can see, there has already been some interest in studying BSM physics with the help of the Glashow resonance. For a good fraction of them, the question whether neutrinos are of Dirac or Majorana nature has an influence on the GR event rate that would be expected. In the analysis we performed in Ref. [1], we did not include any BSM physics. Moreover, the nature of neutrinos did not play a role there. However, the analysis we performed is important to facilitate such studies looking for BSM physics since the main observable that is considered in many such studies is the $\overline{\nu}_e$ fraction $f^{\mathrm{E}}_{\overline{\nu}_e}$. With our analysis, we put constraints on this observable, which can not only be used to identify sources but in principle, if the source or at least the $\overline{\nu}_e$ fraction $f^{\mathrm{E}}_{\overline{\nu}_e}$ that should come from the source is known, a similar analysis could also be used to detect deviations from the expected $f^{\mathrm{E}}_{\overline{\nu}_e}$ that point towards BSM physics.

With the one GR candidate event found so far, it is difficult to examine BSM physics with the help of the GR. However, as discussed in Sec. 3.5, we expect more GR candidate events to be measured in the future. Even if we do not measure many such events, this would still be valuable information to constrain BSM scenarios like the ones given here. If we only consider SM physics, the non-observation of GR candidate events would convey information about astrophysical neutrino sources as discussed in Ch. 3. Moreover, it might help to use multimessenger physics to identify neutrino sources. Besides the detection of UHE neutrinos, gravitational waves are a prime probe to observe the astrophysical objects that emit both the neutrinos and the gravitational waves at the same time [59]. So even though right now it is difficult to test BSM models via the $\overline{\nu}_e$ fraction $f^{\mathrm{E}}_{\overline{\nu}_e}$, it is worth it to think about BSM physics that experiments might be able to find in the future.

4.2 A scalar that carries lepton number

Let us now move on to a specific model that was studied in the context of $0\nu\beta\beta$ while the author was working on this thesis. This one also heavily relies on the introduction of a scalar similar to, e.g., Refs. [192, 193]. Later on, when we discuss its influence on the GR, we do not consider the scalar to be the intermediate particle. Instead, we keep considering the standard GR and the scalar takes on a similar role as the magnetic moment in Ref. [185], i.e., it changes the $\overline{\nu}_e$ fraction $f^{\mathrm{E}}_{\overline{\nu}_e}$ and thus it might also influence the outcome of searches for GR candidate events.

The main idea behind our model is that the addition of the scalar makes non-zero $0\nu\beta\beta$ rates possible without having a zero-density vacuum Majorana neutrino mass. While we consider the capture of this scalar, the experimental signature is not distinguishable from the experimental signature of standard $0\nu\beta\beta$. This will be discussed in more detail in Ch. 5. There, we introduce a complex scalar ϕ that carries two units of lepton number such that $B - L$ is an exact symmetry. We specifically assume that lepton number is conserved in our model. Moreover, the

Lagrangian is chosen such that the complex scalar ϕ does not acquire a vacuum expectation value (vev). This is important to make sure that we do not get a Majorana mass term for light neutrinos in the vacuum. Please note that ϕ will still acquire an expectation value when its own density reaches a critical value; this will be discussed later on in Sec. 5.2.4.

In Ch. 5, we will discuss the capture of such a scalar from a cosmic background. For this to be possible, the scalar needs to be stable on cosmological timescales. Looking at the Lagrangian that is introduced in Eq. 5.1, we can see that (as long as the Higgs portal coupling is very small) the only decay channel is the decay to two right-handed neutrinos. In this thesis, we therefore assume $m_\phi < 2m_{\nu,\mathrm{min}}$. With this, the decay is kinematically forbidden and thus the scalar is stable on cosmological time scales.

While we designed the model such that it affects $0\nu\beta\beta$ in a certain way, it is interesting to see that the existence of such a scalar can also affect other measurements. In the project discussed in Ch. 3, the parameter of interest for our analysis was $f^{\mathrm{E}}_{\overline{\nu}_e}$ (see Eq. 2.30). Therefore, if the existence of our scalar changes the ratio between the amount of neutrinos and antineutrinos that arrive on Earth after being emitted by a certain astrophysical source, this will affect the amount of GR candidate events we expect to see in IceCube and other neutrino telescopes. However, since the scalar only couples to right-handed neutrinos in our model, the influence of the scalar will always be suppressed by the necessary Dirac mass insertions. For now, we will discuss this model in the context of $0\nu\beta\beta$ and after that, when we understand its features, we will come back to the GR and discuss the interplay of the observables of the two processes in Ch. 6.

5

Neutrinoless double beta decay without a Majorana neutrino mass in the zero-density vacuum

As discussed in Sec. 2.4, $0\nu\beta\beta$ is the main probe for a possible Majorana neutrino mass. This is strongly related to the famous Schechter-Valle theorem [28] (see Sec. 2.4.1 for details) that states that - if $0\nu\beta\beta$ is found - this immediately implies that neutrinos have a Majorana mass, at least via the diagram shown in Fig. 2.7. While we do not question that the Schechter-Valle theorem is correct, we do question whether there might be a possibility that we see a signal in experiments searching for $0\nu\beta\beta$ which looks exactly like the signal we would expect from ordinary $0\nu\beta\beta$ but originates from a mechanism where the Schechter-Valle theorem does not apply. Such a scenario requires BSM physics (technically, there is also the capture of two relic neutrinos, which is described in Sec. 5.4; however, the expected half-life of such a process is so large that it is out of the reach of next generation experiments). In this chapter, we will show how a scalar can help to circumvent the Schechter-Valle theorem in certain cases.

We will start by discussing the specific model we use and the role of the scalar in more detail in Sec. 5.1. There, we will investigate both the scenario of scalar capture and scalar emission and argue why the capture mode is the one that can lead to a signal that looks similar to the standard $0\nu\beta\beta$ signal. After that, in Sec. 5.2, we will see how different scalar densities alter the situation. We find that the scalar forms a BE condensate for a higher density (or a smaller mass of the scalar), which has to be taken into account. In the free phase, there is a mechanism which - if a $0\nu\beta\beta$ signal is ever found - might still help to distinguish the capture mode from standard $0\nu\beta\beta$. It is also described in Sec. 5.2. Next, we look into phenomenological implications the existence of the scalar would have beyond $0\nu\beta\beta$ in Sec. 5.3. Lastly,

we briefly discuss the capture of dark vector bosons and fermions in Sec. 5.4 and there is a conclusion for this project in Sec. 5.5. This chapter is based on work that was first published in Ref. [3] and also partly on yet unpublished work [4].

5.1 The role of the scalar

In summary, what we want to achieve is a scenario where non-zero $0\nu\beta\beta$ decay rates are seen with an experimental signature that cannot be distinguished from the one we expect from standard $0\nu\beta\beta$ while, at the same time, retaining the Dirac nature of neutrinos in the vacuum Lagrangian. In other words, we want to propose a scenario where a non-zero $0\nu\beta\beta$ signal is generated without the existence of a Majorana neutrino mass or lepton number violation in the vacuum Lagrangian. We find that our scenario can fulfill all of these with one caveat. The density of the scalar cannot be to high or otherwise it will induce an effective Majorana mass for the neutrino. This issue will be addressed in detail later on in Sec. 5.2.4.

First of all, let us introduce the Lagrangian $\mathcal{L}$ for our model. Besides the complex scalar ϕ, the SM particle spectrum is also present. While the scalar is charged under $B-L$ with a $B-L$ charge of -2 ($B=0$, $L=2$) for ϕ and 2 ($B=0$, $L=-2$) for $\phi^\dagger$, it is a singlet under the other SM symmetries. On top of that, we also introduce right-handed neutrinos ν_R. This is necessary to introduce the Dirac mass term for neutrinos. The relevant part of the Lagrangian reads

$$\begin{aligned}\mathcal{L} \supset\ & m_\phi^2\phi^\dagger\phi + \lambda_\phi(\phi^\dagger\phi)^2 + \lambda_{H\phi}(H^\dagger H)(\phi^\dagger\phi) + Y^\nu_{ij}\overline{L}_i\tilde{H}\nu_{R,j} \\ & + g_{ij}\overline{\nu}_{R,i}\nu^C_{R,j}\phi + \text{kinetic terms} + \text{h.c.}\,,\end{aligned} \tag{5.1}$$

where m_ϕ is the mass of the scalar, λ_ϕ is the coupling constant of the ϕ^4 interaction, $\lambda_{H\phi}$ is the coupling constant of the interaction between the scalar and the Higgs (Higgs portal), H is the Higgs boson, Y^ν_{ij} is the Yukawa coupling constant for the coupling of the right-handed neutrino and the Higgs and g_{ij} is the coupling constant for the interaction between the scalar and the right-handed neutrino. Note that all terms in this Lagrangian are $B-L$ conserving. The neutrinos acquire a Dirac mass $m_D = Y^\nu v_{EW}$ after electroweak symmetry breaking. Here, v_{EW} is the electroweak vev. For the scope of this thesis, we require the coupling of the Higgs portal $\lambda_{H\phi}$ to be small. There is no direct coupling to the left-handed neutrinos and coupling of ϕ to the left-handed neutrinos will always require the mass insertion of the Dirac neutrino mass. Moreover, the Lagrangian was chosen such that ϕ does not acquire a vev. This is relevant since a vev would immediately lead to a Majorana neutrino mass term via the coupling of ϕ to the right-handed neutrinos ν_R

$$g_{ij}\overline{\nu}_{R,i}\nu^C_{R,j}\phi\,. \tag{5.2}$$

In the literature, discussing an extra scalar alongside $0\nu\beta\beta$ is not new. There have been many studies investigating $0\nu\beta\beta$ with additional emission of a so-called Majoron. Majorons are the Goldstone bosons of a spontaneously broken lepton number. Therefore, they are clearly related to a possible Majorana nature of neutrinos. Nowadays, the name Majoron is usually used to refer to massless or light particles

that couple to neutrinos. Due to these properties of the Majoron, it is natural to study how it influences $0\nu\beta\beta$ when it is coupled to the propagating neutrino. In most of the research that has been done so far, the effect of $0\nu\beta\beta$ emitting one or more Majorons was studied. For example, a comprehensive study on massive Majorons that includes Majoron emitting $0\nu\beta\beta$ can be found in Ref. [196]. As we will discuss below, the mode that is relevant for us in this chapter is the capture of a scalar. [119, 197]

So far, there have not been many studies discussing the capture mode. A recent publication that considers the capture of an ultralight real scalar can be found in Ref. [198]. In contrast to our model, the real scalar in Ref. [198] directly couples to the left-handed neutrino ν_L. The authors find a periodic modulation pattern in decay events. Moreover, they find that the existence of such a scalar would have altered the standard results of cosmology, leaving them with strong constraints on the parameter space. The parameter space is constrained so much that future $0\nu\beta\beta$ experiments will most likely not see such a real scalar. Another related study that considers $0\nu\beta\beta$ induced by fermionic DM that couples to the intermediate neutrino in $0\nu\beta\beta$ via a scalar is given in Ref. [199]. Lastly, we also want to mention Ref. [200], which does not consider an external particle, but it does consider a model that predicts an enhanced $0\nu\beta\beta$ rate. For this, they calculate loop-induced contributions from the neutrino self-energy in a scotogenic model.

In this work, we want to discuss whether the capture of a complex scalar that carries two units of lepton number can lead to an experimental signature that looks like the one we would expect from $0\nu\beta\beta$. The Feynman diagrams are shown in Fig. 5.1 for both the capture (left panel) and the emission process (right panel). It is shown that ϕ couples to the right-handed neutrino ν_R, which couples to the left-handed neutrino ν_L via the insertion of the Dirac neutrino mass. Moreover, in the left Feynman diagram ϕ is captured while in the right one $\phi^\dagger$ is emitted. This is immediately clear when we remember that $B - L$ is a conserved quantity in our theory. In ordinary $0\nu\beta\beta$, lepton number is not conserved: The initial state has a lepton number of zero while the final state has a lepton number of two. Since the scalar ϕ carries a lepton number of two (and thus $\phi^\dagger$ carries a lepton number of minus two), we need either a capture of ϕ or an emission of $\phi^\dagger$ for the lepton number to be conserved. In Sec. 2.4.2, it was already mentioned that the PSF would be important for the discussion here. As also pointed out there, the PSF depends on the final state particles and all the relevant integrations are over final state parameters like the energy and momentum of the final state electrons. For the emission of the scalar, the decay can be written as follows:

$$(A, Z) \to (A, Z + 2) + 2e^- + \phi^\dagger \,. \tag{5.3}$$

Obviously, compared to the standard $0\nu\beta\beta$ mode

$$(A, Z) \to (A, Z + 2) + 2e^- \,, \tag{5.4}$$

the final state has one additional particle. This leads to a PSF that is proportional

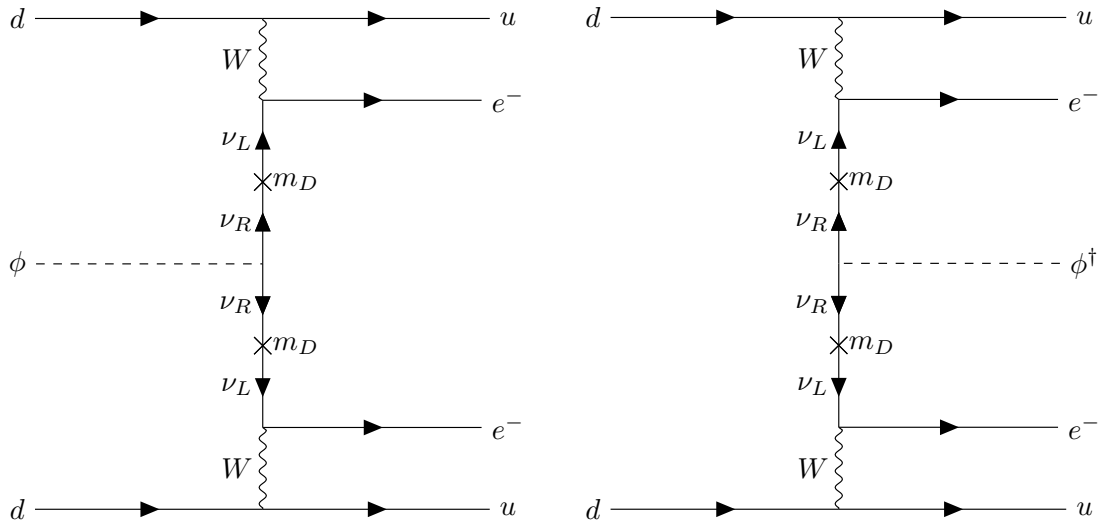

Figure 5.1: Feynman diagrams for neutrinoless double beta decay with an external scalar that carries two units of lepton number. The diagram on the left shows the capture of the scalar and the diagram on the right shows its emission. Moreover, it is shown that the scalar only couples to the right-handed neutrino ν_R, which is coupled to the left-handed neutrino ν_L via an insertion of a Dirac mass. For the single beta decay vertex, we show the standard interaction that is allowed within the Standard Model.

to [124, 196, 201]

$$G^{0\nu\beta\beta}(Q,Z) \propto \int F_0(Z,E_1)F_0(Z,E_2)E_1E_2p_1p_2p_\phi \times \delta(E_1+E_2+E_\phi+M_f-M_i)dqdE_1dE_2d(\hat{\mathbf{p}}_1\cdot\hat{\mathbf{p}}_2)\,, \tag{5.5}$$

where p_ϕ is the momentum of the scalar and E_ϕ is its energy. It can be seen that this clearly depends on the final state and therefore it differs from the PSF for standard $0\nu\beta\beta$ that is given in Eq. 2.45. However, for capture of ϕ

$$(A,Z)+\phi \to (A,Z+2)+2e^-\,, \tag{5.6}$$

the PSF is the same as the one given in Eq. 2.45 except for the fact that the energy of the scalar would enter the delta distribution, which ensures energy conservation. As long as the energy that is transferred by ϕ is below the experimental resolution, the phase space of ordinary $0\nu\beta\beta$ and of the capture mode will look exactly the same in experiment. That is why we look at this mode. Let us briefly emphasize here that the scenario that is outlined in this chapter does not break the Schechter-Valle theorem even though we claim that the detection of an experimental signal that looks like $0\nu\beta\beta$ would not immediately mean that the neutrino has a Majorana mass. This is because the Schechter-Valle theorem does not apply in our case due to the additional external particle, which would then also show up in the diagram given in Fig. 2.7. In the case of a true $0\nu\beta\beta$, the Schechter-Valle theorem is still valid.

The spectra for the different double beta decay modes including $0\nu\beta\beta$ with emission and capture of a scalar alongside the standard $2\nu\beta\beta$ and $0\nu\beta\beta$ are shown

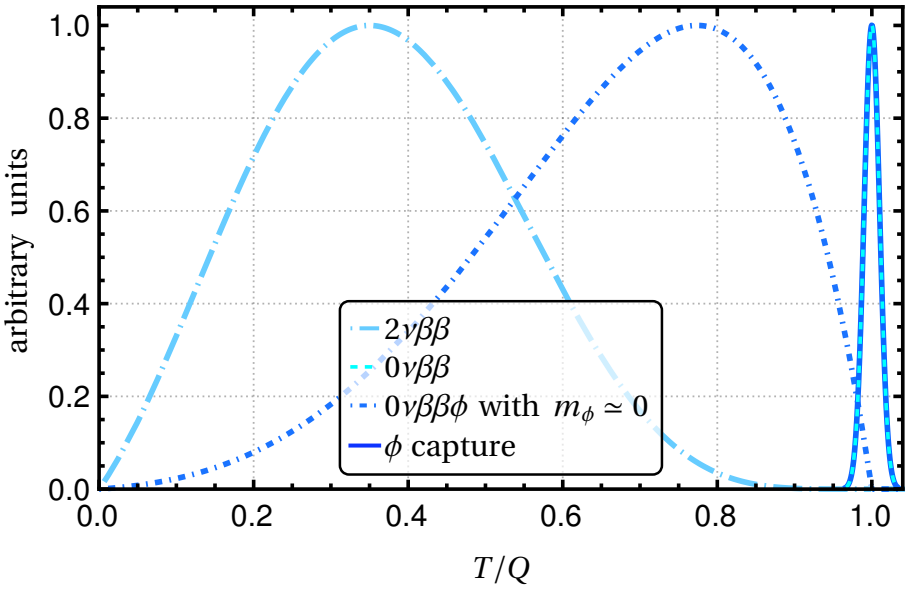

Figure 5.2: Total energy spectra for the two emitted electrons. Here, we consider different modes of double beta decay. The quantity T/Q is shown on the x-axis, where Q is the Q-value and $T = E_1 + E_2 - 2m_e$ is the kinetic energy of the two final state electrons summed up, the E_i are the energies of the electrons and m_e is the electron mass. The two dashed-dotted lines show the spectrum of standard double beta decay (long dash, lighter color) and of neutrinoless double beta decay with emission of a scalar with mass $m_\phi \simeq 0$ (short dash, darker color) [196]. Moreover, a peak at $T/Q = 1$ is shown. This represents the spectra of the ordinary neutrinoless double beta decay mode and the mode with the capture of a scalar. Assuming that the energy, which is transferred by the capture of the scalar, is less than the experimental resolution, these are overlapping delta distributions, which are smeared out due to the experimental accuracy. This smear-out has been exaggerated for better visibility here. Also published in Ref. [3] (licensed under CC BY).

in Fig. 5.2. As already described above, the spectra for standard $0\nu\beta\beta$ and the capture mode are exactly the same as long as the energy transfer from the captured scalar is below the experimental resolution. Moreover, they are easy to distinguish from the other two modes, which do not have a discrete spectrum. For the spectra of $2\nu\beta\beta$ and $0\nu\beta\beta$ with emission of ϕ, we used formulae from Ref. [196].

The complex scalar ϕ can in principle be cold DM [202]. This strongly depends on parameters like its energy, mass or number density. For our purposes, the scalar ϕ needs to be stable over cosmological timescales. There are two ways to ensure this: Either

$$m_{\nu,\mathrm{min}} > m_\phi/2 \tag{5.7}$$

holds or the coupling to all neutrinos that are lighter than half of the mass of ϕ is very small and thus the decay of ϕ is suppressed.

Before the complex scalar ϕ can be captured and induce a $0\nu\beta\beta$ signal, it has to be produced. However, within the work we perform we choose to stay rather agnostic about the production mechanism of the scalar and instead study the effects it has once it is produced. In general, ultralight scalars like the one proposed in

this thesis can be produced in the early universe in a non-relativistic way (for more details see Ref. [203] and references therein).

Before we move on, let us quickly mention that, in principle, it would also be possible to capture or emit any odd number of scalars, as long as the net lepton number they carry together is $L = 2$ for the capture and $L = -2$ for the emission. As long as at least one scalar is emitted, the phase space changes and it can be distinguished from standard $0\nu\beta\beta$ mode. For the capture of an odd number of scalars, the PSF is still the same as for standard $0\nu\beta\beta$. However, we will concentrate on the capture of a single scalar in this thesis - at least in the free phase.

5.2 Influence of the density of the scalar

Current $0\nu\beta\beta$ experiments have shown that - if it exists at all - $0\nu\beta\beta$ is an extremely rare process. Since the capture of a scalar ϕ would give the same signal, the lower limit for the half-life of $0\nu\beta\beta$ found in experiments so far also applies to the capture process. However, for it to be of interest to us, its half-life also should not be too far away from the current limits since then chances of seeing it within our lifetime would be very low. In this section, we will discuss the interplay between the number density of the scalar, the half-life and a possible transition to the condensate phase.

In general, an increase of the number density of the scalar ϕ has two effects: On the one hand, an overdensity of ϕ would lead to an increased capture rate and thus a smaller half-life, making detection of the capture process in next generation experiments more likely. On the other hand, the scalar can undergo BE condensation at high enough densities. Before we go into detail on the behavior in both the free and the condensate phase and how the transition between the two phases takes place, there will be a very brief introduction to BE condensation in ϕ^4 theory.

5.2.1 Bose-Einstein condensation and its contribution to the effective neutrino mass

BE condensation is a thermal effect and the theory that is commonly used to describe thermal effects in QFT is thermal field theory. To keep this section brief, we will not give a complete introduction to thermal field theory. The interested reader is referred to Ref. [204] for this purpose. However, we want to briefly describe BE condensation and give a few results that will be relevant later on before we move on to calculate the half-lives of the capture process in the free and the condensate phase. The concept of BE condensation was developed by S. N. Bose and A. Einstein. In 1924, Bose published a paper [205] on the statistics of light quanta (nowadays called photons). Einstein extended this idea in two consecutive follow-up papers [206], where he first proposed the idea of condensation at low temperatures in the second of the two papers.

In general, BE condensation is a finite temperature effect that appears in a gas of bosons when it is cooled under a critical temperature T_C. Since the calculations are quite extensive, we will only give a few results here. For a detailed calculation see, e.g., Ref. [207]. If we assume that the gas consists of identical, non-interacting

bosons, it is well-known that it follows the BE distribution given by

$$n(E_i) = \frac{1}{\exp((E_i - \mu)/(T)) - 1}\,. \tag{5.8}$$

Here, n is the expected number of particles in a certain state i with energy E_i, μ is the chemical potential and T is the temperature. This distribution has an interesting feature that the analogous one for fermions does not have due to the Pauli exclusion principle: For energies near the chemical potential, $n(E_i)$ can be large. Or in other words: It is possible that many bosons are in the same state. In practice, the different energy levels can be degenerate, which means that there are several states at energy E_i. To account for this, we can multiply Eq. 5.8 by the degeneracy. Let us give a specific example: For bosons with spin 0 that are confined in a box with volume V, the degeneracy is given by

$$g(E_i) = \frac{2}{\sqrt{\pi}} \left(\frac{m}{2\pi}\right)^{3/2} V\sqrt{E_i}\,, \tag{5.9}$$

where m is the mass of the boson. We can see that, while the BE distribution becomes large, the degeneracy goes to zero at low energies. The product of the two functions is still integrable. However, at temperatures below a critical temperature T_C something subtle happens and we cannot simply integrate the product of the degeneracy and n over the energy to get the amount of bosons that are in certain states. This is due to the fact that the chemical potential depends on the temperature. For temperatures above T_C, the chemical potential of the Bose gas is negative and hence most of the atoms will be in excited states, i.e., in states that have a higher energy than the ground state. If the temperature drops below T_C, the chemical potential is approximately zero. This allows for many particles in the ground state. Calculations give

$$N_0 = N - N_{\text{excited}} = \left(1 - \left(\frac{T}{T_C}\right)^{3/2}\right) N \tag{5.10}$$

for $T < T_C$. Here, N is the total number of particles and N_0 is the number of particles in the ground state. This equation clearly indicates that, at low temperatures, a gas of bosons quickly transitions to a BE condensate, where most of the particles are in the ground state. This effect is called BE condensation and it only appears in Bose gases. [207, 208]

Naturally, our complex scalar field ϕ can also undergo BE condensation at low temperatures if its density is high enough. Or, in other words, if we can think of ϕ as single particles that are scattered across the universe, there are not enough particles in one place to actually form a BE condensate. Therefore, a certain density is needed for ϕ to be able to undergo condensation. As we will see later, this is related to the rates of ϕ capture. The interplay between the condensation and the capture rates will be discussed in detail in Sec. 5.2.2 and 5.2.4.

From the non-interacting Bose gas we get that ϕ will form a Bose gas around the critical temperature of [203]

$$T_C = \frac{2\pi}{m_\phi} \left(\frac{n_\phi}{\zeta(3/2)}\right)^{2/3}\,, \tag{5.11}$$

where n_ϕ is the total number density of ϕ and ζ is Riemann's zeta function ($\zeta(3/2) \approx 2.612$). However, this is only partially correct. A careful treatment within thermal effective field theory (EFT) gives that Eq. 5.11 is only valid in the regime of large masses or low densities. The full result reads [209]

$$T_{\text{crit}} = \begin{cases} \frac{2\pi}{m_\phi}\left(\frac{n_\phi}{\zeta(3/2)}\right)^{2/3} & n_\phi \ll m_\phi^3 \\ \left(\frac{3n_\phi}{m_\phi}\right)^{1/2} & n_\phi \gg m_\phi^3 \end{cases} . \tag{5.12}$$

As already discussed above, we get a macroscopic occupation of the ground state when the temperature of the system is smaller than T_C. This comes with a conversion of the conserved particle number that we have for ϕ in the free phase to a non-zero scalar condensate [204]. In the condensate phase, we can therefore treat the scalar as a background field instead and not as individual particles. If we do not think of the scalar as individual particles anymore, the ground state acquires a non-trivial expectation value within a region with a large enough density of ϕ and, as a result, the $B - L$ symmetry is spontaneously broken [203, 204].

As a result of the BE condensation, the right-handed neutrino gets an effective Majorana mass term when it interacts with the scalar medium. This is analogous to the refractive mass of neutrinos as described in Ref. [210]. However, our setup is a bit different since we only consider an effective Majorana mass term and our scalar carries lepton number. An example process for our case is shown in Fig. 5.3. While these processes primarily give an effective Majorana mass to right-handed neutrinos within the medium, the left-handed neutrinos would clearly also get an effective Majorana mass via two Dirac mass insertions. The initial claim of our project was that there might be a $0\nu\beta\beta$ signal without a Majorana neutrino mass term in the vacuum. This effective Majorana mass induced in the condensate phase is the reason why this claim has been restricted to the vacuum or, to be more specific, to the zero-density vacuum.

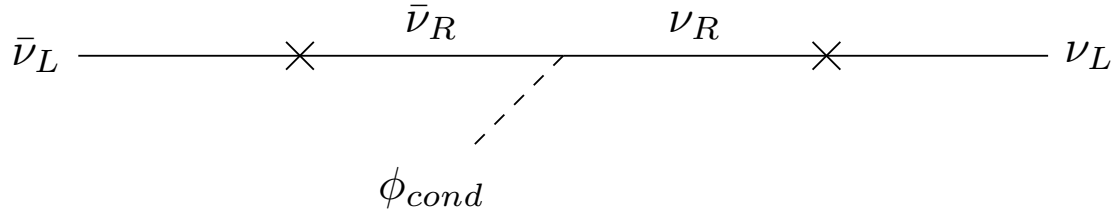

Figure 5.3: How the condensate of ϕ gives an effective Majorana mass to the left-handed neutrino. Here, the expectation value that is acquired by the scalar ϕ in the condensate phase is responsible for the mass term of the right-handed neutrino. With two Dirac mass insertions the left-handed neutrino gets a Majorana mass term. Please note that this is only a mass term in the condensate phase. The Lagrangian of our model was constructed such that ϕ does not have a vacuum expectation value and therefore the diagram shown here can only happen if the scalar has a large enough number density.

5.2.2 The capture mode at low densities - free phase

In the free phase, where the scalar does not form a condensate, a $0\nu\beta\beta$ signal might be detected even without a Majorana neutrino mass within the medium. However, there is one caveat: As shown in Fig. 5.1, there is not only the capture of the scalar ϕ. We can also have emission of $\phi^\dagger$ (in Eq. 5.1, the corresponding vertex is hidden in the hermitian conjugate). This can potentially cause problems. As discussed before, the PSF for the emission mode is different from the one for ordinary $0\nu\beta\beta$ and the capture mode. Therefore, the emission mode could be distinguished from the others in experiment unless it is suppressed. This also implies that experiments could see the difference between standard $0\nu\beta\beta$ and the capture within our model since only the capture mode would be accompanied by the emission mode. Here, we will calculate the decay rate for both the emission and the capture mode. In the end, we will find that there is a part of the parameter space where the emission mode is indeed suppressed. This is the case when the mass of the scalar is small and when its density is large.

To calculate the rates for the scalar capture and the emission, we make use of existing calculations for $0\nu\beta\beta$ with Majoron emission [211, 212]. Throughout this calculation, we assume that the momentum of ϕ is much smaller than the typical Fermi momentum of nucleons:

$$p_\phi \lesssim \mathcal{O}(1\,\mathrm{MeV}) \ll p_F \approx \mathcal{O}(100\,\mathrm{MeV})\,. \tag{5.13}$$

Therefore, we neglect the momentum carried by ϕ. Due to this assumption, the amplitudes for the capture and the emission process are identical and it can be written as

$$\mathcal{A}_{0\nu\beta\beta\phi} = \frac{G_F^2}{2}\overline{e_L}(p_1)\gamma_\mu \sum_{ij} U_{ei}U_{ej}\frac{g_{ij}m_i m_j}{q^4}\gamma_\nu e_L^C(p_2) J^\mu_{V-A}(1) J^\nu_{V-A}(2) + (p_1 \rightleftarrows p_2)\,. \tag{5.14}$$

Here, U is again the PMNS matrix, g_{ij} is the coupling constant of ϕ and the right-handed neutrinos, m_i are the masses of the neutrino mass eigenstates, q is the momentum of the internal neutrino and J_{V-A} is the standard weak charged current [213]

$$J^\mu_{V-A} \propto \bar{u}\gamma^\mu(1-\gamma_5)d\,. \tag{5.15}$$

For an expansion in chiral EFT see, e.g., Ref. [214]. The expression in Eq. 5.14 is equivalent to the one we would get from the standard LνEM [215] except for the neutrino propagator. That is due to the fact that the momenta do not change within the approximation given in Eq. 5.13. However, the neutrino propagator is different due to the coupling to the scalar and the two mass insertions. Moreover, we neglected the neutrino masses in the denominator of the propagator, leading to the factor of $1/q^4$ in this case. In the end, the decay rate for $0\nu\beta\beta$ with emission of $\phi^\dagger$ reads

$$\Gamma^{\mathrm{em}}_{0\nu\beta\beta\phi} = g^2 \log(2) \left(\frac{m_{\beta\beta\phi}}{m_e}\right)^4 |\mathcal{M}_{0\nu\beta\beta\phi}|^2\, G_{0\nu\beta\beta\phi}\,. \tag{5.16}$$

Here, we assumed that g_{ij} from Eq. 5.14 is real, diagonal and the same for all i:

$$g_{ij} = g\delta_{ij} \quad (g \in \mathbb{R})\,. \tag{5.17}$$

Moreover, we defined an effective mass

$$m^2_{\beta\beta\phi} = \sum_i U^2_{ei} m^2_i \,. \tag{5.18}$$

The two leftover constituents that are needed to calculate the decay rate are the NME $\mathcal{M}_{0\nu\beta\beta\phi}$ and the PSF $G_{0\nu\beta\beta\phi}$. We want to point out here that the decay rate does not depend on the number density of ϕ.

Now let us have a look at numerical values for some of the quantities that are needed to calculate the decay rate. For $m_{\beta\beta\phi}$, we assume normal mass ordering with a lightest neutrino that is massless. Moreover, we assume that the CP phases vanish. With $\Delta m^2_{21} \approx 7.53 \times 10^{-5}\,\mathrm{eV}^2$ and $\Delta m^2_{32} \approx 2.455 \times 10^{-3}\,\mathrm{eV}^2$ [39] we get

$$m^2_{\beta\beta\phi} \approx 78\,\mathrm{meV}^2 \,. \tag{5.19}$$

The NME $\mathcal{M}_{0\nu\beta\beta\phi}$ that we need for this process is also found in $0\nu\beta\beta$ with emission of two scalars [211]. These NMEs have been calculated in the framework of the IBM2 model in Ref. [212]. $G_{0\nu\beta\beta\phi}$, the PSF, is also available in the literature. We take it from Ref. [216]. Here, we take ^{136}Xe as an example isotope. For this isotope, the numerical values for the NME and the PSF are [212, 216]

$$\mathcal{M}^{^{136}\mathrm{Xe}}_{0\nu\beta\beta\phi} = 1.112 \times 10^{-3} \quad \text{and} \quad G^{^{136}\mathrm{Xe}}_{0\nu\beta\beta\phi} = 4.09 \times 10^{-16}\,\frac{1}{\mathrm{yr}} \,. \tag{5.20}$$

The formula for the capture rate is overall very similar to Eq. 5.16. It reads

$$\Gamma^{\mathrm{cap}}_{0\nu\beta\beta\phi} = g^2 \log(2) \frac{\alpha \rho_{\mathrm{DM}}}{2 m^2_\phi m^2_e} \left(\frac{m_{\beta\beta\phi}}{m_e}\right)^4 |\mathcal{M}_{0\nu\beta\beta\phi}|^2 \, G_{0\nu\beta\beta} \,. \tag{5.21}$$

This one does depend on the number density of the scalar. Here, it is expressed through the local DM density $\rho_{\mathrm{DM}} \approx 0.3\,\mathrm{GeV/cm}^3$ [217] and α (the fraction of the total DM mass that ϕ accounts for). To keep it simple, we made the assumption that ϕ is non-relativistic and thus $E_\phi \approx m_\phi$. With this, the number density of the scalar can be written as

$$n_\phi = \frac{\alpha \rho_{\mathrm{DM}}}{m_\phi} \,. \tag{5.22}$$

As discussed before, the PSF for the capture mode is the same as the one for ordinary $0\nu\beta\beta$ due to the fact that the final states of the two processes are the same. For ^{136}Xe, its numerical value is [218]

$$G^{^{136}\mathrm{Xe}}_{0\nu\beta\beta} = 1.458 \times 10^{-14}\,\frac{1}{\mathrm{yr}} \,. \tag{5.23}$$

Next, we compare the capture and emission rates by dividing Eq. 5.16 by Eq. 5.21 and get

$$\frac{\Gamma^{\mathrm{em}}_{0\nu\beta\beta\phi}}{\Gamma^{\mathrm{cap}}_{0\nu\beta\beta\phi}} = \frac{2 m^2_\phi m^2_e}{\alpha \rho_{\mathrm{DM}}} \frac{G_{0\nu\beta\beta\phi}}{G_{0\nu\beta\beta}} \,. \tag{5.24}$$

Here, the coupling constant g, the effective neutrino mass $m_{\beta\beta\phi}$ and the NME $\mathcal{M}_{0\nu\beta\beta\phi}$ drop out since they appear in both expressions. With the numerical values for ^{136}Xe, Eq. 5.24 simplifies to

$$\frac{\Gamma^{\mathrm{em},^{136}\mathrm{Xe}}_{0\nu\beta\beta\phi}}{\Gamma^{\mathrm{cap},^{136}\mathrm{Xe}}_{0\nu\beta\beta\phi}} \approx \frac{6.4 \times 10^{-25}}{\alpha} \left(\frac{m_\phi}{10^{-20}\,\mathrm{eV}}\right)^2 \,. \tag{5.25}$$

From the capture rate we can calculate the half-life with Eq. 2.41. For ^{136}Xe, the half-life for the capture mode is given by

$$T^{1/2,^{136}\mathrm{Xe}}_{0\nu\beta\beta\phi} = \frac{\log(2)}{\Gamma^{\mathrm{cap}}_{0\nu\beta\beta\phi}} \simeq \frac{1.4 \times 10^{28}\,\mathrm{yr}}{\alpha g^2} \left(\frac{m_\phi}{10^{-20}\,\mathrm{eV}}\right)^2 . \tag{5.26}$$

From Eq. 5.25 we can see that the emission mode is strongly suppressed with respect to the capture mode for small scalar masses m_ϕ, which is associated with a larger number density. Moreover, Eq. 5.26 shows that the half-life is shorter for a smaller scalar mass m_ϕ. Hence, we can say that - within the regime of small scalar masses - a signal that looks like ordinary $0\nu\beta\beta$ might be induced by the capture mode without a Majorana neutrino mass being present in the zero-density vacuum Lagrangian. Of course, the limitation that the momentum transferred by the scalar ϕ cannot be larger than the experimental sensitivity still holds. Moreover, there is another way in which it would be possible to distinguish the two modes. However, for this one detection in experiments utilizing at least two different isotopes is necessary. This will be discussed in Sec. 5.2.3.

5.2.3 Distinguishing the mechanisms by measuring in different isotopes

In Sec. 5.1, we said that it is impossible to distinguish the ϕ capture mode from standard $0\nu\beta\beta$ as long as the energy carried by the scalar is smaller than the experimental resolution of the energy. This is due to the fact that the single electron spectra and also the angular correlation of the two final state electrons are the same for the capture mode as for the standard LνEM. For both processes, the chiralities of all external fermions are equivalent. However, this is not the full truth. There is one way to distinguish these two modes: If we measure events with a $0\nu\beta\beta$ signature in experiments using (at least) two different isotopes, it is in principle possible to distinguish the two mechanisms as long as we are in the free phase. Therefore, let us briefly discuss this possibility here before we move on to the condensate phase. Since the neutrino potentials of the two processes are different, the way the half-life depends on the isotope used in experiment is different for the different mechanisms.

The idea to distinguish mechanisms mediating $0\nu\beta\beta$ by measuring in different isotopes is actually not new. Over the last twenty years there have been several studies addressing this topic [219–222]. Two recent ones are given in Refs. [213, 223]. Here, we will make use of the ratios of the decay rates (or the half-lives) for the different mechanisms as they were given in Ref. [213]. Using these ratios is also helpful to avoid one of the main problems that physicists usually face within the field of $0\nu\beta\beta$. There are various methods to calculate the NMEs and, unfortunately, the different frameworks tend to give values that are rather far away from each other. However, when using the ratios that we present in this section, the systematic effects are (at least partially) canceled out [223]. In principle, the ratios can be applied to distinguishing mechanisms as long as they are mediated by operators with different hadronic structures. The PSFs also contribute to some extent. Here, we will limit our discussion to the capture mode and standard $0\nu\beta\beta$ via the LνEM.

Similar to Eq. 3.7 in Ref. [213], we can define the half-life ratio

$$R_x({}^A Z) = \frac{T_x^{1/2}({}^A Z)}{T_x^{1/2}({}^{76}\mathrm{Ge})} = \frac{G_x({}^{76}\mathrm{Ge})\left|\mathcal{M}_x({}^{76}\mathrm{Ge})\right|^2}{G_x({}^A Z)\left|\mathcal{M}_x({}^A Z)\right|^2}\,, \tag{5.27}$$

where x denotes the mechanism and ${}^A Z$ is the isotope we consider. Here, we always normalize to the isotope ^{76}Ge as it is done in Ref. [213]. As before, the $G_x({}^A Z)$ are the PSFs corresponding to the isotope ${}^A Z$ and the $\mathcal{M}_x({}^A Z)$ are the NMEs. It can be seen that the PSFs and the NMEs depend on both the mechanism and the isotope. However, Eq. 5.27 is not sufficient to actually distinguish two mechanisms. For that, we need to compare two of these ratios, which we do by defining [213]

$$R_y^x({}^A Z) = \frac{R_x({}^A Z)}{R_y({}^A Z)}\,, \tag{5.28}$$

where x and y denote the two mechanisms we want to compare (in our case the ϕ capture mode and the LνEM). For a few different isotopes, we show the numerical values for the ratio given in Eq. 5.28 in Fig. 5.4. These values have been obtained with the Python tool νDoBe [224] and we used the NMEs calculated within the IBM2 framework. As expected, the ratio is one for ^{76}Ge since all the values are normalized to ^{76}Ge. However, for the other five isotopes that are shown the values are different. Therefore, it is in principle possible to distinguish the two mechanisms if we ever see $0\nu\beta\beta$ events in two different isotopes. From the experimental half-life estimates we can then calculate the ratios and compare with the expected ratios as given in Fig. 5.4. However, so far not a single $0\nu\beta\beta$ event has been measured. Even if $0\nu\beta\beta$ or the capture mode exists, we are still far away from the measurements needed to make this distinction. Nevertheless, if we overcome these difficulties, it is technically possible to distinguish the two mechanisms like this in the free phase even if the energy of the scalar is smaller than the experimental energy resolution.

While the mechanism we described in this section is the most promising way to distinguish the capture of a dark scalar from usual $0\nu\beta\beta$ it might not be the only one. Another rather obvious approach relies on the fact that the capture mode strongly depends on the local number density of the scalar. Within the condensate phase, it affects the effective Majorana neutrino mass and within the free phase it also affects the half-life (cf. Eqs. 5.21 and 5.26). Due to this dependence on the number density of the scalar it is possible that the half-life varies depending on where in the universe the measurement is performed if we assume that the density of the scalar is not the same everywhere. However, this is a rather academic consideration since it is quite unrealistic that $0\nu\beta\beta$ measurements will be performed anywhere besides on Earth within the next decades.

5.2.4 The capture mode at higher densities - condensate phase

From Eq. 5.26 it can be seen that one of the variables that govern the half-life is the number density of the scalar as given in Eq. 5.22. The higher the scalar number

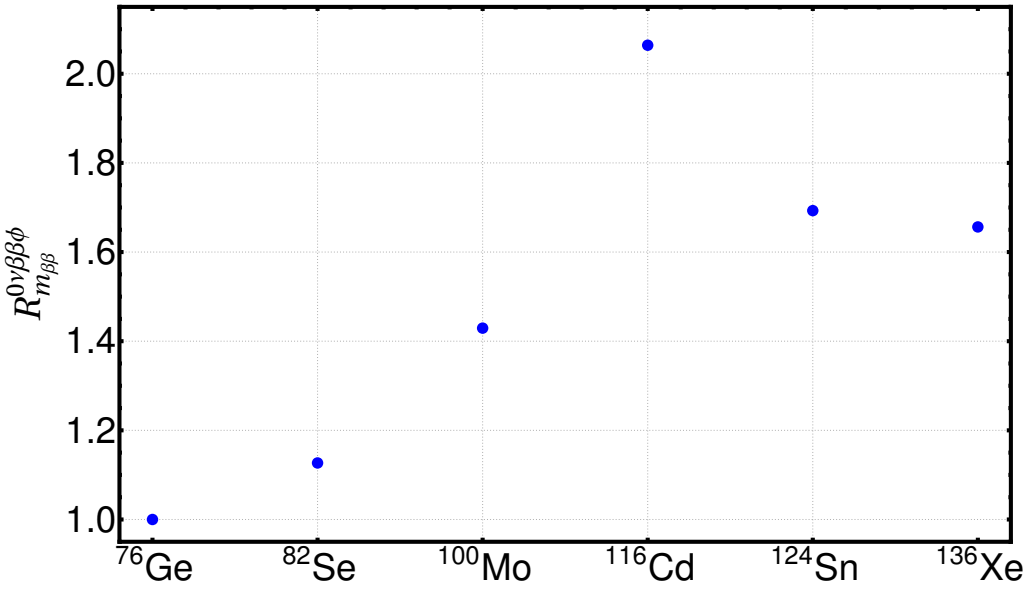

Figure 5.4: In this plot we show the variation of the half-life ratio as given in Eq. 5.28 for different isotopes. The two scenarios we consider here are the standard light-neutrino exchange mechanism and the scalar capture scenario proposed in this thesis. All of the data points were normalized to ^{76}Ge. The ratios have been obtained with the Python tool νDoBe [224].

density, the shorter the half-life and a shorter half-life makes detection more likely. Thus, a high scalar number density is in principle preferred for the capture mode. Since $\rho_{\rm DM}$ is fixed, the scalar number density can be increased either by increasing the fraction α of the total DM mass that ϕ accounts for or by a small scalar mass m_ϕ. However, the scalar number density cannot be increased indefinitely. For scalar masses $m_\phi \ll 1\,\text{eV}$, the perturbative treatment given above does not work anymore since ϕ will form a BE condensate as discussed in Sec. 5.2.1. The formation of such a condensate would result in an effective Majorana mass term for right-handed neutrinos, which comes from interactions with the medium. The critical temperature below which the condensate will form is given in Eq. 5.12. For simplification, we use Eq. 5.11 since the behavior we would get with Eq. 5.12 is not qualitatively different in the range we consider here. Then, the critical temperature can approximately be written as

$$T_C \approx 10^{30}\,\text{eV} \times \alpha \left(\frac{10^{-20}\,\text{eV}}{m_\phi}\right)^{(5/3)} . \tag{5.29}$$

If the temperature of the scalar T_ϕ is fixed, this equation can also be interpreted as a critical number density $n_{\phi,C}$. Or, in the case of a fixed mass density ($\rho_\phi = \alpha\rho_{\rm DM}$), it can be interpreted as a critical scalar mass $m_{\phi,\text{c}}$. The critical mass and the regions in which ϕ is in the free or in the condensate phase are shown in Fig. 5.5. There, we assumed that T_C does not exceed the energy resolution that typical $0\nu\beta\beta$ experiments of the next generation have. A good example for such an experiment is the Large Enriched Germanium Experiment for Neutrinoless $\beta\beta$ Decay (LEGEND) [225] and thus we require $T_C \lesssim 1\,\text{keV}$, which also sets a limit on the ranges of m_ϕ and T_ϕ that are shown in Fig. 5.5.

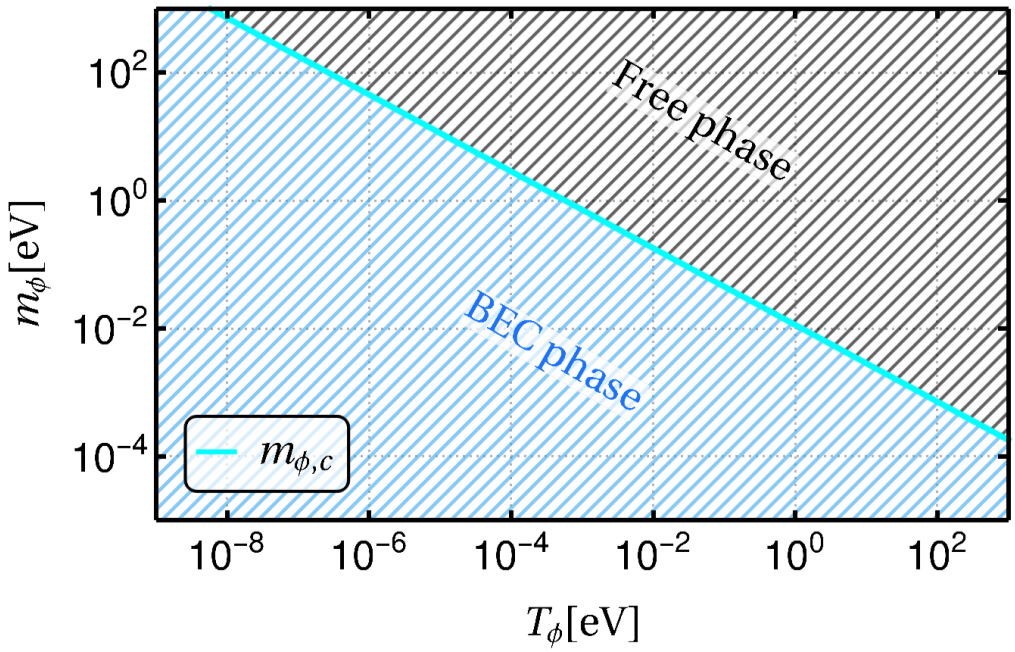

Figure 5.5: The critical scalar mass $m_{\phi,\mathrm{c}}$ for the transition from the free phase to the condensate phase is shown. Here, we assumed that the scalar mass density equals the local dark matter density $\rho_\phi = \rho_{\mathrm{DM}}$. Moreover, the results displayed here correspond to Eq. 5.11, which is a simplification. Taking the more accurate formula given in Eq. 5.12 would, however, not change the behavior qualitatively. For masses below $m_{\phi,\mathrm{c}}$, the scalar is in the condensate phase and for masses above $m_{\phi,\mathrm{c}}$ it is in the free phase. Moreover, we required that m_ϕ and T_ϕ are below the typical energy resolution of neutrinoless double-beta decay experiments ($\Delta E \approx \mathcal{O}(1\,\mathrm{keV})$ [225]). Also published in Ref. [3] (licensed under CC BY).

When the scalar is in the condensate phase, its ground state acquires an expectation value that is different from zero. Then, we can describe ϕ with a mean-field description as follows:

$$\phi = \frac{1}{\sqrt{2}} \left(\langle \phi_{\mathrm{cond}} \rangle + \phi_{\mathrm{exc}} \right) . \tag{5.30}$$

Here, ϕ_{cond} stands for the condensate in the ground state and ϕ_{exc} for excitations. In the limit of an ideal Bose gas, the absolute value of the expectation value for the ground state condensate is given by

$$| \langle \phi_{\mathrm{cond}} \rangle | = \sqrt{\frac{n_{\phi,\mathrm{cond}}}{2m_\phi}} . \tag{5.31}$$

As discussed already, we need to require a large number density such that the capture rate is considerably large. This large number density then translates into a critical temperature that is much larger than, e.g., the CMB temperature. Due to this, it is fair to assume that $T_\phi \ll T_C$ for decay rates that are large enough to detect them in experiments. In this case, ϕ can be completely described in terms of a BE condensate, which means

$$n_{\mathrm{cond},\phi} \simeq n_\phi - n_{\phi^\dagger} \quad \text{and} \quad n_{\phi,\mathrm{exc}} \simeq 0 . \tag{5.32}$$

Please note that we have to use the difference between the number density of ϕ and $\phi^\dagger$ here while we only used the number density of ϕ in the free phase. In the scalar medium, the ground state expectation value behaves like a vev that generates a Majorana mass for the right-handed neutrino. [204]

However, the expectation value given in Eq. 5.31 is not complete for the complex scalar that we have. Now, let us perform a proper treatment including the complex phase of the complex scalar ϕ. This treatment is taken from Ref. [4]. We can parameterize ϕ as

$$\phi = |\langle\phi\rangle| \exp(i\theta) \tag{5.33}$$

and, since our Lagrangian is invariant under the position-independent transformation [204]

$$\phi \to e^{-ix}\phi\,, \quad \phi^\dagger \to e^{ix}\phi^\dagger \quad x \in \mathbb{R}\,, \tag{5.34}$$

we can write the Noether current for our complex scalar as [204]

$$\mathcal{J}_\mu = -2\mathrm{Im}(\phi^* \partial_\mu \phi)\,. \tag{5.35}$$

From this we can get

$$n_\phi = \mathcal{J}_0 = -2|\langle\phi\rangle|^2 \partial_t \theta\,, \tag{5.36}$$

where t is the time. If we plug Eq. 5.31 into this, we arrive at

$$\partial_t \theta = -m_\phi\,. \tag{5.37}$$

Neglecting an additive constant that would only lead to a constant phase shift, integration gives

$$\theta = -m_\phi t \tag{5.38}$$

and therefore we can write

$$\phi = \sqrt{\frac{n_\phi}{2m_\phi}} \exp(-im_\phi t)\,. \tag{5.39}$$

Now that we have found this form, we can rewrite the interaction vertex for the interaction between the scalar and the right-handed neutrinos in Eq. 5.1 as follows:

$$\sqrt{\frac{n_\phi}{2m_\phi}} \exp(i\theta) g_{ij} \overline{\nu_{\mathrm{R},i}} \nu^C_{\mathrm{R},j}\,. \tag{5.40}$$

The scalar number density n_ϕ is given in Eq. 5.22 and the angle θ is time dependent and given in Eq. 5.38. This generates a complex-valued effective Majorana mass in the condensate phase. Therefore, the effects of the condensate are very similar to those of a Higgs scenario. The phase that rotates with time can be identified as a corresponding Goldstone mode. It follows that in the condensate phase we can fully describe the effects of the scalar in terms of an effective Majorana neutrino mass $m_{\beta\beta}$ for the electron neutrino. Here, the exchange of three sterile neutrinos gives an additional contribution, which needs to be included. This can be described in terms of a usual type 1 seesaw mechanism (see, e.g., Refs. [44,226,227] and Sec. 2.1). Given

the standard 2×2 mass matrix known from the seesaw mechanism (see Eq. 2.20), we can identify

$$m_{D,ij} = Y^{\nu}_{ij} \frac{v}{\sqrt{2}} \quad \text{and} \quad m_{R,ij} = 2\sqrt{\frac{n_\phi}{2m_\phi}} \exp(i\theta) g_{ij} \,. \tag{5.41}$$

Here, Y^{ν}_{ij} comes from the Yukawa interaction with the Higgs and v is the Higgs vev. With diagonal couplings we can write

$$m_{D,ij} = m_{D,i}\delta_{ij} \quad \text{and} \quad m_{R,ij} = 2\sqrt{\frac{n_\phi}{2m_\phi}} \exp(i\theta) g \delta_{ij} \,. \tag{5.42}$$

In this way, we do not need to diagonalize a 6×6 neutrino mass matrix including all three generations and are left with diagonalizing three separate 2×2 matrices that correspond to the usual type 1 seesaw matrix in Eq. 2.20. On top of that, the scenario of diagonal couplings conveniently forbids a possible neutrino decay channel $\nu_i \to \phi\nu_j$. Now we are able to rewrite the neutrino mass terms in the Lagrangian in matrix form as

$$\mathcal{L} \supset -\frac{1}{2}\overline{n^C_{L,i}} M_i n_{L,i} + \text{ h.c.}, \quad M_i = \begin{pmatrix} 0 & m_{D,i} \\ m_{D,i} & |m_R| \exp i\theta \end{pmatrix} , \tag{5.43}$$

where we introduced the left- and right-handed fields

$$n_{R,i} = \begin{pmatrix} \nu^C_{L,i} \\ \nu_{R,i} \end{pmatrix}, \quad n_{L,i} = n^C_{R,i} \,. \tag{5.44}$$

In Eq. 5.43, we also defined

$$|m_R| = g\sqrt{\frac{2n_\phi}{m_\phi}} \,. \tag{5.45}$$

In general, such a complex-valued type 1 seesaw matrix can be diagonalized making use of a unitary matrix [228, 229] such that

$$M_{i,\text{diag}} = \begin{pmatrix} m_i^- & 0 \\ 0 & m_i^+ \end{pmatrix} = S_i^T M_i S_i \,, \quad S_i^{-1} = S_i^\dagger \,, \tag{5.46}$$

where m_i^- and m_i^+ are real and non-negative. Therefore, we can also write the mass term in the Lagrangian in terms of the mass states $N_{L,i} = (N^-_{L,i}, N^+_{L,i})^T$, which fulfill

$$N_{L,i} = S_i^\dagger n_{L,i} \,. \tag{5.47}$$

The rewritten mass term is

$$\overline{n^C_{L,i}} M_i n_L = \overline{n^C_{L,i}} S_i^* S_i^T M_i S_i S_i^\dagger n_{L,i} = \overline{N^C_{L,i}} M_{i,\text{diag}} N_{L,i} \,. \tag{5.48}$$

Now we will look at the effects that the mechanism that has been described here has on neutrino mixing. The three sterile right-handed neutrinos that were introduced in our model will also change the neutrino mixing, which is usually described by the PMNS matrix U_{PMNS}. One of the standard parametrizations for this matrix is

given in Eq. 2.7. In the standard scenario with three neutrinos, the charged-current interaction between the neutrino mass states $\nu_{L,i}$ and the left-handed charged leptons $l_{L,\sigma}$ is given by

$$\overline{l_{L,\sigma}}\gamma^\mu(U_{\text{PMNS}})_{\sigma i}\nu_{L,i}\,. \tag{5.49}$$

Here, σ denotes the flavor of the charged leptons. We can denote this interaction term in terms of the effective mass states $N_{L,i} = (N^-_{L,i}, N^+_{L,i})^T$. For that, let us introduce the mixing matrices

$$\mathcal{V}^-_{\sigma i} = (U_{\text{PMNS}})_{\sigma i}(S_i)_{11}, \qquad \mathcal{V}^+_{\sigma i} = (U_{\text{PMNS}})_{\sigma i}(S_i)_{12} \tag{5.50}$$

for the light and heavy states. Please note that we do not sum over i here. Using this definition, the interaction term in Eq. 5.49 can be rewritten as

$$\begin{aligned}\sum_i \overline{l_{L,\sigma}}\gamma^\mu(U_{\text{PMNS}})_{\sigma i}\nu_{L,i} &= \sum_i \overline{l_{L,\sigma}}\gamma^\mu(U_{\text{PMNS}})_{\sigma i}\,(S_i)_{1j}\,(N_{L,i})_j \\ &= \sum_i \overline{l_{L,\sigma}}\gamma^\mu\left(\mathcal{V}^-_{\sigma i}N^-_{L,i} + \mathcal{V}^+_{\sigma i}N^+_{L,i}\right)\,,\end{aligned} \tag{5.51}$$

where $N^+_{L,i}$ and $N^-_{L,i}$ are the components of the effective mass states $N_{L,i}$ within the condensate.

The mixing angles θ_{ij} that are used to calculate the PMNS matrix (cf. Eq. 2.8) are fixed with the help of oscillation data [230]. Besides these, we need to know a few other parameters to determine m_i^+ and m_i^-. These are the parameters m_ϕ, g and α, which are relevant for the effective Majorana mass m_R of the right-handed neutrinos and the Dirac masses $m_{D,i}$. For the Dirac masses, we require that at $t = 0$ (or at $m_R = |m_R|$) the three light masses m_i^- fulfill the differences of the squared masses $\Delta m_{ij} = m_i^2 - m_j^2$ as they are observed in oscillation experiments. Then, the only free parameters that are leftover are the neutrino mass ordering, the two Majorana CP phases of the PMNS matrix and the smallest neutrino mass m_{min}.

In the end, we can write the corresponding half-life as [231]

$$\left(T^{1/2}_{0\nu\beta\beta}\right)^{-1} = g_A^4 G_{0\nu\beta\beta}\left|\sum_{i=1}^{3}(\mathcal{V}^-_{ei})^2\frac{m_i^-}{m_e}\mathcal{M}(0) + \sum_{i=4}^{6}(\mathcal{V}^+_{ei})^2\frac{m^+_{i-3}(n_\phi)}{m_e}\mathcal{M}(m_{\nu,i})\right|^2. \tag{5.52}$$

Here, m_e is the electron mass and for the NMEs we used a simple interpolation formula to display the mass dependence [231–234]:

$$\mathcal{M}(m_i) = \frac{4m_N^2|\mathcal{M}^{(9)}_\nu|}{\langle p^2\rangle + m_i^2} \quad \text{and} \quad \left\langle p^2\right\rangle = 4m_N^2\frac{|\mathcal{M}^{(9)}_\nu|}{|\mathcal{M}^{(3)}_\nu|}\,. \tag{5.53}$$

In this equation, m_N denotes the proton mass. In Eq. 5.53, we also used the NMEs $\mathcal{M}^{(3)}_\nu$ and $\mathcal{M}^{(9)}_\nu$. Details on these and on the interpolation itself are given in Appendix C.

The $0\nu\beta\beta$ half-life for ^{136}Xe in dependence on the scalar mass m_ϕ is shown in Fig. 5.6 for both NO and IO. The parameters g and α are both set to one. The Dirac CP phase is set to its best-fit value [39] and the Majorana CP phases are set to zero. For both NO and IO, the smallest neutrino mass m_{min} is varied within

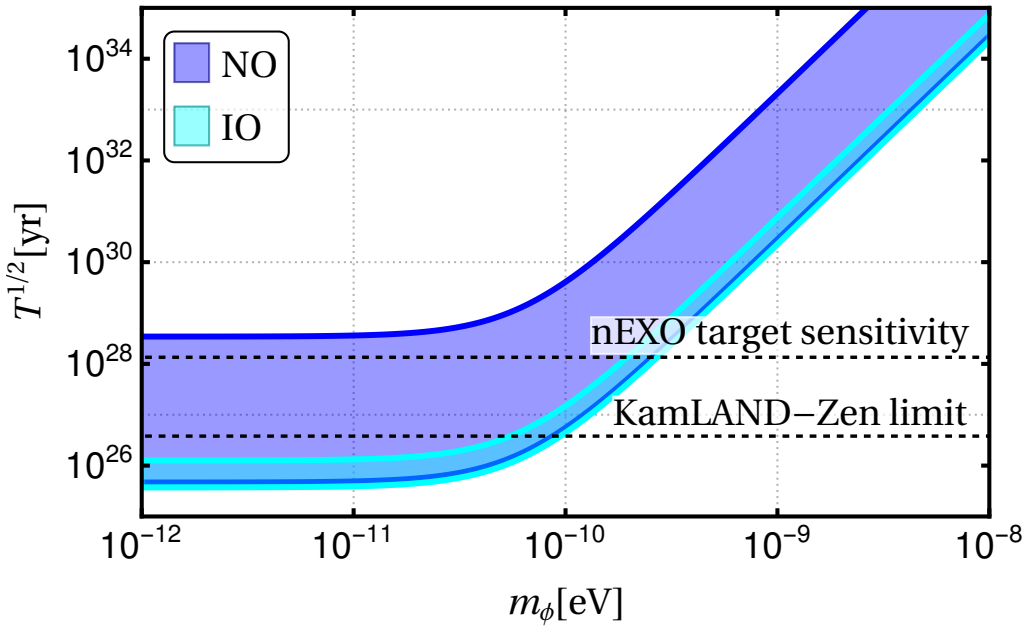

Figure 5.6: The half-life for $0\nu\beta\beta$ in ^{136}Xe within the condensate phase is shown in dependence on the scalar mass m_ϕ. For larger scalar masses (equivalent to smaller number densities of the scalar), neutrinos behave like pseudo-Dirac particles when they are in the medium. In this plot, we assumed $\alpha = g = 1$, the Majorana CP phases are set to zero and the Dirac CP phase is set to its best-fit value as it is given in Ref. [39]. The blue region is for normal ordering and the turquoise one represents inverted ordering. For both of them, the mass of the lightest neutrino is varied between zero (upper contours) and the highest value that is still in agreement with $\sum_{i=1}^{3} m_i < 260\,\text{meV}$ [39, 43] (lower contours). As a reference we also show the recent limit on the half-life set by KamLAND-Zen [139] and the expected sensitivity of nEXO [235]. Also published in Ref. [3] (licensed under CC BY).

the range that is currently allowed from cosmology ($\sum_{i=1}^{3} m_i \leq 260\,\text{meV}$ [39]). We can see that, for small masses (or, equivalently, larger scalar number densities), the standard half-life regime for the LνEM is reproduced. However, for larger masses (or smaller scalar number densities), the neutrinos behave like pseudo-Dirac particles. A pseudo-Dirac regime like this can be strongly constrained from cosmology and oscillation data [236], but it is not our main region of interest. For $m_\phi \lesssim 10^{-10}\,\text{eV}$ (with $g = \alpha = 1$), we get that active and sterile neutrinos actually decouple almost completely within our scenario.

5.3 Phenomenological implications beyond neutrinoless double beta decay

So far, we have only studied the influence that the complex scalar ϕ introduced in this thesis would have on $0\nu\beta\beta$. However, this is obviously not the full story. If we assume that a scalar carrying two units of lepton number couples to right-handed neutrinos, which, in turn, couple to left-handed neutrinos via the Dirac

mass insertion, this will have an impact on several other physical observables. One of these is the GR for which we will give a brief discussion in Ch. 6. Here, the focus will be on other processes and experiments that would be affected by our extension of the SM.

The first and most obvious class of experiments that might be influenced by the scalar are high-energy collider experiments. Since the scalar carries two units of lepton number, its emission would lead to a lepton number that differs from the expected one for a certain final state by an even number. For emission of the scalar, we would expect a characteristic production signature with two leptons carrying a lepton number of the same sign from an initial state that has a total lepton number of zero. On top of that, we would expect a process like this to come with missing energy and forward jets [237]. Such a signature is due to a ϕ generated in vector boson fusion processes, which carries away energy that manifests itself in the missing energy detected in the experiment. Emission of a lepton number carrying scalar ϕ can contribute to decay modes of different particles, some of which are

$$
\begin{aligned}
&\text{muon:} \quad \mu \to e\nu\nu\phi\,, \\
&\text{tau lepton:} \quad \tau \to e\nu\nu\phi, \mu\nu\nu\phi\,, \\
&\text{Higgs boson:} \quad h \to \nu\nu\phi\,, \\
&W \text{ boson:} \quad W \to \ell\nu\phi\,, \\
&Z \text{ boson:} \quad Z \to \nu\nu\phi\,, \\
&\text{charged mesons:} \quad P \to \ell\nu\phi \text{ with } P = \pi, K, D, D_S, B\,,
\end{aligned}
$$

where ℓ stands for a lepton. We did not indicate the charges and whether the participating particles are antiparticles since there are multiple possibilities. For example, if we look at the W boson there are the two possibilities $W^- \to \ell^- \nu_\ell \phi^\dagger$ and $W^+ \to \ell^+ \bar{\nu}_\ell \phi$ when assuming that not only lepton number but also lepton family number is conserved.

When neutrinos from a neutrino beam experiment interact with matter fields, emission of a scalar would alter the momentum distributions of the final state charged leptons, leaving us with a unique signature. While this might already be enough to distinguish the case where ϕ is present from the SM case, there is also the feature that the final state charged lepton has a wrong sign compared to the SM case. Due to the different behavior in magnetic fields, this could be detected in magnetized detectors like the Deep Underground Neutrino Experiment (DUNE) or the Main Injector Neutrino Oscillation Search (MINOS) [238]. Even though there are quite strict experimental limits, the combination of mass and coupling that we choose relaxes these constraints due to the fact that, within our model, the scalar only couples to the right-handed neutrinos directly, which then requires one or two insertions of the Dirac neutrino mass to couple to the active neutrinos.

Collider experiments are not the only probe besides $0\nu\beta\beta$ that would be influenced by the scalar. Another important field that is to some extent sensitive to its existence is the field of astrophysics and cosmology. The most important contribution here are neutrino self-interactions (NSIs). The ultra-light scalar we introduced in this work could induce a relevant amount of NSIs, leading to an impact on neutrinos, which originate from astrophysical sources and subsequently travel through the

cosmic neutrino background. Like this, the NSIs induced by the scalar could lead to distortions of the spectrum that are observable in IceCube [239, 240]. Moreover, the NSIs might impact the neutrino mixing patterns in environments that have different densities of the scalar. It is difficult to construct a model that is renormalizable and, at the same time, allows significant NSIs. Within the model proposed in this thesis, the scalar leads to both long- and short-range NSIs. The short-range interactions can take place in the condensate via an exchange of massive excitations [203]. It is possible that, during the epoch of recombination, neutrino free-streaming has been impacted by the NSIs. This could be a way to resolve Hubble tension [241–243]. As mentioned several times already, in our model the scalar only couples to the right-handed sterile neutrinos. Within the parameter region we are interested in, these sterile neutrinos are effectively decoupled from the active neutrinos. Thus bounds from, e.g., Big Bang nucleosynthesis or active-sterile oscillations are weakened significantly.

Next we want to have a look at BE condensate DM, which has been studied in several articles, see, e.g., Refs. [203, 244–247]. In our work, we do not consider that our scalar necessarily accounts for the full DM density. Therefore, limits that are deduced from gravitational effects, which are induced by the mass density of the scalar, can be relaxed in our case - as long as ϕ does not account for the total observed DM density (which is equivalent to $\alpha < 1$). In a similar way, bounds on the coupling g can, in most cases, be weakened significantly by increasing the number density n_ϕ unless these two parameters are constrained at once.

Let us mention one last possible implication of our model that might become important in the future, depending on future measurements of neutrino masses. As we already mentioned earlier, cosmology sets an upper limit on the sum of neutrino masses (see Sec. 2.1 where we gave the limit from Planck 2018 [43] that is widely used in the community). However, there are stronger limits. In the same publication that we took the value used in this thesis from [43], they get a value as low as 120 meV when combining multiple measurements. The limit published in Ref. [248] is even lower than that with

$$\sum_{i=1}^{3} m_i < 82\,\text{meV}\,. \tag{5.54}$$

On the other hand, we can get a lower limit from neutrino oscillations. The current best-fit values for Δm^2_{12} and Δm^2_{23} are given in Eqs. 2.11 and 2.12. Since the masses of the neutrinos have to be bigger than or equal to zero, we can directly translate the best-fit values for Δm^2_{12} and Δm^2_{23} into a lower limit on the sum of neutrino masses if we assume that the smallest mass (m_1 for NO and m_3 for IO) is equal to zero. This results in

$$\sum_{i=1}^{3} m_i \geq \begin{cases} 100\,\text{meV} & \text{for IO} \\ 59\,\text{meV} & \text{for NO} \end{cases}\,. \tag{5.55}$$

While the limit in Eq. 5.54 is so far not widely accepted in the community (and it would also be necessary to do a calculation that carefully considers the uncertainties), it is noticeable that possible stricter limits from cosmology might call for a scenario to resolve the tension if the lower limit from neutrino oscillations is ever larger than the upper limit from cosmology in the future. In principle, the complex

scalar that was presented in this thesis might help alleviate this tension. If there was a larger scalar density in the early universe, this would have lead to a larger effective mass for the right-handed neutrinos and, consequently, to a smaller mass of the active neutrinos. Due to the expansion of the universe until today, the density of the scalar may have decreased, leading to larger active neutrino masses, which we can measure in neutrino oscillations today. Therefore, if there is a discrepancy between the limits on neutrino masses from cosmology and oscillations in the future, it might be worth it to consider a model similar to the one we presented in this thesis to resolve the problem.

5.4 Capture of dark vector bosons and fermions

So far we have focused on the capture of a complex scalar that can account for part of the DM observed in the universe. Nonetheless, the dark sector can also contain dark vector bosons and dark fermions [249]. In this section, we will briefly discuss these two cases without performing a full study.

Let us start with the capture of dark vector bosons. Just like the scalar we discussed in this chapter, the vector bosons follow the BE statistics given in Eq. 5.8. Because of that, the vector bosons can also undergo BE condensation and thus form a condensate. It differs from the scalar as its Lorentz structure is different to the one of the scalar. Therefore, a vector interaction cannot induce a standard fermion mass term from the expectation value of the vector boson. However, it can give a refractive mass term from elastic forward scattering to neutrinos that are coupled to the vector background field [210]. We do not expect a qualitative difference for $0\nu\beta\beta$ induced by the capture of a vector boson compared to the capture of the scalar discussed in this thesis.

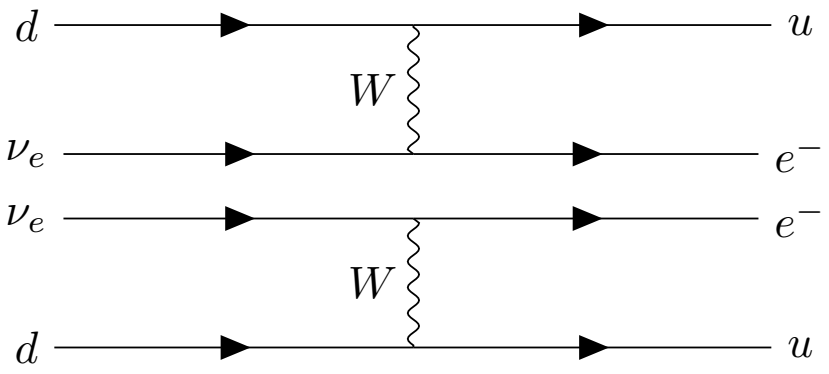

Figure 5.7: Capture of two (electron) neutrinos in double beta decay. As for $0\nu\beta\beta$, there are no neutrinos in the final state. This process is allowed within the Standard Model and it does not violate lepton number conversation.

For dark fermions, the situation is a bit different. For fermions, the possibility of seeing a $0\nu\beta\beta$ signal without a Majorana neutrino mass is actually covered by the SM (see also Ch. 1). The relevant process is the capture of two relic neutrinos that is shown in Fig. 5.7. This process has previously been studied in Refs. [29, 30].

Within the Standard Model, the capture of two electron neutrinos would lead to a signature like the one we would expect in $0\nu\beta\beta$. However, the same caveat as for the capture of the scalar is relevant: If the two neutrinos carry more energy than the experimental energy resolution, it is possible to distinguish the double neutrino capture mode from $0\nu\beta\beta$. All these discussions are of rather theoretical nature. For a hypothetical experiment using ^{100}Mo [250], the authors of Ref. [29] find the expected number of capture events to be

$$N_{\text{cap}}^{^{100}\text{Mo}} \approx 1.0 \times 10^{-48} n_{\nu_{\text{relic}}}^2 \,\text{yr}^{-1}\,, \tag{5.56}$$

given that the detector is made from one ton ^{100}Mo. Here, $n_{\nu_{\text{relic}}}$ is the number density of one flavor of relic neutrinos (or antineutrinos), which is expected to be [29]

$$\langle n_{\nu_{\text{relic}}} \rangle \approx 56\,\text{cm}^{-3}\,. \tag{5.57}$$

The expected event number is clearly too small for the process to be observed in any available experiment.

One way to increase the amount of double capture events would be to assume that the measurement takes place in a region where the relic neutrinos are clustering and thus have an increased density. However, due to the Pauli exclusion principle that holds for fermions we cannot increase the density of the relic neutrinos indefinitely. For a degenerate fermion gas, the maximum number density is known to be [251]

$$n_{\text{max}} = \frac{g_s}{(2\pi)^3} \frac{4}{3} \pi p_{\text{max}}^3 \tag{5.58}$$

for momenta $p < p_{\text{max}}$. Here, g_s is the number of spin degrees of freedom; we assume $g_s = 2$. From Eq. 5.58 we can see that putting an upper limit on the number density of a fermion is equivalent to putting an upper limit on the maximal momentum p_{max}. A natural choice for this upper bound for massless fermions is to to assume that the energy density of the fermions should not be larger than the average energy density of the CMB photons, which is $\rho_\gamma \simeq 260\,\text{meV/cm}^3$ [39]. From this, we can get

$$n_{\text{max}}^{\text{massless}} \approx 4 \times 10^3\,\text{cm}^{-3}\,. \tag{5.59}$$

For massive fermions, on the other hand, it is more reasonable to assume that the mass density should not exceed the local dark matter density. Then we can use the Tremaine-Gunn bound [252], which gives a lower limit for the mass of fermionic DM bound in a galactic halo. This lower limit is $m \gtrsim \mathcal{O}(100\,\text{eV})$. Moreover, according to the Tremaine-Gunn bound, we can also require that p_{max} is smaller than the escape velocity of typical galaxies, leading to an upper limit of

$$n_{\text{max}}^{\text{massive}} \approx 3 \times 10^6\,\text{cm}^{-3} \tag{5.60}$$

on the fermionic number density.

In principle, it is possible to relax these bounds by introducing more fermion species as it is done in Ref. [253] and thus evade Pauli exclusion to some extent. However, the number of species that would be required scales with $N_F \gtrsim (100\,\text{eV}/m_f)^4$ [253] and thus we would need to introduce $N_F \gtrsim 10^{21}$ fermionic species

to get local number densities of $n_f / \langle n_\nu \rangle \approx 10^{10}$. We can see that - to get observable half-lives for a fermionic capture model - we would either have to introduce a large amount of fermionic DM species or the interaction cross section would need to be much larger than for the capture of the relic neutrinos. On top of that, such scenarios would be expected to change the outcome of beta decay experiments like the Karlsruhe Tritium Neutrino Experiment (KATRIN) [29, 30, 254].

5.5 Conclusion

In this chapter, we studied the possibility that the underlying mechanism of a $0\nu\beta\beta$ signal, which might be found in future experiments, is the capture of a lepton number carrying scalar. As long as the energy carried by the scalar is smaller than the experimental resolution, the capture mode and ordinary $0\nu\beta\beta$ are practically indistinguishable in experiment. With this, there is no LNV physics and Majorana neutrino mass necessary in the zero-density vacuum Lagrangian (a possible Lagrangian facilitating the capture with these properties is given in Eq. 5.1). This scenario is theoretically interesting because it is able to circumvent the well-known Schechter-Valle theorem (cf. Sec. 2.4.1). Within our analysis, we found that this scenario is in principle feasible, but also sensitive to the density of the scalar. At high densities, the scalar can form a BE condensate, leading to an effective Majorana neutrino mass within the medium. We want to stress, however, that in the vacuum Lagrangian there is still no Majorana neutrino mass. Both the behavior in the free phase and in the condensate phase have been discussed in detail. Within this chapter, we also described a possibility how we could still distinguish the different mechanisms in the free phase even if the energy carried by the scalar is smaller than the experimental resolution. This would require that $0\nu\beta\beta$ is detected in experiments using (at least) two different isotopes. Moreover, we discussed phenomenological implications that our model and the existence of a complex scalar carrying two units of lepton number would have beyond $0\nu\beta\beta$ and we briefly looked into modified settings where, instead of a scalar, a dark vector boson or fermion would be captured.

Even though the observations we made in this project are theoretically interesting, we found that the capture rate of the scalar would be too low to be measured in future experiments if we require that the density of the scalar is low enough such that the scalar is still in the free phase. Therefore, to generate a signal that can realistically be measured in experiment, the density of the scalar needs to be high enough. In this case, we will always be in the condensate phase and neutrinos will, in fact, acquire an effective Majorana mass in the medium, where $B - L$ symmetry is then effectively broken. With this, the connection between the detection of $0\nu\beta\beta$ and a Majorana neutrino mass as we know it from the Schechter-Valle theorem is restored for realistically testable half-lives of $0\nu\beta\beta$. However, we want to stress here that the reasons for its validity within the medium are more subtle and also different from the ones in the usual $0\nu\beta\beta$ scenarios.

6

Influence of the complex scalar on Glashow resonance measurements in neutrino telescopes

Now that we have discussed the two main topics of this thesis, let us see how they are connected. The first project the author worked on was aiming to infer the type of astrophysical neutrino source that neutrinos are emitted from. To achieve this, we used the GR candidate event that was measured in IceCube so far. This project heavily relied on the ratio between the number of neutrinos and the number of antineutrinos that a certain source emits to distinguish the different sources. The calculation and results are summarized in Ch. 3. They were published in Ref. [1] before. The second topic deals with the question whether a complex scalar ϕ that carries two units of lepton number can induce a $0\nu\beta\beta$ signal without an actual Majorana neutrino mass or lepton number violation being present in the zero-density vacuum Lagrangian. We found that, under certain circumstances, the capture of such a scalar can indeed lead to an experimental signal, which we would normally expect from $0\nu\beta\beta$. All of this is described in detail in Ch. 5 and it is based on Ref. [3] and partly on Ref. [4].

When the complex scalar ϕ, which behaves according to the Lagrangian given in Eq. 5.1, interacts with right-handed (anti-)neutrinos, it can change a neutrino into an antineutrino and vice versa. For left-handed neutrinos, at least one or two additional Dirac mass insertions are needed. Obviously, if the scalar exists, this effect would not only take place in a $0\nu\beta\beta$-like situation but also when a neutrino or antineutrino that comes from an astrophysical source moves through a medium of ϕ (or $\phi^\dagger$). Moreover, emission of one or more scalar(s) might be relevant even if the neutrinos are propagating in a vacuum. Implications that it would have on other physical processes beyond $0\nu\beta\beta$ are discussed in Sec. 5.3. A possible setup

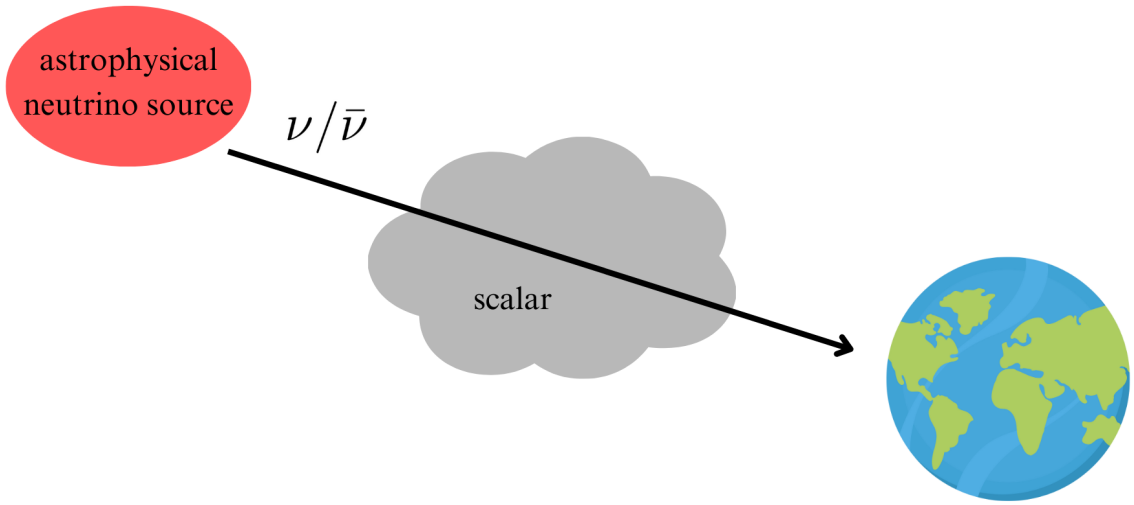

Figure 6.1: A scenario that is discussed in this chapter. The neutrinos and antineutrinos that are produced by an astrophysical neutrino source travel to Earth before they can be detected in neutrino telescopes such as IceCube. If the complex scalar that was introduced in Ch. 5 exists and the (anti-)neutrino flies through an area where a certain density of the complex scalar is prevalent, this might change the ν:$\bar{\nu}$ ratio that is measured on Earth. Therefore, it can in principle have an influence on the events measured via the Glashow resonance (cf. Ch. 3). Figure made with Canva [255].

is shown in Fig. 6.1, where a neutrino source emits (anti-)neutrinos, which then fly through a cloud containing the scalar before they reach a detector like, e.g., IceCube on Earth. In principle, the cloud of the scalar can also enclose the Earth, the astrophysical neutrino source or both as long as the neutrinos fly through the medium at some point on their way to Earth. Another scenario is, as mentioned before, that the (anti-)neutrino emits some amount of scalars ϕ or $\phi^\dagger$ on its way to Earth. Both these scenarios might have an influence on the ratio between neutrinos and antineutrinos that originate from an astrophysical source and that arrive at IceCube or another neutrino telescope and thus, if such a scalar exists, it does make sense to think about its influence on our results. In this chapter, we will discuss a few possible scenarios qualitatively and find that the influence of the scalar on the measurement of GR candidate events should not be large. However, a proper quantitative treatment is left for future work.

Let us start with the behavior in the free phase. Here, we will discuss how the scalar could affect the $\overline{\nu}_e$ fraction $f^{\mathrm{E}}_{\overline{\nu}_e}$ that arrives on Earth in general. One observation that can be made is that an odd number of external scalars (capture or emission) can change between neutrino and antineutrino. This is due to the fact that the net change in lepton number has to be ± 2. However, it is crucial to carefully take into account which process is allowed kinematically. For example, let us start with the case where we have only one external scalar. The capture mode ($\nu\phi^\dagger \to \bar{\nu}$, $\bar{\nu}\phi \to \nu$) is forbidden due to kinematics (unless the initial state (anti-)neutrino is lighter than the final state one and the mass and momentum of the captured scalar is such that on-shell production of the final state (anti-)neutrino

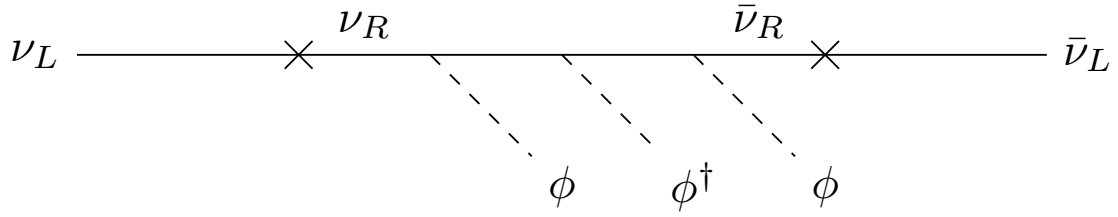

Figure 6.2: Feynman diagram for an example process with more than one external scalar that contributes to the change in the $\overline{\nu}_e$ fraction $f^{\mathrm{E}}_{\overline{\nu}_e}$. Here, the emission of three scalars is shown, which leads to an overall change of two units for the lepton number. As long as the process is allowed kinematically, we could also consider the capture of a scalar/several scalars instead of the emission. Here, we need two mass insertions since the scalars only couple to right-handed neutrinos.

works out; however, this is a rather theoretical consideration). Also, the emission mode ($\nu \to \bar{\nu}\phi$, $\bar{\nu} \to \nu\phi^\dagger$) is only allowed if the final state (anti-)neutrino is lighter than the one in the initial state [256] (see Sec. 5.2.4 as well). Therefore, this is strongly dependent on the choice of g_{ij}. For more than one external scalar, the situation is not so different. It is still important to check carefully whether a certain process is kinematically allowed. An example for a process that is allowed as long as the masses work out is given in Fig. 6.2. However, all these processes will most likely be suppressed due to the necessary mass insertions and the momentum in the propagators. Nonetheless, a quantitative analysis should be performed to properly judge the impact such processes have on the measurement of GR candidate events in neutrino telescopes. Neutrino decay with the emission of a scalar, Majoron or singlet Higgs has been discussed in various models before, see, e.g., Refs. [257–260]

Such emission and capture processes can happen in both directions, i.e., from neutrinos to antineutrinos and the other way around. For the capture modes, it does depend on the background though. Naively, we could think that therefore the processes in the two directions should not change much overall. However, this is only partially true. If we consider the μ-damped pγ source, we expect $f^{\mathrm{E}}_{\overline{\nu}_e} \approx 0$. In such a case, the situation is not symmetric and the interaction with the complex scalar might lead to the appearance of GR candidate events where we would usually expect to see no such events.

Besides the change in $f^{\mathrm{E}}_{\overline{\nu}_e}$, the scalar could also lead to another effect that might affect the GR. Since the GR only happens at quite high energies of the incoming electron antineutrino, it may not happen anymore if too much energy is lost on the way to Earth due to the emission of scalars or scattering with the scalars in general. Capture of scalars does not play a role for this as long as the scalar background does not carry too much energy - if we stick with the assumption that the energy it carries is less than the experimental resolution in IceCube that we used in Ch. 5, this is definitely true. Therefore, a sensitive study should also include how the expected amount of measured GR candidate events changes due to the loss of energy. As before, we do expect that the effects are not too large. Here, the energy loss is not exclusive to an odd number of external scalars. If the emission of two scalars carries away too much energy such that the energy is below the energy that is needed for the

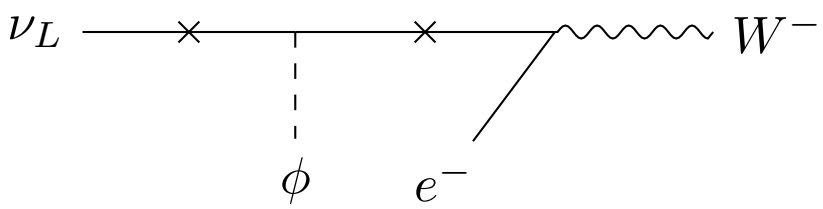

Figure 6.3: Feynman diagram for the Glashow resonance process with an extra external scalar ϕ. Since the model is such that the ϕ only couples to the right-handed neutrinos, two mass insertions are needed. Like this, an incoming left-handed neutrino can induce a process that is similar to the Glashow resonance. In this Feynman diagram, the ϕ symbolizes either an incoming $\phi^\dagger$ or an outgoing ϕ such that $B - L$ is conserved. The W boson will subsequently decay to other particles.

GR, the number of GR candidate events is potentially reduced as well. Technically, emission processes might also reduce the energy of neutrinos with an energy above the GR energy such that they can induce a GR candidate event. However, we expect this to be less relevant since the flux decreases with higher neutrino energies (cf. Fig. 2.2).

Please note that the scalar can mediate a GR-like process also for an incoming neutrino. If a neutrino arrives to IceCube, the two processes

$$\nu + e^- + \phi^\dagger \to W^- \to \dots \quad \text{and} \quad \nu + e^- \to W^- + \phi \to \dots \tag{6.1}$$

are allowed. A Feynman diagram is shown in Fig. 6.3. While this is not really different from what we considered before, we do not need to require that the intermediate antineutrino is on-shell here. The incoming particle can be a left-handed neutrino, which couples to a scalar (either an incoming $\phi^\dagger$ or an outgoing ϕ) via a Dirac mass insertion and then, via another Dirac mass insertion, the resulting anti-neutrino can couple to the electron and produce a W boson, which will subsequently decay. Of course, the antineutrino needs to be of electron flavor since we still assume that the coupling to the W boson is the one from the SM. If the antineutrino also has the correct energy, an on-shell W boson can be produced. However, we do not expect such processes to have a huge influence since they are suppressed due to the mass insertions.

Now, let us briefly have a look at the condensate phase. As discussed in Sec. 5.2.4, the neutrino gets an effective Majorana mass while it is in an area where the density of the scalar is large enough for a BE condensate to form. In some sense, the phenomenology of such a setting is not as interesting as in the free phase since the behavior would be the same as for a Majorana mass that is not induced by the existence of our scalar. Here, we want to mention Refs. [184,185] again: If neutrinos have a Majorana mass, their magnetic moment allows for conversion of neutrinos and antineutrinos, which, in turn, can lead to changes in $f^{\mathrm{E}}_{\overline{\nu}_e}$. A strong magnetic field would facilitate these interconversions. Of course, for this to be feasible, the strong magnetic field has to be inside a cloud of our scalar condensate. For example, there might be an accretion of a scalar background around a magnetar. All in all, it is fair to say that, in the condensate phase, the behavior does not only depend on the scalar but also on a magnetic field that might be present at the same time.

7

Summary and conclusion

Back in 1930, when Pauli first came up with the idea of an additional neutral particle that is emitted in beta decay, nobody knew what rich phenomenology was hidden behind it. In this thesis, we looked into two different rare events that can teach us a lot about neutrinos and their sources. Moreover, we also looked at a connection between the two scenarios.

In Ch. 3, we described how the famous GR can be used to distinguish different astrophysical neutrino sources. Here, we chose the ideal pp, pγ and μ-damped pγ source. Moreover, we included a pγ source with an equal mixture of single- and multi-pion production. Before we started with the actual analysis, we first calculated higher-order corrections to the GR cross section. Once future experiments have measured more GR candidate events, it will be more and more relevant to know the cross section precisely. Therefore, we also published the values for the cross section that takes DB and ISR into account alongside the corresponding paper. We found that the two corrections combined lead to a reduction of the peak by about 30% as well as a so-called radiative return, which is caused by the ISR. After incorporating these two corrections, we introduced two flux models that we used in our analysis, namely the single power law flux model with and without an exponential energy cutoff. With these prerequisites, we were able to perform both a Bayesian and a frequentist analysis. For this analysis, the relevant variable is the $\overline{\nu}_e$ fraction $f^{\mathrm{E}}_{\overline{\nu}_e}$ and for the different source types we expect different values of $f^{\mathrm{E}}_{\overline{\nu}_e}$. The main result of this project is given in Fig. 3.7. While we cannot make strong claims yet due to the fact that only one GR candidate event has been measured so far, we can exclude the ideal μ-damped pγ source at around 2σ for all cases (flux model and Bayesian/frequentist analysis). Out of all the ideal sources, the ideal pp source is slightly favored. However, it will be necessary to redo such an analysis once more GR candidate events have been measured in experiment. For now, we did a few projections for future measurements of IceCube-Gen2. Here, we

find that for the neutrino flux model without a cutoff ten years of runtime would be sufficient to distinguish between the ideal pp and pγ source at 2σ level. With the exponential cutoff, a longer runtime would be required. While we only took into account IceCube-Gen2, it is not the only neutrino telescope that will be build in the future. Our calculation can also be applied to other neutrino telescopes and to a combination of different experiments. This would lead to a larger effective volume overall and thus the runtime that is needed for certain distinctions would decrease for a study that combines all future neutrino telescopes.

We also looked into different BSM models that could have an influence on GR measurements in Ch. 4 and introduced a complex scalar, which could, in principle, also change the $\overline{\nu}_e$ fraction $f^{\mathrm{E}}_{\overline{\nu}_e}$. In Ch. 5, we presented a proof-of concept showing that a $0\nu\beta\beta$ signal could be induced by the capture of the complex scalar as well. Since this scalar carries two units of lepton number, the capture process conserves lepton number. Moreover, in the zero-density vacuum, the neutrinos do not acquire a Majorana mass. In this thesis, we have discussed how we can circumvent the famous Schechter-Valle theorem with the help of such a scalar. As long as the energy of the captured scalar is smaller than the energy resolution of the experiment, a future $0\nu\beta\beta$ signal could also come from the capture of such a scalar. In this case, the detection of such a signal would not immediately imply that neutrinos have a Majorana mass. We want to stress here once again that we do not claim that the Schechter-Valle theorem is wrong. It just does not apply in our case due to the additional external particle. While $0\nu\beta\beta$ with emission of other particles (oftentimes a Majoron) has been discussed in the literature, this possibility has been overlooked so far. For our causes, it is, however, crucial that we look at capture and not at emission since the PSF is different for the emission and it can thus be distinguished from standard $0\nu\beta\beta$ via, e.g., the LνEM. Besides these general considerations, we also addressed some subtleties in Ch. 5. The most important one is that our scalar will form a BE condensate if its density is large. For the capture process to be possible, we need it to happen within a background of our scalar and the capture rate strongly depends on the density of the scalar. We found that the capture rate will be too small (and thus the half-life too large) to be detectable in any experiments that are in reach so far if the density of the scalar is such that the scalar does not form a BE condensate. If we allow for the scalar to form a BE condensate and thus the density to be large enough such that a detection would not be unrealistic, the scalar acquires an in-medium expectation value, leading to an effective Majorana neutrino mass. While this is basically the same as a normal Majorana mass as long as we are within the medium, let us stress that the mechanism behind it is still different and it does not make use of a Majorana neutrino mass within the vacuum Lagrangian. Besides that, we also discussed how the capture mode can still be distinguished from the $0\nu\beta\beta$ if a signal is ever found in experiment. While the signal will look the same when it is first measured, enough statistics and measurements in different isotopes will help to distinguish the different mechanisms that could be the underlying one. Then, we also discussed other phenomenological implications that the existence of such a scalar would have and we briefly looked into the capture of dark fermions and vector bosons.

While the two different topics the author worked on during her PhD studies

may at first glance seem to be quite different, they are still connected. In Ch. 6, we discussed how the existence of the complex scalar would affect the measurement of GR candidate events qualitatively. In the condensate phase, the behavior is similar to the behavior of Majorana neutrinos. In the free phase, several different processes can have an effect since the capture or emission of an odd number of scalars would change neutrinos into antineutrinos and vice versa, which affects the $\overline{\nu}_e$ fraction $f^{\mathrm{E}}_{\overline{\nu}_e}$. However, it is important to be cautious about whether or not a process is kinematically allowed. Moreover, all of these processes are suppressed by at least two Dirac mass insertions since the scalar only couples to right-handed neutrinos in our model. Overall, we can see that the variable $f^{\mathrm{E}}_{\overline{\nu}_e}$ - which is the most important variable for the analysis we performed to infer the neutrino sources from the GR - is strongly entangled with other parameters once we introduce new physics.

In general, the observation and also the non-observation of rare events can yield rich information on the origin and also on the properties of neutrinos. This shows how valuable searches for events like the GR or the $0\nu\beta\beta$ can be even though they are difficult. While IceCube has already detected a GR candidate event, we want to stress that the non-observation of such candidate events would have also conveyed valuable information. For the case of the GR within the framework of our analysis, it would have been a strong hint towards the μ-damped pγ source. In the case of $0\nu\beta\beta$, the non-observation we see so far points towards the non-existence of a Majorana neutrino mass. However, the current lower limit for the half-life that is set by experiments is not even close to the one that has been calculated for the double capture of relic neutrinos, which is the background process that is allowed within the SM.

In this thesis, we took a detailed look at two aspects of what we can learn from such measurements and, in the case of the $0\nu\beta\beta$ induced by the capture, also where we might need to be cautious when interpreting experimental results that we might see in the future. For the GR, we showed how these measurements can be used to infer information on astrophysical neutrino sources and did the calculation for the one GR candidate event that IceCube found so far. In the future, if more such candidate events have been found in neutrino telescopes, this calculation can be redone to find stronger constraints on $f^{\mathrm{E}}_{\overline{\nu}_e}$, which can, in turn, be used to identify astrophysical neutrino sources.

As we discussed, there might also be BSM effects that influence this variable. An example is the complex scalar that we introduced here in connection with $0\nu\beta\beta$. Besides this, we extended the understanding of the LNV process $0\nu\beta\beta$ by presenting a proof-of-concept that a possible future $0\nu\beta\beta$ signal does not necessarily mean that neutrinos have a Majorana mass in the zero-density vacuum. Here, we proposed the capture, which has barely been studied in the literature so far, especially compared to the well-studied emission mode. While we focused on a small fraction of neutrino physics, we have seen that this small part already comes with a very rich phenomenology and that there is still much to learn.

In the beginning of this thesis, we quoted Pauli where he said that, by proposing the neutrino, he has "done something very bad" since the neutrino "cannot be detected". Now we have seen that, while he was right with his proposal that a second particle should be emitted in beta decay, this statement is not correct. In

fact, he opened the door to the broad world of neutrino physics. However, he is in good company with that: Albert Einstein once called the cosmological constant he introduced the "biggest blunder" of his life [261]. Today, the cosmological constant is part of the standard cosmological model.

Acknowledgments

First of all, I would like to thank my supervisor Prof. Manfred Lindner for giving me the opportunity to be a part of his group at the Max-Planck-Institut für Kernphysik and to work on up-to-date neutrino physics. Without him, this work would not have been possible. Moreover, I would like to thank my second supervisor Priv.-Doz. Werner Rodejohann and my third supervisor Dr. Florian Goertz for always being there and for their helpful advice. I would also like to thank Prof. Joerg Jaeckel for being the second referee and Prof. Matthias Bartelmann and Prof. Belina von Krosigk for being part of the examination committee. Furthermore, I would like to thank Dr. Ting Cheng, Oliver Scholer and Musa Rajamov for proofreading this thesis.

Next, I would like to thank the people I was working with in the last years, my collaborators Dr. Lukáš Gráf, Dr. Guo-yuan Huang, Dr. Sudip Jana, Oliver Scholer and Dr. Manibrata Sen. I am very grateful for all the discussions we had and for everything I learned from you. Moreover, I would like to thank all my friends at the institute for making this time so special, for the chats in the hallway, for organizational advice and in general for the supportive atmosphere in our group. Special thanks to my office mate Dr. Ting Cheng. It would not have been the same without you.

Science cannot be done without the people organizing everything around it. I would like to thank Anja Berneiser and Britta Schwarz for everything they did to keep this group running smoothly in the past years and for always looking out for us PhD students.

During the years in Heidelberg, I also found some wonderful friends outside of physics. Thanks to Bonyad, Darya, Julius, Line, Lukas, Marla, Miriam, Paula, Sophie, Soraya and others for everything we experienced together. I will always have fond memories of my time here.

I am also deeply indebted to my parents Anne and Thomas and my brother Mats for all their moral support not only during these last years but during my whole studies. And, last but not least, to Musa, for always being there for me.

List of abbreviations

$0\nu\beta\beta$ neutrinoless double beta decay

$2\nu\beta\beta$ two-neutrino double beta decay

AMANDA Antarctic Muon And Neutrino Detector Array

ANTARES Astronomy with a Neutrino Telescope and Abyss environmental RE-Search project

ARCA Astroparticle Research with Cosmics in the Abyss

Baikal-GVD Baikal Gigaton Volume Detector

BE Bose-Einstein

BSM beyond the Standard Model

CC charged current

CMB cosmic microwave background

CNO carbon-nitrogen-oxygen

COM center-of-mass

CP charge conjugation parity

CUORE Cryogenic Underground Observatory for Rare Events

DB Doppler broadening

DIS deep inelastic scattering

DM dark matter

DUMAND Deep Underwater Muon And Neutrino Detector

DUNE Deep Underground Neutrino Experiment

EFT effective field theory

EXO Enriched Xenon Observatory

GERDA GERmanium Detector Array

GR Glashow resonance

HESE high energy starting event

IBM2 Interacting Boson Model-2

IO inverted ordering

ISR initial state radiation

KamLAND Kamioka Liquid Scintillator Antineutrino Detector

KamLAND-Zen KamLAND ZEro-Neutrino double-beta decay

KATRIN Karlsruhe Tritium Neutrino Experiment

KM3NeT Cubic Kilometre Neutrino Telescope

LECs low-energy constants

LEGEND Large Enriched Germanium Experiment for Neutrinoless $\beta\beta$ Decay

LEP Large Electron-Positron Collider

LνEM light-neutrino exchange mechanism

LNV lepton number violating

MINOS Main Injector Neutrino Oscillation Search

NC neutral current

NEMO NEutrino Mediterranean Observatory

NESTOR Neutrino Extended Submarine Telescope with Oceanographic Research Project

nEXO next EXO

NME nuclear matrix element

NO normal ordering

NOνA NuMi Off-Axis ν_e Appearance

NT-200 Neutrino Telescope 200

NSIs neutrino self-interactions

ORCA Oscillation Research with Cosmics in the Abyss

P-ONE Pacific Ocean Neutrino Experiment

PDF probability density function

PEPE PeV energy partially contained event

PMNS Pontecorvo-Maki-Nakagawa-Sakata

PMT photomultiplier tube

PSF phase space factor

QFT quantum field theory

SM Standard Model

TAMBO Tau Air Shower Mountain-Based Observatory

TRIDENT The tRopIcal DEep-sea Neutrino Telescope

UHE ultrahigh-energy

vev vacuum expectation value

A

Electron velocity distribution in atoms

In Sec. 3.1.2, we used the electron velocity distributions of electrons in atoms to calculate the distributions averaged over the electrons in a molecule. However, we did not discuss how to calculate the electron velocity distributions of electrons in a given orbital of an atom in the first place. This is done here. Note that we also closely follow Ref. [162] in this Appendix. Since the calculations in this thesis are done for ice, there will be a special focus on the distributions for hydrogen and oxygen.

The first thing we need is the wave function for an electron with quantum numbers n, l and m. For the wave function, the following proportionality holds after the angular integration of the Fourier transformation [162]:

$$\Psi_{nl}(\mathbf{k}) \propto Y^*_{lm}(\Omega_k) \int_0^\infty \mathrm{d}r\, r^{n+1} e^{-\mu r} j_l(kr)\,. \tag{A.1}$$

Here, $k = m_e\beta$ and $\mu_{nl} = \xi_{nl}/a_0$. a_0 is the Bohr radius and $\xi_{nl} = Z_{\mathrm{eff}}/n = (Z - \sigma_{nl})/n$, where σ_{nl} accounts for the screening of the nuclear charge seen by the test electron that is decreased by other electrons in the atom. Note that we only need the proportionality since the wave functions need to be normalized anyways and thus we can take overall constants into account by normalizing in the end. Using this wave function, the distribution for quantum numbers n and l reads [162]

$$f_{nl}(\beta) = m_e \int \mathrm{d}\Omega_k k^2 |\Psi_{nl}(k)|^2\,. \tag{A.2}$$

After performing the remaining integral, the velocity distributions that are sufficient

for atoms with an atomic number up to $Z = 26$ are the following:

$$f_{1s}(k) = \frac{32}{\pi} \frac{\mu_{1s}^5 k^2}{(\mu_{1s}^2 + k^2)^4} , \tag{A.3}$$

$$f_{2s}(k) = \frac{32}{3\pi} \frac{\mu_{2s}^5 (3\mu_{2s}^2 k - k^3)^2}{(\mu_{2s}^2 + k^2)^6} , \tag{A.4}$$

$$f_{2p}(k) = \frac{512}{3\pi} \frac{\mu_{2p}^7 k^4}{(\mu_{2p}^2 + k^2)^6} , \tag{A.5}$$

$$f_{3s}(k) = \frac{1024}{5\pi} \frac{\mu_{3s}^7 (\mu_{3s}^3 k - \mu_{3s} k^3)^2}{(\mu_{3s}^2 + k^2)^8} , \tag{A.6}$$

$$f_{3p}(k) = \frac{1024}{45\pi} \frac{\mu_{3p}^7 (5\mu_{3p}^2 k^2 - k^4)^2}{(\mu_{3p}^2 + k^2)^8} , \tag{A.7}$$

$$f_{3d}(k) = \frac{4096}{5\pi} \frac{\mu_{3d}^9 k^6}{(\mu_{3d}^2 + k^2)^8} , \tag{A.8}$$

$$f_{4s}(k) = \frac{512}{35\pi} \frac{\mu_{4s}^9 (5\mu_{4s}^4 k - 10\mu_{4s}^2 k^3 + k^5)^2}{(\mu_{4s}^2 + k^2)^{10}} . \tag{A.9}$$

These are similar to the ones found in Ref. [162]. However, we corrected possible typos in Eqs. A.4 and A.9.

For ice, hydrogen and oxygen are the relevant elements. Hydrogen has one electron in the $1s$ orbital. Thus, the electron velocity distribution for hydrogen is given by Eq. A.3 with $\xi_{1s} = 1$. Oxygen contains eight electrons, two of which are in the $1s$ orbital, two in the $2s$ and four in the $2p$ orbital. Therefore, the electron velocity distribution averaged over the electrons in oxygen is

$$F_O(k) = \frac{f_{1s}(k) + f_{2s}(k) + 2f_{2p}(k)}{4} . \tag{A.10}$$

The constants used here are $\xi_{1s} = 7.6579$, $\xi_{2s} = 2.2458$ and $\xi_{2p} = 2.2266$ [262].

B

Maximum likelihood theory

For the statistical analysis in Ch. 3, we used the maximum likelihood method. Here, a short description of this method and of the Bayesian and the frequentist interpretation is given. We will follow Ch. 6 of Ref. [263]. Please note that we discuss the maximum likelihood analysis for unbinned data since this is the one that is used in this thesis. For the analysis of binned data, the interested reader is referred to Sec. 6.10 of Ref. [263]. Now, let us assume that we have a PDF

$$f(x;\theta)\,, \tag{B.1}$$

where x is the random variable and θ is a set of parameters ($\theta = (\theta_1, \theta_2, \ldots)$) or a single parameter. In the case that the functional form of $f(x;\theta)$ is known but at least one parameter is unknown, maximum likelihood theory is useful to infer information on the unknown parameter(s) if n measurements of x have been performed. To derive the so-called likelihood function, first consider the probability for the first measurement of x that was found in experiment to be in the interval $[x_1, x_1 + dx_1]$. For a given hypothesis for the PDF $f(x;\theta)$ and the parameter(s) θ, this probability is $f(x_1;\theta)dx_1$. If we now consider n independent measurements that give values in the intervals $[x_i, x_i + dx_i]$ for $i = 1$ to $i = n$, the probability reads

$$\prod_{i=1}^{n} f(x_i;\theta)dx_i\,. \tag{B.2}$$

Intuitively, this is reasonable: The expression gives a high probability if the values measured are what we would expect given the functional form of $f(x;\theta)$ and the assumed parameter(s) θ. However, if the assumed parameter value(s) are not close to the correct value(s), we get a low value. Therefore, with a given functional form of $f(x;\theta)$, the expression above gives us an estimate of how well the parameter(s) θ are chosen. The dx_i do not depend on the parameter(s) θ and thus the so-called

likelihood function

$$L(\theta) = \prod_{i=1}^{n} f(x_i; \theta) \tag{B.3}$$

is just as good as the expression in Eq. B.2 when it comes to estimating how well the parameter(s) θ are chosen. If we now assume that the maximum of the likelihood function $L(\theta)$ is not on the boundary of the parameter range and that the function is differentiable in the parameter(s) θ, we can find the best estimate for the parameter(s) θ by standard differentiation:

$$\frac{\partial L}{\partial \theta_i} = 0, \quad i = 1, \ldots, n\,. \tag{B.4}$$

For a lot of measurements, this is rather inconvenient since we need to take the derivative of a product with many factors. The standard way to deal with this is to take the log-likelihood function instead of the likelihood function. Due to the fact that the logarithm is a monotonically increasing function, $\log(L)$ will be maximized by the same parameter value as L. Conveniently, taking the logarithm converts the product in Eq. B.3 into a sum

$$\log(L(\theta)) = \log\left(\prod_{i=1}^{n} f(x_i; \theta)\right) = \sum_{i=1}^{n} \log(f(x_i; \theta))\,, \tag{B.5}$$

which is much less tedious to differentiate. The log-likelihood function we used in our analysis is given in Eq. 3.16.

There are two common ways to interpret the likelihood - the Bayesian and the frequentist interpretation. Since we do the analysis for both interpretations, they will both be introduced in the following sections.

B.1 Bayesian interpretation

The Bayesian approach heavily relies on Bayes' theorem, which gives a relation between different probabilities. If we assume that we have two propositions A and B, the probability of both A and B happening is denoted as $P(A, B)$. This probability can also be written as

$$P(A, B) = P(A|B)P(B)\,, \tag{B.6}$$

where $P(A|B)$ is the probability for A given that B is happening. Of course this can also be written with A and B exchanged. Therefore,

$$P(A|B)P(B) = P(B|A)P(A) \tag{B.7}$$

holds and thus

$$P(A|B) = \frac{P(B|A)P(A)}{P(B)} \tag{B.8}$$

is also true. This is Bayes' theorem [264]. Now, let us introduce some important names that are also used in the analysis. For this, we assume that A is a model parameter having a certain value and B is the data that was measured. Then $P(A|B)$

is the so-called posterior, which reflects the probability for the model parameter to have a certain value given the measured data. $P(B|A)$ is the likelihood and $P(A)$ is the model prior. The prior encodes what was known about the model before the data was measured. Lastly, $P(B)$ is the model evidence. [265]

In general, it is fair to say that the Bayesian approach is the one that takes into account what we knew about the parameter(s) in question before the data was obtained. The posterior probability reflects what we can say about the parameter(s) after measuring the data and this is expressed in terms of the likelihood and the prior. This prior is a way to express what we knew about the parameter(s) before the measurement. Therefore, the Bayesian approach updates what we know about the parameter(s) in question from the prior to the posterior. [266]

B.2 Frequentist interpretation

The frequentist approach is rather different from the Bayesian one. For this, no prior knowledge is taken into account. Instead, for this approach we assume that probability only depends on the frequency of outcomes if an experiment is conducted many times. The frequentist definition of probability can be written as follows:

$$P(x) = \lim_{n\to\infty} \frac{n_x}{n}\,. \tag{B.9}$$

Here, n is the total amount of measurements and n_x is the number of measurements that had outcome x. If the number of measurements goes to infinity, we get the exact probability. While this is easier compute than the Bayesian approach, to get to these high numbers of measurements it is necessary that the measurement is repeatable. [265, 266]

C

Nuclear matrix elements for the calculation of the half-life in the condensate phase

The half-life for $0\nu\beta\beta$ in the condensate phase is given in Eq. 5.52. There, we introduced a NME that depends on the neutrino mass. Its dependence on this neutrino mass is then given by the interpolation in Eq. 5.53. For the calculations of $0\nu\beta\beta$ half-lives done in this thesis, we worked in the framework of chiral EFT [214, 267]. Moreover, we used the Python tool νDoBe [224] for our calculations. In Eq. 5.53, we used the short-range NME $\mathcal{M}_\nu^{(9)}$ and the long-range NME $\mathcal{M}_\nu^{(3)}$. These can be written as

$$\mathcal{M}_\nu^{(3)} = \frac{M_F}{g_A^2} - M_{GT} - M_T - 2\frac{m_\pi^2 g_\nu^{NN}}{g_A^2} M_{F,sd}\,, \tag{C.1}$$

$$\begin{aligned}\mathcal{M}_\nu^{(9)} = {} & \frac{5}{6}\frac{g_1^{\pi\pi} m_\pi^2}{m_N^2}\left(\frac{1}{2}M_{GT,sd}^{AP} + M_{GT,sd}^{PP} + \frac{1}{2}M_{T,sd}^{AP} + M_{T,sd}^{PP}\right) \\ & + \left(g_1^{\pi N} - \frac{5}{6}g_1^{\pi\pi}\right)\frac{m_\pi^2}{2m_N^2}\left(M_{GT,sd}^{AP} + M_{T,sd}^{AP}\right) - 2\frac{g_1^{NN}}{g_A^2}\frac{m_\pi^2}{m_N^2}M_{F,sd}\,.\end{aligned} \tag{C.2}$$

Here, m_N is the mass of the nucleon and m_π is the mass of the pion. Besides these two masses, there are two types of new variables here. The first one are the low-energy constants (LECs). These constants represent the couplings that are present in the chiral EFT Lagrangian. The relevant LECs are given in Table C.1. However, two of the LECs ($g_1^{\pi N}$ and g_1^{NN}) are unknown. For these two, we make use of an estimate utilizing naive dimensional analysis as introduced in Refs. [268,269], leading to

$$g_1^{\pi N} \approx g_1^{NN} \approx 1\,. \tag{C.3}$$

Besides the LECs, Eqs. C.1 and C.2 also contain different NMEs. In this thesis, we use values for the NMEs that have been calculated in the IBM2 framework. These are given in Table C.2.

Table C.1: Summary of the low-energy constants used for the calculation. The values are taken from Ref. [224]. Since $g_1^{\pi N}$ and g_1^{NN} are unknown, naive dimensional analysis was utilized to estimate their value.

g_a	1.271 [270]
$g_1^{\pi\pi}$	0.36 [271]
g_ν^{NN}	$-92.9\,\mathrm{GeV}^{-2}$ [272–274]
$\lvert g_1^{\pi N}\rvert$	$\mathcal{O}(1)$
$\lvert g_1^{NN}\rvert$	$\mathcal{O}(1)$

Table C.2: Nuclear matrix elements for ^{136}Xe calculated in the framework of the Interacting Boson Model-2. Values taken from Ref. [233].

long-range		short-range	
M_F	-0.522	$M_{F,sd}$	-0.734
M_{GT}	5.704	$M_{GT,sd}^{AP}$	-0.690
M_T	0.092	$M_{GT,sd}^{PP}$	0.167
		$M_{T,sd}^{AP}$	-0.363
		$M_{T,sd}^{PP}$	0.115

Bibliography

[1] G.-y. Huang, M. Lindner, and N. Volmer, "*Inferring astrophysical neutrino sources from the Glashow resonance*," JHEP **11** (2023) 164, arXiv:2303.13706.

[2] N. Volmer, "*On neutrino telescopes and their ability to infer astrophysical neutrino sources via the Glashow resonance*," to be published.

[3] L. Gráf, S. Jana, O. Scholer, and N. Volmer, "*Neutrinoless Double Beta Decay without Vacuum Majorana Neutrino Mass*," arXiv:2312.15016.

[4] L. Gráf, O. Scholer, M. Sen, and N. Volmer, "*to be published*," 2024.

[5] J. Chadwick, "*The intensity distribution in the magnetic spectrum of β particles from radium (B + C)*," Verh. Phys. Gesell. **16** (1914) 383–391.

[6] L. M. Brown, "*The idea of the neutrino*,"Physics Today **31** (09, 1978) 23–28.

[7] W. Pauli, "*Letter about his neutrino hypothesis to the participants of the Tübingen conference on radioactivity*," 1930. https://cds.cern.ch/record/83282/files/meitner_0393.pdf.

[8] C. L. Cowan, F. Reines, F. B. Harrison, H. W. Kruse, and A. D. McGuire, "*Detection of the free neutrino: A Confirmation*," Science **124** (1956) 103–104.

[9] E. Fermi, "*An attempt of a theory of beta radiation. 1.*," Z. Phys. **88** (1934) 161–177.

[10] C. Giunti and C. W. Kim, *Fundamentals of Neutrino Physics and Astrophysics*. Oxford University Press, 03, 2007.

[11] G. Rajasekaran, "*The Story of the Neutrino*," arXiv:1606.08715.

[12] F. W. Stecker, "*Chapter 1: Neutrino Physics and Astrophysics Overview*," arXiv:2301.02935.

[13] J. A. Formaggio, A. L. C. de Gouvêa, and R. G. H. Robertson, "*Direct Measurements of Neutrino Mass*," Phys. Rept. **914** (2021) 1–54, arXiv:2102.00594.

[14] F. Cavanna, M. L. Costantini, O. Palamara, and F. Vissani, "*Neutrinos as astrophysical probes*," ICTP Lect. Notes Ser. **14** (2003) 415–437, arXiv:astro-ph/0311256.

[15] "*High-Energy Neutrino Astronomy*," Nuclear Physics A **752** (2005) 3–13. Proceedings of the 22nd International Nuclear Physics Conference (Part 2).

[16] **IceCube**, M. G. Aartsen *et al.*, "*Detection of a particle shower at the Glashow resonance with IceCube*," Nature **591** (2021) no. 7849, 220–224, arXiv:2110.15051. [Erratum: Nature 592, E11 (2021)].

[17] **IceCube**, J. Ahrens *et al.*, "*Icecube - the next generation neutrino telescope at the south pole*," Nucl. Phys. B Proc. Suppl. **118** (2003) 388–395, arXiv:astro-ph/0209556.

[18] S. L. Glashow, "*Resonant Scattering of Antineutrinos*," Phys. Rev. **118** (1960) 316–317.

[19] **KM3Net**, S. Adrian-Martinez *et al.*, "*Letter of intent for KM3NeT 2.0*," J. Phys. G **43** (2016) no. 8, 084001, arXiv:1601.07459.

[20] **Baikal-GVD**, A. D. Avrorin *et al.*, "*Baikal-GVD: status and prospects*," EPJ Web Conf. **191** (2018) 01006, arXiv:1808.10353.

[21] **IceCube-Gen2**, M. G. Aartsen *et al.*, "*IceCube-Gen2: the window to the extreme Universe*," J. Phys. G **48** (2021) no. 6, 060501, arXiv:2008.04323.

[22] M. D. Schwartz, *Quantum Field Theory and the Standard Model*. Cambridge University Press, 3, 2014.

[23] B. Pontecorvo, "*Mesonium and antimesonium*," Zhur. Eksptl'. i Teoret. Fiz. **33** (1957) .

[24] S. M. Bilenky, "*Bruno Pontecorvo and Neutrino Oscillations*," Adv. High Energy Phys. **2013** (2013) 873236.

[25] K. Zuber, *Neutrino Physics*. Taylor & Francis, Boca Raton, 2020.

[26] W. Altmannshofer, J. Davighi, and M. Nardecchia, "*Gauging the accidental symmetries of the standard model, and implications for the flavor anomalies*," Phys. Rev. D **101** (2020) no. 1, 015004, arXiv:1909.02021.

[27] W. H. Furry, "*On transition probabilities in double beta-disintegration*," Phys. Rev. **56** (1939) 1184–1193.

[28] J. Schechter and J. W. F. Valle, "*Neutrinoless Double beta Decay in SU(2) x U(1) Theories*," Phys. Rev. D **25** (1982) 2951.

[29] R. Hodak, S. Kovalenko, and F. Simkovic, "*Capturing relic neutrinos with beta-and double beta-decaying nuclei*," AIP Conf. Proc. **1180** (2009) no. 1, 50–54.

[30] R. Hodák, F. Šimkovic, S. Kovalenko, and A. Faessler, "*Towards the detection of light and heavy relic neutrinos*," Progress in Particle and Nuclear Physics **66** (2011) no. 2, 452–456. Particle and Nuclear Astrophysics.

[31] F. Englert and R. Brout, "*Broken Symmetry and the Mass of Gauge Vector Mesons*," Phys. Rev. Lett. **13** (1964) 321–323.

[32] P. W. Higgs, "*Broken symmetries, massless particles and gauge fields*," Phys. Lett. **12** (1964) 132–133.

[33] P. W. Higgs, "*Broken Symmetries and the Masses of Gauge Bosons*," Phys. Rev. Lett. **13** (1964) 508–509.

[34] S. Bilenky, *Introduction to the Physics of Massive and Mixed Neutrinos*. Lecture Notes in Physics. Springer Berlin Heidelberg, 2010.

[35] R. Davis, Jr., D. S. Harmer, and K. C. Hoffman, "*Search for neutrinos from the sun*," Phys. Rev. Lett. **20** (1968) 1205–1209.

[36] B. T. Cleveland, T. Daily, R. Davis, Jr., J. R. Distel, K. Lande, C. K. Lee, P. S. Wildenhain, and J. Ullman, "*Measurement of the solar electron neutrino flux with the Homestake chlorine detector*," Astrophys. J. **496** (1998) 505–526.

[37] M. Gell-Mann and A. Pais, "*Behavior of neutral particles under charge conjugation*," Phys. Rev. **97** (1955) 1387–1389.

[38] A. De Angelis and M. Pimenta, *Introduction to Particle and Astroparticle Physics: Multimessenger Astronomy and its Particle Physics Foundations*. Undergraduate Lecture Notes in Physics. Springer Nature, Heidelberg, 2018.

[39] **Particle Data Group**, R. L. Workman *et al.*, "*Review of Particle Physics*," PTEP **2022** (2022) 083C01.

[40] **NOvA**, "*New NOvA results add to mystery of neutrinos*." `https://news.fnal.gov/2024/06/new-nova-results-add-to-mystery-of-neutrinos/`. Accessed: 27.07.2024.

[41] L. Stanco, "*The next challenge for neutrinos: the mass ordering*," EPJ Web Conf. **164** (2017) 01031, `arXiv:1610.05533`.

[42] E. Majorana, "*Teoria simmetrica dell'elettrone e del positrone*," Nuovo Cim. **14** (1937) 171–184.

[43] **Planck**, N. Aghanim *et al.*, "*Planck 2018 results. VI. Cosmological parameters*," Astron. Astrophys. **641** (2020) A6, `arXiv:1807.06209`. [Erratum: Astron.Astrophys. 652, C4 (2021)].

[44] R. N. Mohapatra and A. Y. Smirnov, "*Neutrino Mass and New Physics*," Ann. Rev. Nucl. Part. Sci. **56** (2006) 569–628, `arXiv:hep-ph/0603118`.

[45] Y. Cai, T. Han, T. Li, and R. Ruiz, "*Lepton Number Violation: Seesaw Models and Their Collider Tests*," Front. in Phys. **6** (2018) 40, arXiv:1711.02180.

[46] **T2K**, K. Abe *et al.*, "*The T2K Experiment*," Nucl. Instrum. Meth. A **659** (2011) 106–135, arXiv:1106.1238.

[47] M. Sajjad Athar *et al.*, "*Status and perspectives of neutrino physics*," Prog. Part. Nucl. Phys. **124** (2022) 103947, arXiv:2111.07586.

[48] C. Fabjan and H. Schopper, *Particle Physics Reference Library Volume 2: Detectors for Particles and Radiation*. 01, 2020.

[49] J. Lesgourgues and S. Pastor, "*Massive neutrinos and cosmology*," Phys. Rept. **429** (2006) 307–379, arXiv:astro-ph/0603494.

[50] U. K. Dey, "*Cosmic neutrino background: a minireview*,".

[51] A. Mirizzi, I. Tamborra, H.-T. Janka, N. Saviano, K. Scholberg, R. Bollig, L. Hudepohl, and S. Chakraborty, "*Supernova Neutrinos: Production, Oscillations and Detection*," Riv. Nuovo Cim. **39** (2016) no. 1-2, 1–112, arXiv:1508.00785.

[52] H. T. Janka, "*Neutrino Emission from Supernovae*," arXiv:1702.08713.

[53] T. K. Gaisser, F. Halzen, and T. Stanev, "*Particle astrophysics with high-energy neutrinos*," Phys. Rept. **258** (1995) 173–236, arXiv:hep-ph/9410384. [Erratum: Phys.Rept. 271, 355–356 (1996)].

[54] P. Bhattacharjee and G. Sigl, "*Origin and propagation of extremely high-energy cosmic rays*," Phys. Rept. **327** (2000) 109–247, arXiv:astro-ph/9811011.

[55] J. J. Beatty and S. Westerhoff, "*The Highest-Energy Cosmic Rays*," Ann. Rev. Nucl. Part. Sci. **59** (2009) 319–345.

[56] T. K. Gaisser, R. Engel, and E. Resconi, *Cosmic Rays and Particle Physics*. Cambridge University Press, 6, 2016.

[57] L. A. Anchordoqui, "*Ultra-High-Energy Cosmic Rays*," Phys. Rept. **801** (2019) 1–93, arXiv:1807.09645.

[58] J. Becker Tjus and L. Merten, "*Closing in on the origin of Galactic cosmic rays using multimessenger information*," Phys. Rept. **872** (2020) 1–98, arXiv:2002.00964.

[59] K. Murase and I. Bartos, "*High-Energy Multimessenger Transient Astrophysics*," Ann. Rev. Nucl. Part. Sci. **69** (2019) 477–506, arXiv:1907.12506.

[60] K. Murase and F. W. Stecker, "*Chapter 10: High-Energy Neutrinos from Active Galactic Nuclei*," arXiv:2202.03381.

[61] S. V. Troitsky, "*Constraints on models of the origin of high-energy astrophysical neutrinos*," Usp. Fiz. Nauk **191** (2021) no. 12, 1333–1360, arXiv:2112.09611.

[62] Z.-z. Xing and S. Zhou, *Neutrinos in particle physics, astronomy and cosmology*. 2011.

[63] **IceCube**, M. G. Aartsen *et al.*, "*Flavor Ratio of Astrophysical Neutrinos above 35 TeV in IceCube*," Phys. Rev. Lett. **114** (2015) no. 17, 171102, arXiv:1502.03376.

[64] E. Roulet and F. Vissani, "*On the energy of the protons producing the very high-energy astrophysical neutrinos*," JCAP **03** (2021) 050, arXiv:2011.12769.

[65] D. Biehl, A. Fedynitch, A. Palladino, T. J. Weiler, and W. Winter, "*Astrophysical Neutrino Production Diagnostics with the Glashow Resonance*," JCAP **01** (2017) 033, arXiv:1611.07983.

[66] D. F. G. Fiorillo, "*High-Energy and Ultra-High-Energy Neutrino Astrophysics*," Universe **10** (2024) no. 3, 149.

[67] S. Hummer, M. Ruger, F. Spanier, and W. Winter, "*Simplified models for photohadronic interactions in cosmic accelerators*," Astrophys. J. **721** (2010) 630–652, arXiv:1002.1310.

[68] P. Baerwald, S. Hummer, and W. Winter, "*Magnetic Field and Flavor Effects on the Gamma-Ray Burst Neutrino Flux*," Phys. Rev. D **83** (2011) 067303, arXiv:1009.4010.

[69] P. A. Cherenkov, "*Visible luminescence of pure liquids under the influence of γ-radiation*," Dokl. Akad. Nauk SSSR **2** (1934) no. 8, 451–454.

[70] E. P. Cherenkova, "*The discovery of the Cherenkov radiation*," Nucl. Instrum. Meth. A **595** (2008) 8–11.

[71] W. Demtroeder, *Experimental physics. Vol. 4: Nuclear, particle and astrophysics*. 1998.

[72] F. Halzen and S. R. Klein, "*IceCube: An Instrument for Neutrino Astronomy*," Rev. Sci. Instrum. **81** (2010) 081101, arXiv:1007.1247.

[73] **IceCube**, R. Abbasi *et al.*, "*Low energy event reconstruction in IceCube DeepCore*," Eur. Phys. J. C **82** (2022) no. 9, 807, arXiv:2203.02303.

[74] **IceCube-Gen2**, L. Lu *et al.*, "*Shower angular resolution in IceCube-Gen2 and implications on diffuse science*," PoS **ICRC2023** (2023) 1188.

[75] **IceCube**, M. G. Aartsen *et al.*, "*Evidence for High-Energy Extraterrestrial Neutrinos at the IceCube Detector*," Science **342** (2013) 1242856, arXiv:1311.5238.

[76] H. Faissner, H. Reithler, and P. M. Zerwas, eds., *Proceedings, International Neutrino Conference 1976: Aachen, Germany, June 8-12, 1976*. Vieweg, Braunschweig, 1977.

[77] C. Spiering, "*High energy neutrinos and neutrino telescopes*," in *International Conference on History of the Neutrino: 1930-2018*. 3, 2019. arXiv:1903.11481.

[78] A. Roberts, "*The birth of high-energy neutrino astronomy: A personal history of the DUMAND project*,"Rev. Mod. Phys. **64** (Jan, 1992) 259–312.

[79] U. F. Katz and C. Spiering, "*High-Energy Neutrino Astrophysics: Status and Perspectives*," Prog. Part. Nucl. Phys. **67** (2012) 651–704, arXiv:1111.0507.

[80] **BAIKAL**, I. A. Belolaptikov *et al.*, "*The Baikal underwater neutrino telescope: Design, performance and first results*," Astropart. Phys. **7** (1997) 263–282.

[81] **BAIKAL**, V. A. Balkanov *et al.*, "*The BAIKAL neutrino project: Status report*," Nucl. Phys. B Proc. Suppl. **118** (2003) 363–370.

[82] R. I. Bagduev *et al.*, "*The Optical module of the Baikal deep underwater neutrino telescope*," Nucl. Instrum. Meth. A **420** (1999) 138–154, arXiv:astro-ph/9903347.

[83] F. Halzen and J. G. Learned, "*High-energy neutrino detection in deep polar ice*,".

[84] **AMANDA**, E. Andres *et al.*, "*AMANDA: Status, results and future*," in *8th International Workshop on Neutrino Telescopes*, pp. 63–79. 2, 1999. arXiv:astro-ph/9906205.

[85] **IceCube**, A. Achterberg *et al.*, "*Five years of searches for point sources of astrophysical neutrinos with the AMANDA-II neutrino telescope*," Phys. Rev. D **75** (2007) 102001, arXiv:astro-ph/0611063.

[86] F. Halzen, "*The Case for a kilometer scale high-energy neutrino detector*," Nucl. Phys. B Proc. Suppl. **38** (1995) 472–483, arXiv:hep-ph/9410386.

[87] **ANTARES**, E. Aslanides *et al.*, "*A deep sea telescope for high-energy neutrinos*," arXiv:astro-ph/9907432.

[88] **NEMO**, A. Capone *et al.*, "*Recent results and perspectives of the NEMO project*," Nucl. Instrum. Meth. A **602** (2009) 47–53.

[89] **NESTOR**, L. K. Resvanis *et al.*, "*NESTOR: A Neutrino particle astrophysics underwater laboratory for the Mediterranean*," Nucl. Phys. B Proc. Suppl. **35** (1994) 294–300.

[90] **NEMO-3, SuperNEMO**, T. Le Noblet, "*Latest results from NEMO-3 and commissioning status of the SuperNEMO demonstrator*," J. Phys. Conf. Ser. **1342** (2020) no. 1, 012029.

[91] M. Ageron *et al.*, "*ANTARES: the first undersea neutrino telescope*," Nuclear Instruments and Methods in Physics Research Section A: Accelerators, Spectrometers, Detectors and Associated Equipment **656** (2011) no. 1, 11–38, arXiv:1104.1607.

[92] **IceCube**, "*Description of IceCube*." icecube.wisc.edu/science/icecube/. Accessed: 14.04.2024.

[93] **IceCube**, A. Achterberg *et al.*, "*First Year Performance of The IceCube Neutrino Telescope*," Astropart. Phys. **26** (2006) 155–173, arXiv:astro-ph/0604450.

[94] **IceCube**, R. Abbasi *et al.*, "*The IceCube Data Acquisition System: Signal Capture, Digitization, and Timestamping*," Nucl. Instrum. Meth. A **601** (2009) 294–316, arXiv:0810.4930.

[95] **IceCube**, S. Yu and J. Micallef, "*Recent neutrino oscillation result with the IceCube experiment*," in *38th International Cosmic Ray Conference*. 7, 2023. arXiv:2307.15855.

[96] **IceCube**, "*Timeline of IceCube*." icecube.wisc.edu/about-us/icecube10/timeline/. Accessed: 14.04.2024.

[97] **IceCube**, M. G. Aartsen *et al.*, "*First observation of PeV-energy neutrinos with IceCube*," Phys. Rev. Lett. **111** (2013) 021103, arXiv:1304.5356.

[98] **IceCube**, M. G. Aartsen *et al.*, "*Observation of High-Energy Astrophysical Neutrinos in Three Years of IceCube Data*," Phys. Rev. Lett. **113** (2014) 101101, arXiv:1405.5303.

[99] **IceCube**, M. G. Aartsen *et al.*, "*Evidence for Astrophysical Muon Neutrinos from the Northern Sky with IceCube*," Phys. Rev. Lett. **115** (2015) no. 8, 081102, arXiv:1507.04005.

[100] **IceCube**, M. G. Aartsen *et al.*, "*Neutrino emission from the direction of the blazar TXS 0506+056 prior to the IceCube-170922A alert*," Science **361** (2018) no. 6398, 147–151, arXiv:1807.08794.

[101] **IceCube, Fermi-LAT, MAGIC, AGILE, ASAS-SN, HAWC, H.E.S.S., INTEGRAL, Kanata, Kiso, Kapteyn, Liverpool Telescope, Subaru, Swift NuSTAR, VERITAS, VLA/17B-403**, M. G. Aartsen *et al.*, "*Multimessenger observations of a flaring blazar coincident with high-energy neutrino IceCube-170922A*," Science **361** (2018) no. 6398, eaat1378, arXiv:1807.08816.

[102] R. Stein *et al.*, "*A tidal disruption event coincident with a high-energy neutrino*," Nature Astron. **5** (2021) no. 5, 510–518, arXiv:2005.05340.

[103] S. Reusch *et al.*, "*Candidate Tidal Disruption Event AT2019fdr Coincident with a High-Energy Neutrino*," Phys. Rev. Lett. **128** (2022) no. 22, 221101, arXiv:2111.09390.

[104] **IceCube**, R. Abbasi *et al.*, "*Evidence for neutrino emission from the nearby active galaxy NGC 1068*," Science **378** (2022) no. 6619, 538–543, arXiv:2211.09972.

[105] **IceCube**, M. G. Aartsen *et al.*, "*Determining neutrino oscillation parameters from atmospheric muon neutrino disappearance with three years of IceCube DeepCore data*," Phys. Rev. D **91** (2015) no. 7, 072004, arXiv:1410.7227.

[106] **IceCube**, M. G. Aartsen *et al.*, "*Measurement of Atmospheric Neutrino Oscillations at 6–56 GeV with IceCube DeepCore*," Phys. Rev. Lett. **120** (2018) no. 7, 071801, arXiv:1707.07081.

[107] **IceCube**, R. Abbasi *et al.*, "*Measurement of atmospheric neutrino mixing with improved IceCube DeepCore calibration and data processing*," Phys. Rev. D **108** (2023) no. 1, 012014, arXiv:2304.12236.

[108] **IceCube**, M. G. Aartsen *et al.*, "*Measurement of Atmospheric Tau Neutrino Appearance with IceCube DeepCore*," Phys. Rev. D **99** (2019) no. 3, 032007, arXiv:1901.05366.

[109] **IceCub-Gen2e**, "*Outline of IceCube-Gen2*." icecube-gen2.de/project/index_eng.html. Accessed: 16.04.2024.

[110] **IceCube**, M. G. Aartsen *et al.*, "*IceCube-Gen2: A Vision for the Future of Neutrino Astronomy in Antarctica*," arXiv:1412.5106.

[111] **IceCube**, M. G. Aartsen *et al.*, "*Neutrino astronomy with the next generation IceCube Neutrino Observatory*," arXiv:1911.02561.

[112] **P-ONE**, M. Agostini *et al.*, "*The Pacific Ocean Neutrino Experiment*," Nature Astron. **4** (2020) no. 10, 913–915, arXiv:2005.09493.

[113] A. Romero-Wolf *et al.*, "*An Andean Deep-Valley Detector for High-Energy Tau Neutrinos*," in *Latin American Strategy Forum for Research Infrastructure*. 2, 2020. arXiv:2002.06475.

[114] Z. P. Ye *et al.*, "*Proposal for a neutrino telescope in South China Sea*," arXiv:2207.04519.

[115] **Baikal-GVD**, R. Dvornicky, "*Baikal-GVD neutrino telescope: recent status*," PoS **TAUP2023** (2024) 343.

[116] **KM3NeT**, S. R. Gozzini, "*Latest Results with the KM3NeT Neutrino Telescope*," PoS **TAUP2023** (2024) 176.

[117] **Super-Kamiokande**, Y. Fukuda *et al.*, "*Evidence for oscillation of atmospheric neutrinos*," Phys. Rev. Lett. **81** (1998) 1562–1567, arXiv:hep-ex/9807003.

[118] J. J. Gómez-Cadenas, J. Martín-Albo, J. Menéndez, M. Mezzetto, F. Monrabal, and M. Sorel, "*The search for neutrinoless double-beta decay*," Riv. Nuovo Cim. **46** (2023) no. 10, 619–692.

[119] W. Rodejohann, "*Neutrino-less Double Beta Decay and Particle Physics*," Int. J. Mod. Phys. E **20** (2011) 1833–1930, arXiv:1106.1334.

[120] B. J. P. Jones, "*The Physics of Neutrinoless Double Beta Decay: A Primer*," in *Theoretical Advanced Study Institute in Elementary Particle Physics: The Obscure Universe: Neutrinos and Other Dark Matters*. 8, 2021. arXiv:2108.09364.

[121] E. Takasugi, "*Can the Neutrinoless Double Beta Decay Take Place in the Case of Dirac Neutrinos?*," Phys. Lett. B **149** (1984) 372–376.

[122] K. Enqvist, J. Maalampi, and K. Mursula, "*Neutrinoless Double Beta Decay in the Case of Dirac Neutrinos*," Phys. Lett. B **124** (1983) 89–93.

[123] M. Duerr, M. Lindner, and A. Merle, "*On the Quantitative Impact of the Schechter-Valle Theorem*," JHEP **06** (2011) 091, arXiv:1105.0901.

[124] M. Doi, T. Kotani, and E. Takasugi, "*Double beta Decay and Majorana Neutrino*," Prog. Theor. Phys. Suppl. **83** (1985) 1.

[125] F. F. Deppisch, M. Hirsch, and H. Pas, "*Neutrinoless Double Beta Decay and Physics Beyond the Standard Model*," J. Phys. G **39** (2012) 124007, arXiv:1208.0727.

[126] J. Engel and J. Menéndez, "*Status and Future of Nuclear Matrix Elements for Neutrinoless Double-Beta Decay: A Review*," Rept. Prog. Phys. **80** (2017) no. 4, 046301, arXiv:1610.06548.

[127] J. Hyvärinen and J. Suhonen, "*Nuclear matrix elements for $0\nu\beta\beta$ decays with light or heavy Majorana-neutrino exchange*," Phys. Rev. C **91** (2015) no. 2, 024613.

[128] E. L. Fireman, "*A measurement of the half-life of double beta-decay from (50)Sn-124*," Phys. Rev. **75** (1949) 323–324.

[129] A. S. Barabash, "*75 years of double beta decay: yesterday, today and tomorrow*," DAE Symp. Nucl. Phys. **55** (2010) I13, arXiv:1101.4502.

[130] H. V. Klapdor-Kleingrothaus, A. Dietz, H. L. Harney, and I. V. Krivosheina, "*Evidence for neutrinoless double beta decay*," Mod. Phys. Lett. A **16** (2001) 2409–2420, arXiv:hep-ph/0201231.

[131] H. V. Klapdor-Kleingrothaus, I. V. Krivosheina, A. Dietz, C. Tomei, O. Chkvoretz, and H. Strecker, "*Search for neutrinoless double beta decay with enriched Ge-76 1990-2003: HEIDELBERG-MOSCOW experiment*," arXiv:hep-ph/0404062.

[132] C. E. Aalseth *et al.*, "*Comment on 'Evidence for neutrinoless double beta decay'*," Mod. Phys. Lett. A **17** (2002) 1475–1478, arXiv:hep-ex/0202018.

[133] M. Gunther *et al.*, "*Heidelberg - Moscow beta-beta experiment with Ge-76: Full setup with five detectors*," Phys. Rev. D **55** (1997) 54–67.

[134] H. V. Klapdor-Kleingrothaus *et al.*, "*Latest results from the Heidelberg-Moscow double beta decay experiment*," Eur. Phys. J. A **12** (2001) 147–154, arXiv:hep-ph/0103062.

[135] **GERDA**, M. Agostini *et al.*, "*Final Results of GERDA on the Search for Neutrinoless Double-β Decay*," Phys. Rev. Lett. **125** (2020) no. 25, 252502, arXiv:2009.06079.

[136] **nEXO**, S. A. Kharusi *et al.*, "*nEXO Pre-Conceptual Design Report*," arXiv:1805.11142.

[137] **EXO-200**, G. Anton *et al.*, "*Search for Neutrinoless Double-β Decay with the Complete EXO-200 Dataset*," Phys. Rev. Lett. **123** (2019) no. 16, 161802, arXiv:1906.02723.

[138] **KamLAND-Zen**, S. Abe *et al.*, "*Search for the Majorana Nature of Neutrinos in the Inverted Mass Ordering Region with KamLAND-Zen*," Phys. Rev. Lett. **130** (2023) no. 5, 051801, arXiv:2203.02139.

[139] **KamLAND-Zen**, S. Abe *et al.*, "*Search for Majorana Neutrinos with the Complete KamLAND-Zen Dataset*," arXiv:2406.11438.

[140] **KamLAND-Zen**, K. Asakura *et al.*, "*Search for double-beta decay of ^{136}Xe to excited states of ^{136}Ba with the KamLAND-Zen experiment*," Nucl. Phys. A **946** (2016) 171–181, arXiv:1509.03724.

[141] **CUORE**, D. Q. Adams *et al.*, "*Search for Majorana neutrinos exploiting millikelvin cryogenics with CUORE*," Nature **604** (2022) no. 7904, 53–58, arXiv:2104.06906.

[142] V. S. Berezinsky and A. Z. Gazizov, "*Cosmic neutrino and the possibility of Searching for W bosons with masses 30-100 GeV in underwater experiments*," JETP Lett. **25** (1977) 254–256.

[143] R. W. Brown and F. W. Stecker, "*Cosmic Ray Neutrino Tests for Heavier Weak Bosons and Cosmic Antimatter*," Phys. Rev. D **26** (1982) 373.

[144] L. A. Anchordoqui, H. Goldberg, F. Halzen, and T. J. Weiler, "*Neutrinos as a diagnostic of high energy astrophysical processes*," Phys. Lett. B **621** (2005) 18–21, arXiv:hep-ph/0410003.

[145] S. Hummer, M. Maltoni, W. Winter, and C. Yaguna, "*Energy dependent neutrino flavor ratios from cosmic accelerators on the Hillas plot*," Astropart. Phys. **34** (2010) 205–224, arXiv:1007.0006.

[146] Z.-z. Xing and S. Zhou, "*The Glashow resonance as a discriminator of UHE cosmic neutrinos originating from p-gamma and p-p collisions*," Phys. Rev. D **84** (2011) 033006, arXiv:1105.4114.

[147] A. Bhattacharya, R. Gandhi, W. Rodejohann, and A. Watanabe, "*The Glashow resonance at IceCube: signatures, event rates and pp vs. $p\gamma$ interactions*," JCAP **10** (2011) 017, arXiv:1108.3163.

[148] A. Bhattacharya, R. Gandhi, W. Rodejohann, and A. Watanabe, "*On the interpretation of IceCube cascade events in terms of the Glashow resonance*," arXiv:1209.2422.

[149] V. Barger, J. Learned, and S. Pakvasa, "*IceCube PeV Cascade Events Initiated by Electron-Antineutrinos at Glashow Resonance*," Phys. Rev. D **87** (2013) no. 3, 037302, arXiv:1207.4571.

[150] V. Barger, L. Fu, J. G. Learned, D. Marfatia, S. Pakvasa, and T. J. Weiler, "*Glashow resonance as a window into cosmic neutrino sources*," Phys. Rev. D **90** (2014) 121301, arXiv:1407.3255.

[151] A. Palladino, G. Pagliaroli, F. L. Villante, and F. Vissani, "*Double pulses and cascades above 2 PeV in IceCube*," Eur. Phys. J. C **76** (2016) no. 2, 52, arXiv:1510.05921.

[152] I. M. Shoemaker and K. Murase, "*Probing BSM Neutrino Physics with Flavor and Spectral Distortions: Prospects for Future High-Energy Neutrino Telescopes*," Phys. Rev. D **93** (2016) no. 8, 085004, arXiv:1512.07228.

[153] L. A. Anchordoqui, M. M. Block, L. Durand, P. Ha, J. F. Soriano, and T. J. Weiler, "*Evidence for a break in the spectrum of astrophysical neutrinos*," Phys. Rev. D **95** (2017) no. 8, 083009, arXiv:1611.07905.

[154] M. D. Kistler and R. Laha, "*Multi-PeV Signals from a New Astrophysical Neutrino Flux Beyond the Glashow Resonance*," Phys. Rev. Lett. **120** (2018) no. 24, 241105, arXiv:1605.08781.

[155] S. Sahu and B. Zhang, "*On the non-detection of Glashow resonance in IceCube*," JHEAp **18** (2018) 1–4, arXiv:1612.09043.

[156] G.-y. Huang and Q. Liu, "*Hunting the Glashow Resonance with PeV Neutrino Telescopes*," JCAP **03** (2020) 005, arXiv:1912.02976.

[157] S. Zhou, "*Cosmic Flavor Hexagon for Ultrahigh-energy Neutrinos and Antineutrinos at Neutrino Telescopes*," arXiv:2006.06181.

[158] Q. Liu, D. F. G. Fiorillo, C. A. Argüelles, M. Bustamante, N. Song, and A. C. Vincent, "*Identifying Energy-Dependent Flavor Transitions in High-Energy Astrophysical Neutrino Measurements*," arXiv:2312.07649.

[159] **CDF**, T. Aaltonen *et al.*, "*High-precision measurement of the W boson mass with the CDF II detector*," Science **376** (2022) no. 6589, 170–176.

[160] L. Lu, "*Multi-flavour PeV neutrino search with IceCube*," in *Proceedings of 35th International Cosmic Ray Conference; PoS(ICRC2017)*, vol. 301, p. 1002. 2017.

[161] M. Aartsen *et al.*, "*Observation of High-Energy Astrophysical Neutrinos in Three Years of IceCube Data*,"Physical Review Letters **113** (Sept., 2014) , arXiv:1405.5303.

[162] A. Loewy, S. Nussinov, and S. L. Glashow, "*The Effect of Doppler Broadening on the* 6.3 *PeV* W^- *Resonance in* $\bar{\nu}_e e^-$ *Collisions*," arXiv:1407.4415.

[163] **ALEPH, DELPHI, L3, OPAL, SLD, LEP Electroweak Working Group, SLD Electroweak Group, SLD Heavy Flavour Group**, S. Schael *et al.*, "*Precision electroweak measurements on the Z resonance*," Phys. Rept. **427** (2006) 257–454, arXiv:hep-ex/0509008.

[164] A. Garcia, R. Gauld, A. Heijboer, and J. Rojo, "*Complete predictions for high-energy neutrino propagation in matter*," JCAP **09** (2020) 025, arXiv:2004.04756.

[165] M. Cacciari *et al.*, "*QED structure functions: A Systematic approach*," EPL **17** (1992) 123–128.

[166] **IceCube**, L. Mohrmann, "*Combined Analysis of the High-Energy Cosmic Neutrino Flux at the IceCube Detector*," PoS **ICRC2015** (2016) 1066, arXiv:1510.05223.

[167] A. M. Hillas, "*The Origin of Ultrahigh-Energy Cosmic Rays*," Ann. Rev. Astron. Astrophys. **22** (1984) 425–444.

[168] U. Stroth, *Plasmaphysik: Phänomene, Grundlagen, Anwendungen*. Vieweg+Teubner Verlag, 2011.

[169] F. M. Rieger, "*Active Galactic Nuclei as Potential Sources of Ultra-High Energy Cosmic Rays*," Universe **8** (2022) , arXiv:2211.12202.

[170] M. Bustamante *et al.*, "*High-energy cosmic-ray acceleration*," in *CERN-Latin-American School of High-Energy Physics, CLASHEP 2009 - Proceedings*, pp. 533–539. 2010.

[171] **IceCube**, R. Abbasi *et al.*, "*The IceCube high-energy starting event sample: Description and flux characterization with 7.5 years of data*," Phys. Rev. D **104** (2021) 022002, arXiv:2011.03545.

[172] S. Palomares-Ruiz, A. C. Vincent, and O. Mena, "*Spectral analysis of the high-energy IceCube neutrinos*," Phys. Rev. D **91** (2015) no. 10, 103008, arXiv:1502.02649.

[173] A. M. Dziewonski and D. L. Anderson, "*Preliminary reference Earth model*," Physics of the Earth and Planetary Interiors **25** (1981) no. 4, 297–356.

[174] R. Gandhi, C. Quigg, M. H. Reno, and I. Sarcevic, "*Ultrahigh-energy neutrino interactions*," Astropart. Phys. **5** (1996) 81–110, arXiv:hep-ph/9512364.

[175] R. Gandhi, C. Quigg, M. H. Reno, and I. Sarcevic, "*Neutrino interactions at ultrahigh-energies*," Phys. Rev. D **58** (1998) 093009, arXiv:hep-ph/9807264.

[176] T.-J. Hou *et al.*, "*New CTEQ global analysis of quantum chromodynamics with high-precision data from the LHC*," Phys. Rev. D **103** (2021) no. 1, 014013, arXiv:1912.10053.

[177] D. B. Clark, E. Godat, and F. I. Olness, "*ManeParse : A Mathematica reader for Parton Distribution Functions*," Comput. Phys. Commun. **216** (2017) 126–137, arXiv:1605.08012.

[178] A. Palladino and W. Winter, "*A multi-component model for observed astrophysical neutrinos*," Astron. Astrophys. **615** (2018) A168, arXiv:1801.07277.

[179] J. G. Learned and S. Pakvasa, "*Detecting tau-neutrino oscillations at PeV energies*," Astropart. Phys. **3** (1995) 267–274, arXiv:hep-ph/9405296.

[180] **IceCube**, R. Abbasi *et al.*, "*Detection of astrophysical tau neutrino candidates in IceCube*," Eur. Phys. J. C **82** (2022) no. 11, 1031, arXiv:2011.03561.

[181] **LHAASO**, Z. Cao *et al.*, "*Ultrahigh-energy photons up to 1.4 petaelectronvolts from 12 γ-ray Galactic sources*," Nature **594** (2021) no. 7861, 33–36.

[182] **LHAASO*†, LHAASO**, Z. Cao *et al.*, "*Peta–electron volt gamma-ray emission from the Crab Nebula*," Science **373** (2021) no. 6553, 425–430, arXiv:2111.06545.

[183] T. Sudoh and J. F. Beacom, "*Where are Milky Way's hadronic PeVatrons?*," Phys. Rev. D **107** (2023) no. 4, 043002, arXiv:2209.03970.

[184] Q. Liu, N. Song, and A. C. Vincent, "*Probing neutrino production in high-energy astrophysical neutrino sources with the Glashow resonance*," Phys. Rev. D **108** (2023) no. 4, 043022, arXiv:2304.06068.

[185] T. Cheng, H.-J. Kuan, Y.-Y. Li, and V. Brdar, "*Magnetar-powered Neutrinos and Magnetic Moment Signatures at IceCube*," arXiv:2312.14113.

[186] A. Y. Smirnov, "*The MSW effect and matter effects in neutrino oscillations*," Phys. Scripta T **121** (2005) 57–64, arXiv:hep-ph/0412391.

[187] Q. Liu, N. Song, and A. C. Vincent, "*Constraints on Heavy Asymmetric and Symmetric Dark Matter from the Glashow Resonance*," arXiv:2406.14602.

[188] K. Petraki and R. R. Volkas, "*Review of asymmetric dark matter*," Int. J. Mod. Phys. A **28** (2013) 1330028, arXiv:1305.4939.

[189] M. Bustamante, J. F. Beacom, and K. Murase, "*Testing decay of astrophysical neutrinos with incomplete information*," Phys. Rev. D **95** (2017) no. 6, 063013, arXiv:1610.02096.

[190] M. Bustamante, "*New limits on neutrino decay from the Glashow resonance of high-energy cosmic neutrinos*," arXiv:2004.06844.

[191] D.-H. Xu and S.-J. Rong, "*Connect the Lorentz violation to the Glashow resonance event*," Mod. Phys. Lett. A **38** (2023) no. 04, 2350029, arXiv:2211.05478.

[192] K. S. Babu, P. S. Dev, S. Jana, and Y. Sui, "*Zee-Burst: A New Probe of Neutrino Nonstandard Interactions at IceCube*," Phys. Rev. Lett. **124** (2020) no. 4, 041805, arXiv:1908.02779.

[193] K. S. Babu, P. S. B. Dev, and S. Jana, "*Probing neutrino mass models through resonances at neutrino telescopes*," Int. J. Mod. Phys. A **37** (2022) no. 11n12, 2230003, arXiv:2202.06975.

[194] A. Zee, "*A Theory of Lepton Number Violation, Neutrino Majorana Mass, and Oscillation*," Phys. Lett. B **93** (1980) 389. [Erratum: Phys.Lett.B 95, 461 (1980)].

[195] U. K. Dey, N. Nath, and S. Sadhukhan, "*Charged Higgs effects in IceCube: PeV events and NSIs*," JHEP **09** (2021) 113, arXiv:2010.05797.

[196] T. Brune and H. Päs, "*Massive Majorons and constraints on the Majoron-neutrino coupling*," Phys. Rev. D **99** (2019) no. 9, 096005, arXiv:1808.08158.

[197] J. Heeck, "*Phenomenology of Majorons*," in *13th Patras Workshop on Axions, WIMPs and WISPs*, pp. 212–215. 2018. arXiv:1709.07670.

[198] G.-y. Huang and N. Nath, "*Neutrino meets ultralight dark matter: $0\nu\beta\beta$ decay and cosmology*," JCAP **05** (2022) no. 05, 034, arXiv:2111.08732.

[199] F. Nozzoli and C. Cernetti, "*Dark Matter stimulated neutrinoless double beta decay*," arXiv:2212.07832.

[200] J. Herms, S. Jana, V. P. K., and S. Saad, "*Light neutrinophilic dark matter from a scotogenic model*," Phys. Lett. B **845** (2023) 138167, arXiv:2307.15760.

[201] M. Doi, T. Kotani, and E. Takasugi, "*Neutrinoless double-beta decay with Majoron emission*,"Phys. Rev. D **37** (May, 1988) 2575–2589.

[202] K. Tuominen, "*Cold Particle Dark Matter*," Symmetry **13** (2021) no. 10, 1945.

[203] E. G. M. Ferreira, "*Ultra-light dark matter*," Astron. Astrophys. Rev. **29** (2021) no. 1, 7, arXiv:2005.03254.

[204] M. Laine and A. Vuorinen, *Basics of Thermal Field Theory*, vol. 925. Springer, 2016. arXiv:1701.01554.

[205] Bose, "*Plancks Gesetz und Lichtquantenhypothese*," Zeitschrift für Physik **26** (1924) 178–181.

[206] A. Einstein, *Quantentheorie des einatomigen idealen Gases; part 1 and 2*. Sitzungsberichte der Preussischen Akademie der Wissenschaften. Physikalisch-mathematische Klasse. Verlag d. Akad. d. Wiss., 1924/25.

[207] D. V. Schroeder, *An Introduction to Thermal Physics*. Addison Wesley, San Francisco, CA, 2000.

[208] D. J. Griffiths, *Introduction to Quantum Mechanics*. Prentice Hall, 1995.

[209] J. I. Kapusta and C. Gale, *Finite-Temperature Field Theory: Principles and Applications*. Cambridge Monographs on Mathematical Physics. Cambridge University Press, 2006.

[210] M. Sen and A. Y. Smirnov, "*Refractive neutrino masses, ultralight dark matter and cosmology*," JCAP **01** (2024) 040, arXiv:2306.15718.

[211] M. Hirsch, H. V. Klapdor-Kleingrothaus, S. G. Kovalenko, and H. Pas, "*On the observability of majoron emitting double beta decays*," Phys. Lett. B **372** (1996) 8–14, arXiv:hep-ph/9511227.

[212] J. Kotila and F. Iachello, "*Nuclear matrix elements for Majoron-emitting double- β decay*," Phys. Rev. C **103** (2021) no. 4, 044302, arXiv:2104.02327.

[213] L. Gráf, M. Lindner, and O. Scholer, "*Unraveling the $0\nu\beta\beta$ decay mechanisms*," Phys. Rev. D **106** (2022) no. 3, 035022, arXiv:2204.10845.

[214] V. Cirigliano, W. Dekens, J. de Vries, M. L. Graesser, and E. Mereghetti, "*Neutrinoless double beta decay in chiral effective field theory: lepton number violation at dimension seven*," JHEP **12** (2017) 082, arXiv:1708.09390.

[215] W. Dekens, J. de Vries, K. Fuyuto, E. Mereghetti, and G. Zhou, "*Sterile neutrinos and neutrinoless double beta decay in effective field theory*," JHEP **06** (2020) 097, arXiv:2002.07182.

[216] J. Kotila, J. Barea, and F. Iachello, "*Phase-space factors and half-life predictions for Majoron-emitting decay*," Phys. Rev. C **91** (2015) no. 6, 064310, arXiv:1509.05154. [Erratum: Phys.Rev.C 92, 029903 (2015)].

[217] **XENON**, E. Aprile *et al.*, "*Dark Matter Search Results from a One Ton-Year Exposure of XENON1T*," Phys. Rev. Lett. **121** (2018) no. 11, 111302, arXiv:1805.12562.

[218] J. Kotila and F. Iachello, "*Phase space factors for double-β decay*," Phys. Rev. C **85** (2012) 034316, arXiv:1209.5722.

[219] F. Deppisch and H. Pas, "*Pinning down the mechanism of neutrinoless double beta decay with measurements in different nuclei*," Phys. Rev. Lett. **98** (2007) 232501, arXiv:hep-ph/0612165.

[220] V. M. Gehman and S. R. Elliott, "*Multiple-Isotope Comparison for Determining 0 nu beta beta Mechanisms*," J. Phys. G **34** (2007) 667–678, arXiv:hep-ph/0701099. [Erratum: J.Phys.G 35, 029701 (2008)].

[221] G. L. Fogli, E. Lisi, and A. M. Rotunno, "*Probing particle and nuclear physics models of neutrinoless double beta decay with different nuclei*," Phys. Rev. D **80** (2009) 015024, arXiv:0905.1832.

[222] A. Faessler, G. L. Fogli, E. Lisi, A. M. Rotunno, and F. Simkovic, "*Multi-Isotope Degeneracy of Neutrinoless Double Beta Decay Mechanisms in the Quasi-Particle Random Phase Approximation*," Phys. Rev. D **83** (2011) 113015, arXiv:1103.2504.

[223] S.-L. Chen and Y.-Q. Xiao, "*Neutrinoless double beta decay in multiple isotopes for fingerprints identification of operators and models*," JHEP **05** (2024) 252, arXiv:2402.04600.

[224] O. Scholer, J. de Vries, and L. Gráf, "*νDoBe — A Python tool for neutrinoless double beta decay*," JHEP **08** (2023) 043, arXiv:2304.05415.

[225] **LEGEND**, N. Abgrall *et al.*, "*The Large Enriched Germanium Experiment for Neutrinoless $\beta\beta$ Decay: LEGEND-1000 Preconceptual Design Report*," arXiv:2107.11462.

[226] S. F. King, "*Neutrino mass models*," Rept. Prog. Phys. **67** (2004) 107–158, arXiv:hep-ph/0310204.

[227] S. M. Bilenky and C. Giunti, "*Neutrinoless Double-Beta Decay: a Probe of Physics Beyond the Standard Model*," Int. J. Mod. Phys. A **30** (2015) no. 04n05, 1530001, arXiv:1411.4791.

[228] W. Flieger and J. Gluza, "*General neutrino mass spectrum and mixing properties in seesaw mechanisms*," Chin. Phys. C **45** (2021) no. 2, 023106, arXiv:2004.00354.

[229] H. E. Haber, "*A tale of three diagonalizations*," Int. J. Mod. Phys. A **36** (2021) no. 04, 2130003, arXiv:2009.03990.

[230] **Particle Data Group**, R. L. Workman *et al.*, "*Review of Particle Physics*," PTEP **2022** (2022) 083C01.

[231] P. D. Bolton, F. F. Deppisch, and P. S. Bhupal Dev, "*Neutrinoless double beta decay versus other probes of heavy sterile neutrinos*," JHEP **03** (2020) 170, arXiv:1912.03058.

[232] A. Faessler, M. González, S. Kovalenko, and F. Šimkovic, "*Arbitrary mass Majorana neutrinos in neutrinoless double beta decay*," Phys. Rev. D **90** (2014) no. 9, 096010, arXiv:1408.6077.

[233] F. F. Deppisch, L. Graf, F. Iachello, and J. Kotila, "*Analysis of light neutrino exchange and short-range mechanisms in $0\nu\beta\beta$ decay*," Phys. Rev. D **102** (2020) no. 9, 095016, arXiv:2009.10119.

[234] W. Dekens, J. de Vries, E. Mereghetti, J. Menéndez, P. Soriano, and G. Zhou, "*Neutrinoless double-β decay in the neutrino-extended standard model*," Phys. Rev. C **108** (2023) no. 4, 045501, arXiv:2303.04168.

[235] **nEXO**, G. Adhikari *et al.*, "*nEXO: neutrinoless double beta decay search beyond 10^{28} year half-life sensitivity*," J. Phys. G **49** (2022) no. 1, 015104, arXiv:2106.16243.

[236] G.-y. Huang, M. Lindner, P. Martínez-Miravé, and M. Sen, "*Cosmology-friendly time-varying neutrino masses via the sterile neutrino portal*," Phys. Rev. D **106** (2022) no. 3, 033004, arXiv:2205.08431.

[237] A. de Gouvêa, P. S. B. Dev, B. Dutta, T. Ghosh, T. Han, and Y. Zhang, "*Leptonic Scalars at the LHC*," JHEP **07** (2020) 142, arXiv:1910.01132.

[238] J. M. Berryman, A. De Gouvêa, K. J. Kelly, and Y. Zhang, "*Lepton-Number-Charged Scalars and Neutrino Beamstrahlung*," Phys. Rev. D **97** (2018) no. 7, 075030, arXiv:1802.00009.

[239] K. C. Y. Ng and J. F. Beacom, "*Cosmic neutrino cascades from secret neutrino interactions*," Phys. Rev. D **90** (2014) no. 6, 065035, arXiv:1404.2288. [Erratum: Phys.Rev.D 90, 089904 (2014)].

[240] K. Ioka and K. Murase, "*IceCube PeV–EeV neutrinos and secret interactions of neutrinos*," PTEP **2014** (2014) no. 6, 061E01, arXiv:1404.2279.

[241] C. D. Kreisch, F.-Y. Cyr-Racine, and O. Doré, "*Neutrino puzzle: Anomalies, interactions, and cosmological tensions*," Phys. Rev. D **101** (2020) no. 12, 123505, arXiv:1902.00534.

[242] M. Berbig, S. Jana, and A. Trautner, "*The Hubble tension and a renormalizable model of gauged neutrino self-interactions*," Phys. Rev. D **102** (2020) no. 11, 115008, arXiv:2004.13039.

[243] E. Di Valentino, O. Mena, S. Pan, L. Visinelli, W. Yang, A. Melchiorri, D. F. Mota, A. G. Riess, and J. Silk, "*In the realm of the Hubble tension—a review of solutions*," Class. Quant. Grav. **38** (2021) no. 15, 153001, arXiv:2103.01183.

[244] C. G. Boehmer and T. Harko, "*Can dark matter be a Bose-Einstein condensate?*," JCAP **06** (2007) 025, arXiv:0705.4158.

[245] S. Das and R. K. Bhaduri, "*Dark matter and dark energy from a Bose–Einstein condensate*," Class. Quant. Grav. **32** (2015) no. 10, 105003, arXiv:1411.0753.

[246] A. Sharma, J. Khoury, and T. Lubensky, "*The Equation of State of Dark Matter Superfluids*," JCAP **05** (2019) 054, arXiv:1809.08286.

[247] E. Castellanos, C. Escamilla-Rivera, and J. Mastache, "*Is a Bose–Einstein condensate a good candidate for dark matter? A test with galaxy rotation curves*," Int. J. Mod. Phys. D **29** (2020) no. 09, 2050063, arXiv:1910.03791.

[248] S. Brieden, H. Gil-Marín, and L. Verde, "*Model-agnostic interpretation of 10 billion years of cosmic evolution traced by BOSS and eBOSS data*," JCAP **08** (2022) no. 08, 024, arXiv:2204.11868.

[249] J. L. Feng, "*Dark Matter Candidates from Particle Physics and Methods of Detection*," Ann. Rev. Astron. Astrophys. **48** (2010) 495–545, arXiv:1003.0904.

[250] H. Ejiri *et al.*, "*MOON for neutrino-less double beta decays*," Eur. Phys. J. ST **162** (2008) 239–250.

[251] F. Schwabl, *Statistische Mechanik*. SpringerLink : Bücher. Springer Berlin Heidelberg, Berlin, Heidelberg, dritte, aktualisierte auflage ed., 2006. http://dx.doi.org/10.1007/3-540-31097-5.

[252] S. Tremaine and J. E. Gunn, "*Dynamical Role of Light Neutral Leptons in Cosmology*," Phys. Rev. Lett. **42** (1979) 407–410.

[253] H. Davoudiasl, P. B. Denton, and D. A. McGady, "*Ultralight fermionic dark matter*," Phys. Rev. D **103** (2021) no. 5, 055014, arXiv:2008.06505.

[254] **KATRIN**, M. Aker *et al.*, "*KATRIN: status and prospects for the neutrino mass and beyond*," J. Phys. G **49** (2022) no. 10, 100501, arXiv:2203.08059.

[255] Canva. https://www.canva.com/. Accessed: 16.07.2024.

[256] A. de Gouvêa, M. Sen, and J. Weill, "*Visible neutrino decays and the impact of the daughter-neutrino mass*," Phys. Rev. D **106** (2022) no. 1, 013005, arXiv:2203.14976.

[257] Y. Chikashige, R. N. Mohapatra, and R. D. Peccei, "*Spontaneously Broken Lepton Number and Cosmological Constraints on the Neutrino Mass Spectrum*," Phys. Rev. Lett. **45** (1980) 1926.

[258] J. Schechter and J. W. F. Valle, "*Neutrino Decay and Spontaneous Violation of Lepton Number*," Phys. Rev. D **25** (1982) 774.

[259] K. S. Babu and R. N. Mohapatra, "*Geometrical neutrino mass hierarchy and a 17-keV tau-neutrino*," Phys. Rev. Lett. **67** (1991) 1498–1501.

[260] I. M. Shoemaker, K. Petraki, and A. Kusenko, "*Collider signatures of sterile neutrinos in models with a gauge-singlet Higgs*," JHEP **09** (2010) 060, arXiv:1006.5458.

[261] P. J. E. Peebles and B. Ratra, "*The Cosmological Constant and Dark Energy*," Rev. Mod. Phys. **75** (2003) 559–606, arXiv:astro-ph/0207347.

[262] E. Clementi and D. L. Raimondi, "*Atomic Screening Constants from SCF Functions*," jcp **38** (1963) no. 11, 2686–2689.

[263] G. Cowan, *Statistical data analysis*. Clarendon Press, 1998.

[264] T. Bayes, "*An Essay towards solving a Problem in the Doctrine of Chances*,"Biometrika **45** (12, 1958) 296–315.

[265] J. VanderPlas, "*Frequentism and Bayesianism: A Python-driven Primer*," arXiv:1411.5018.

[266] R. Trotta, "*Bayesian Methods in Cosmology*," 1, 2017. arXiv:1701.01467.

[267] V. Cirigliano, W. Dekens, J. de Vries, M. L. Graesser, and E. Mereghetti, "*A neutrinoless double beta decay master formula from effective field theory*," JHEP **12** (2018) 097, arXiv:1806.02780.

[268] A. Manohar and H. Georgi, "*Chiral Quarks and the Nonrelativistic Quark Model*," Nucl. Phys. B **234** (1984) 189–212.

[269] E. E. Jenkins, A. V. Manohar, and M. Trott, "*Naive Dimensional Analysis Counting of Gauge Theory Amplitudes and Anomalous Dimensions*," Phys. Lett. B **726** (2013) 697–702, arXiv:1309.0819.

[270] C. C. Chang *et al.*, "*A per-cent-level determination of the nucleon axial coupling from quantum chromodynamics*," Nature **558** (2018) no. 7708, 91–94, arXiv:1805.12130.

[271] A. Nicholson *et al.*, "*Heavy physics contributions to neutrinoless double beta decay from QCD*," Phys. Rev. Lett. **121** (2018) no. 17, 172501, arXiv:1805.02634.

[272] V. Cirigliano, W. Dekens, J. de Vries, M. Hoferichter, and E. Mereghetti, "*Toward Complete Leading-Order Predictions for Neutrinoless Double β Decay*," Phys. Rev. Lett. **126** (2021) no. 17, 172002, arXiv:2012.11602.

[273] V. Cirigliano, W. Dekens, J. de Vries, M. Hoferichter, and E. Mereghetti, "*Determining the leading-order contact term in neutrinoless double β decay*," JHEP **05** (2021) 289, arXiv:2102.03371.

[274] R. Wirth, J. M. Yao, and H. Hergert, "*Ab Initio Calculation of the Contact Operator Contribution in the Standard Mechanism for Neutrinoless Double Beta Decay*," Phys. Rev. Lett. **127** (2021) no. 24, 242502, arXiv:2105.05415.